

DIONÍSIO DE CARVALHO

**Assessment of a software-defined radio aiming at
microwave breast cancer detection**

São Paulo
2023

DIONÍSIO DE CARVALHO

**Assessment of a software-defined radio aiming at
microwave breast cancer detection**

Corrected Version

Thesis presented to the Polytechnic School
of the University of São Paulo in partial
fulfillment of the requirements for the degree
of Doctor of Science.

Concentration Area:
Microelectronics

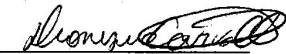
Supervisor:
Prof. Dr. Wilhelmus A. M. Van Noije

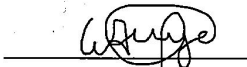
São Paulo
2023

Autorizo a reprodução e divulgação total ou parcial deste trabalho, por qualquer meio convencional ou eletrônico, para fins de estudo e pesquisa, desde que citada a fonte.

Este exemplar foi revisado e corrigido em relação à versão original, sob responsabilidade única do autor e com a anuência de seu orientador.

São Paulo, 05 de Abril de 2024

Assinatura do autor: 

Assinatura do orientador: 

Catálogo-na-publicação

de Carvalho, Dionísio

Assessment of a software-defined radio aiming at microwave breast cancer detection / D. de Carvalho -- versão corr. -- São Paulo, 2023.
140 p.

Tese (Doutorado) - Escola Politécnica da Universidade de São Paulo.
Departamento de Engenharia de Sistemas Eletrônicos.

1.Deteccção de câncer de mama 2.Radio definido por software 3.Imagiologia médica 4.Pulso sintético de banda ultralarga I.Universidade de São Paulo. Escola Politécnica. Departamento de Engenharia de Sistemas Eletrônicos II.t.

Nome: Carvalho, Dionísio de

Título: Avaliação de um rádio definido por software objetivando detecção de câncer de mama por micro-ondas.

Tese apresentada à Escola Politécnica da Universidade de São Paulo para a obtenção do título de Doutor em Ciências.

Aprovado em : 29/Nov/2023

Banca Examinadora

Nome dos Participantes da Banca	Função	Sigla da CPG	Resultado
Wilhelmus Adrianus Maria Van Noije	Presidente	EP - USP	<u>Aprovado</u>
Fatima Salete Correra	Titular	EP - USP	<u>Aprovado</u>
Robson Luiz Moreno	Titular	UNIFEI - Externo	<u>Aprovado</u>
Márcio Bender Machado	Titular	IFSP - Externo	<u>Aprovado</u>
André Augusto Mariano	Titular	UFPR - Externo	<u>Aprovado</u>

Resultado Final: Aprovado

Acknowledgements

Nothing in my life was accomplished alone. The most important things are those that produce the best memories. For all the memories that are forever in my heart, I would like to thank my mother, Heloisa Helena, my father, Marcos Moreira, my stepfather Delfim Vieira (in memoriam), my girlfriend and partner Bruna Fávoro, and all my friends from DMPSV, in special Silvana Leonor and Alexandre Aragão.

Also, nothing significant is accomplished for free. So, I would like to thank my advisor, Professor Wilhelmus Adrianus Maria van Noije, for pushing me to do great work. Your help and guidance were essential for this Thesis.

I would like to thank the Centro Interdisciplinar em Tecnologias Interativas da Universidade de São Paulo (CITI-USP), for lending the instruments (VNA and Spectrum Analyzer) used.

Last but not least, my many thanks to the Porvas climber friends for supporting me in different ways during my journey as a Ph.D. student.

This work was partially supported by CAPES, which provided a scholarship by the PROEX program and by grants No. 313215/2017-0 from CNPq: National Council for Scientific and Technological Development.

"Lá no Sertão, quase ninguém tem estudo
Um ou outro que lá aprendeu ler
Mas tem homem capaz de fazer tudo, doutor
Que antecipa o que vai acontecer "
Oricuri (O Segredo do Sertanejo) - João do Vale

Resumo

A detecção precoce de um tumor na mama feminina proporciona uma taxa de cura próxima de cem por cento. A imagiologia médica empregando micro-ondas (ondas eletromagnéticas com faixa de frequência variando de 300 MHz a 30 GHz) é uma modalidade que tem sido investigada há mais de 30 anos. Nesta tese propôs-se a investigar os sistemas atuais que são capazes de gerar uma imagem a partir da interação das ondas eletromagnéticas com o tecido mamário e as células cancerígenas. Paralelamente, realizou-se um estudo dos equipamentos utilizados por tais sistemas para gerar e recuperar os sinais de micro-ondas que iluminam a mama. Dentre os que apresetam imagens clínicas, o *vector network analyzer* (VNA) é o mais utilizado. Porém, o *software-defined radio* (SDR) também é capaz de gerar e receber sinais de micro-ondas na faixa de frequência necessária para imagiologia médica, além de ser economicamente mais acessível, possibilitar o desenvolvimento de um sistema portátil e ser facilmente testável. A partir disso, a tese analisou a viabilidade técnica de uma placa de VNA chamada BladeRF 2.0, a fim de comprovar sua capacidade em termos de potência de transmissão e recepção dos sinais de micro-ondas. Os testes realizados empregaram antenas Vivaldi posicionadas frente a frente a 15.0 cm de distância entre elas e se diferenciaram pelo meio de propagação das micro-ondas. No primeiro cenário, considerou-se o ar como meio de propagação; enquanto no segundo, uma mama postíça que mimetizou os tecidos internos. Além disso, no primeiro cenário foram utilizados um VNA, que gerou sinais recebidos pelo SDR; e um analisador de espectro, que mediu os sinais gerados pelo SDR. Já no segundo cenário, o próprio SDR foi responsável por gerar e captar os sinais de micro-ondas. Os resultados mostraram que, com os sinais propagando-se pelo ar, a BladeRF 2.0 é capaz de transmitir uma potência de + 18,0 dBm em 1,0 GHz e próximo de + 10,0 dBm em 6.0 GHz; e captar um sinal de -80,0 dBm gerado pelo VNA e transmitido pela antena Vivaldi. Ressalta-se que foram acoplados ao SDR amplificadores de potência tanto no canal de transmissão quanto de recepção. Já no cenário considerando a mama postíça e apenas o SDR, esse apresenta uma relação de sinal-ruído de 52,0 dB para a faixa de frequência de 1,0 a 6,0 GHz. Com esses resultados, concluiu-se que o SDR atende às especificações quanto à potência dos sinais de micro-ondas para um sistema de imagiologia médica. Nesta tese também simulou-se e testou-se um pulso sintético de banda ultralarga a partir da modulação de onda contínua de frequência escalonada. O resultado dessa simulação comprovou sua operação, enquanto a programação do SDR não conseguiu eliminar o efeito de interferência ao transmitir e receber os sinais que compuseram o pulso sintético.

Palavras-chaves: Imagiologia médica. Micro-ondas. Detecção de câncer de mama. Rádio definido por software. Pulso sintético de banda ultralarga.

Abstract

Early detection of breast cancer by women provides a cure rate close to a hundred percent. Medical imaging based on microwave (electromagnetic wave with frequency range from 300 MHz to 30 GHz) is a modality that has been investigated for more than 30 years. This thesis proposed to research current systems that are capable of generating an image from the interaction of the microwave with breast tissue and cancer cells. At the same time, a study was carried out of the equipment used by such systems to generate and recover the signals that illuminate the breast. Among those presenting clinical images, the vector network analyzer (VNA) is the most used. However, the software-defined radio (SDR) is also capable of generating and receiving microwave signals in the frequency range necessary for medical imaging, in addition to being more economically accessible, enabling the development of a portable system, and being easily testable. From this, the thesis analyzed the technical viability of an SDR board known as BladeRF 2.0, in order to prove its capacity in terms of transmitting and receiving power of microwave signals. The tests used two Vivaldi antennas that were placed in line at a 15.0 cm distance between them, and differentiated by the microwave propagation media. In the first scenario, air was considered as the propagation medium; while in the second, a breast phantom that mimicked internal tissues. Furthermore, in the first scenario, an VNA was used, which generated signals received by the SDR; and a spectrum analyzer, which measured the signals generated by the SDR. In the second scenario, the SDR itself was responsible for generating and capturing the microwave signals. The results showed that, with the signals propagating through the air, BladeRF 2.0 is capable of transmitting a power of +18.0 dBm at 1.0 GHz and close to +10.0 dBm at 6.0 GHz; and capture a -80.0 dBm signal generated by the VNA and transmitted by the Vivaldi antenna. Note that the power amplifiers were coupled to the SDR in both the transmission and reception channels. In the scenario considering the breast phantom and only the SDR, this presents a signal-to-noise ratio of 52.0 dB for the frequency range from 1.0 to 6.0 GHz. With these results, it was concluded that the SDR meets the specifications regarding the power of microwave signals for a medical imaging system. This thesis also simulated and tested an ultra-wideband synthetic pulse from step-frequency continuous wave modulation. The result of this simulation proved its operation, while the SDR programming was unable to eliminate the interference effect when transmitting and receiving the signals that composed the synthetic pulse.

Key-words: Medical imaging. Microwave. Breast cancer detection. Software-defined radio. Ultra-wideband synthetic pulse.

List of Figures

Figure 1 – Simulated electric-field distributions applied over a zone with a target.	31
Figure 2 – Generic MwI screening system.	32
Figure 3 – Phantoms measured values: (a) relative permittivity and (b) conductivity.	41
Figure 4 – Testbench for simulations to extract propagation loss and signal penetration.	43
Figure 5 – Attenuation of transmitted signal from TX to RX over frequency for different breast tissue compositions.	43
Figure 6 – Microwave signal representation for MwI tomography.	45
Figure 7 – Target energy map using the improved confocal algorithm. The axes X and Y are in cm.	47
Figure 8 – Typical time domain system blocks.	50
Figure 9 – Time waveform and frequency domain SFCW signals.	52
Figure 10 – Typical frequency domain system blocks.	52
Figure 11 – Radio options: Analog, DSP, and SDR.	54
Figure 12 – Typical SDR blocks.	55
Figure 13 – Baseband signal - Time Domain.	57
Figure 14 – Transmitter SDR blocks.	58
Figure 15 – Receiver SDR blocks.	58
Figure 16 – Medical imaging technology evolutionary timeline.	62
Figure 17 – Photograph of the second-generation MwI prototype made up of a cylindrical array of 16 monopole sensors.	63
Figure 18 – Photography of the microwave electronic subsystem fully assembled.	64
Figure 19 – SAFE design in a clinical surrounding.	66
Figure 20 – MARIA M6 system block diagram.	68
Figure 21 – Photograph of the system composed of the table, one VNA, and cables.	69
Figure 22 – System prototype illustration and some equipment.	71
Figure 23 – Wearable prototype fitted to a volunteer.	72
Figure 24 – Photograph of the Wavelia device in a hospital.	73
Figure 25 – Results from different acquisition days.	74
Figure 26 – Photograph of the system prototype devices.	75
Figure 27 – Mammowave system apparatus.	76
Figure 28 – Architecture system diagram.	77
Figure 29 – USP System results.	78
Figure 30 – SDRadar proposed by Marimuthu.	79
Figure 31 – Architecture system diagram.	80
Figure 32 – BladeRF2.0 board. FX3-blue square, FPGA-yellow square, Transceiver-green square.	86

Figure 33 – Transceiver block diagram.	87
Figure 34 – Simulated radiation pattern of the Vivaldi antenna at 6.0 GHz.	88
Figure 35 – Picture of the employed vivaldi antenna.	89
Figure 36 – Simulation scenario with the breast phantom between TX and RX Vivaldi antennas.	89
Figure 37 – S_{21} (dB) x frequency curves considering the Vivaldi antennas and different propagation media.	90
Figure 38 – GNU radio blocks for BladeRF 2.0 RF communication.	91
Figure 39 – SNR of RF signal at: (a)1.0 GHz and (b)5.0 GHz.	91
Figure 40 – BladeRF 2.0 transmitting RF signal to SA-E4404B.	93
Figure 41 – BladeRF 2.0 receiving RF signal from VNA-ZVA24.	93
Figure 42 – BladeRF 2.0 coupled with the PA and LNA illuminating the breast phantom through the Vivaldi antennas.	94
Figure 43 – S_{21} (dB) x frequency of air link using two Vivaldi antennas.	95
Figure 44 – BladeRF 2.0 output power for different TX gains.	96
Figure 45 – Measured RF power vs. TX Carrier Frequency.	96
Figure 46 – Measured noise floor with RX carrier frequency varying from 1 GHz to 6 GHz.	97
Figure 47 – BladeRF 2.0 time (a) and frequency (b) responses to the transmitted -40 dBm VNA signal at 6.0 GHz.	98
Figure 48 – SNR plot related to BladeRF 2.0 transmission.	99
Figure 49 – SFCW applied signal (a), and its respective frequency response (b). . .	101
Figure 50 – CST setup of a bra model mimicking a breast.	102
Figure 51 – Calculated range profile of the SFCW collected signals from the simulated platform.	103
Figure 52 – C code sample developed aiming at SFCW radar implementation. . . .	104
Figure 53 – BladeRF 2.0 loopback measurement (Magnitude x Sample).	105

List of Tables

Table 1 – Imaging techniques summary for breast cancer detection	30
Table 2 – Mwl tomography systems review	62
Table 3 – Mwl radar-based systems review	67
Table 4 – Summary of Mwl requirements and SDR - VNA performance over the air.	100
Table 5 – Characteristics of the SFCW signal applied in the simulation setup . . .	101

List of abbreviations and acronyms

ABUS	Automated Breast Ultrasound System
ACS	American Cancer Society
ADS	Advanced Design System
ADC	Analog to Digital Converter
AGC	Automatic Gain Control
ASIC	Application Specific Integrated Circuit
BW	BandWidth
BI-RADS	Breast Imaging-Reporting and Data System
CSAR	Circular Synthetic Aperture Radar
CST	Simulia CST Studio suite
CW	Continuous Wave
CMOS	Complementary Metal-Oxide Semiconductor
Δf	Narrowband Tone
ΔR	Range Resolution
DAC	Digital to Analog Converter
DAS	Delay and Sum
DBT	Digital Breast Tomosynthesis
DSP	Digital Signal Processing
DMAS	Delay-Multiply And Sum
DUC	Digital Up Converter

DDC	Digital Down Converter
EM	Electromagnetic
FCC	Federal Communications Commission
FFT	Fast Fourier Transform
FPGA	Field Programmable Gate Array
FMCW	Frequency Modulated Continuous Wave
G_{tx}	Antenna Transmission Gain
G_{rx}	Antenna Reception Gain
GPP	General Purpose Processor
GPR	Ground Penetrating Radar
I	In-Phase
IC	Intergrated Circuit
IEEE	Institute of Electrical and Electronic Engineers
INCA	Instituto Nacional de Câncer
IF	Intermediate Frequency
IFFT	Inverse Fast Fourier Transform
LO	Local Oscillator
LNA	Low Noise Amplifier
MIR	Micropower Impulse Radar
MIST	Microwave Imaging via Space-Time
MRI	Magnetic Resonance Imaging
MwI	Microwave Imaging
PA	Power Amplifier
PET	Positron Emission Tomography
PRI	Pulse Repetition Interval
Q	In-Quadrature

RADAR	RADio Detection And Ranging
RF	Radio-Frequency
P_{RX}	Received Power
S_{11}	Return Loss
S_{21}	Propagation Loss
SAR	Specific Absorption Rate
SBM	Sociedade Brasileira de Mastologia
SDR	Software-Defined Radio
SUS	Sistema Único de Saúde
SFCW	Stepped Frequency Continuous Wave
SVM	Support Vector Machine
TSAR	Tissue Sensing Adaptive Radar
UWB	Ultra Wideband
VNA	Vector Network Analyzer
VCO	Voltage-Controlled Oscillator
WHO	World Health Organization

List of symbols

ω	Angular Frequency
α	Attenuation Constant
σ	Conductivity
ϵ^*	Complex Dielectric Constant
ϵ_s	Static Frequency Dielectric Constant
ϵ_∞	Infinite Frequency Dielectric Constant
ϵ	Dielectric Constant
μ	Permeability
ϵ	Permittivity
τ	Time Constant

Contents

1	INTRODUCTION	27
1.1	Context	27
1.2	Motivation	36
1.3	Objectives	36
1.4	Contributions	37
1.4.1	Monograph - PECE - USP	37
1.5	Thesis Organization	38
2	BACKGROUND AND DEFINITIONS	39
2.1	Woman breast	39
2.1.1	Breast classification	39
2.1.2	Breast and tumor dielectric properties	40
2.1.3	Signal propagation	42
2.2	Microwave Medical Imaging	44
2.2.1	Tomography Approach	45
2.2.2	Radar-Based approach	46
2.3	Radar Overview	47
2.3.1	Radar for Mwl	48
2.3.2	Radar Waveforms Classification	49
2.3.2.1	Pulsed Radar and Time Domain	49
2.3.2.2	Continuous Wave Radar and Frequency Domain	50
2.4	Synthetic Pulse	53
2.5	Software Defined Radio - SDR	53
2.5.1	SDR - Platform Overview	55
2.5.1.1	Host Interface	55
2.5.1.2	DSP Unit	55
2.5.1.3	RF - Analog blocks	56
2.5.2	Software Framework	59
2.6	Scattering parameter	59
2.7	Discussion	60
3	MICROWAVE IMAGING SYSTEMS	61
3.1	Tomography approach	62
3.1.1	Dartmouth College - USA	62
3.1.1.1	SDR-based system	64
3.1.2	McMaster University - CA	65

3.1.3	Istanbul Technical University - TR	65
3.2	Radar-based UWB approach	66
3.2.1	University of Bristol - ENG	67
3.2.2	University of Calgary - CA	69
3.2.3	McGill University - CA	70
3.2.4	Galway University - IE	73
3.2.5	Chalmers University of Technology - SE	74
3.2.5.1	SDR-based system	75
3.2.6	University of Perugia - IT	75
3.2.7	Hiroshima University - JP	76
3.2.8	University of São Paulo (USP) - BR	78
3.2.9	University of Queensland - AU	79
3.3	Combined approach	80
3.3.1	Politecnico di Torino - IT	80
3.4	Mwl system - Spin-off	81
3.5	Discussion	82
3.5.1	Apparatus	82
3.5.1.1	VNA based	82
3.5.1.2	IC based	83
3.5.1.3	SDR based	83
3.5.1.4	Antenna	83
3.5.2	Clinical Acceptance	84
	 4 SDR ASSESSMENT	 85
4.1	Nuand - BladeRF 2.0	86
4.1.1	Transceiver AD9361	87
4.2	Vivaldi Antennas	88
4.2.1	Simulation with Phantom	89
4.3	BladeRF 2.0 - First Steps Programming	90
4.4	Assessment Setup	92
4.4.1	Tests Procedure Over the Air	92
4.4.2	Tests Procedure Over the Breast Phantom	94
4.5	Power Measurements	94
4.5.1	Over the Air	94
4.5.1.1	Antennas S-parameter	94
4.5.1.2	Transmitted Power	95
4.5.1.3	Receiver - Noise Floor	97
4.5.1.4	Received Power	97
4.5.2	Over the Phantom	98
4.5.3	Discussion	99

4.6	Synthetic Pulse Simulation and Measurement	100
4.6.1	Simulation Setup	100
4.6.2	Simulation Results	102
4.6.3	BladeRF 2.0 Programming	104
4.6.4	BladeRF 2.0 operation	105
4.6.5	Discussion	106
	5 CONCLUSIONS AND SUGGESTIONS FOR FUTURE WORKS	107
5.1	Conclusions	107
5.2	Future works suggestion	109
	BIBLIOGRAPHY	111
	APPENDIX	127
	APPENDIX A – PUBLICATIONS DURING CANDIDATURE . . .	129
A.1	Thesis Related	129
A.1.1	First Author	129
A.1.2	Co-author	130
A.2	Not Thesis Related	130
	APPENDIX B – BLADERF 2.0 - SFCW C CODE	133

Chapter 1

Introduction

This chapter presents the context and underlying motivation of this Thesis. Breast screening modalities for tumor detection are described and compared, focusing on the microwave imaging approach. The objectives, original contributions, and paper publications along with the Thesis organization are outlined in the final section of this Chapter.

1.1 Context

The most precious thing in a person's life is its health, and hence its welfare. A relevant disease that has affected millions of people annually around the World is named cancer. More than 100 diseases could be diagnosed as cancer, having in common uncontrolled and disordered cell growth, which invades tissues and organs, resulting in a tumor, also known as neoplasm. Cancer is considered aggressive when it forms, grows, or spreads quickly into distant tissues or organs, ending in metastases. This is the patient's worst scenario for healing, once the long-term survival chances are reduced and the recovery process is much more demanding. Therefore, it is important to be especially cautious about some types of cancer, such as prostate for men and breast for women. Considering that cancer is an age-related disease, as mentioned by (WHITE et al., 2014), and the fact that more and more women live longer lives, it is crucial to pay greater attention to more preventive exams, thus more accurate or complementary medical imaging procedures. Screening, which refers to the process of tests and exams to find a disease in people who do not have symptoms, is paramount to the early detection of breast cancer. Thus, the more efficient it is, the better for health.

Currently, breast cancer is the most common and leading cause of death among women according to (GENTILINI; PARTRIDGE; PAGANI, 2020), with close to 8 million diagnoses in the last 5 years around the world. Breast cancer is also observed in men,

but it is low likely, just 1% of the cases which led to 207 deaths in 2020, according to (INCA, 2022). On the other side, in 2020 alone, 2.3 million women were diagnosed with this disease, reaching 685 thousand deaths worldwide (WHO, 2020). In the USA, in 2023, there will be an estimated 300 thousand new cases of invasive breast cancer diagnosed in women, representing close to 31% of female cancers according to (SIEGEL et al., 2023), which mentioned the remarkable outcomes of diagnoses and treatments in high-income countries. In Brazil, the Instituto Nacional de Câncer José Alencar Gomes da Silva (INCA) reported approximately 17 thousand deaths only in 2017 and had an estimated risk of 61,61 patients for each 100 thousand women from 2020 to 2022 (INCA, 2020). Moreover, (INCA, 2022) estimates 73,610 new cases of breast cancer in 2023, which means a risk of 41,89 cases for each 100 thousand women. Amazonas is the Brazilian state with the highest number of new cases estimated, drawing attention to low-income regions.

The 5-year survival rates for breast cancer are in great contrast between high-income countries, which exceed 90%, compared to 66% in India and 40% in South Africa (WHO, 2023). One reason for this outcome is the more frequent screening test performed by women, which reinforces the need to develop affordable and portable solutions to perform such an exam. Early detection of breast cancer and improved treatment have contributed to reduced mortality rates in recent decades, according to the American Cancer Society (ACS, 2019). In fact, mortality was reported to have reached its peak in the USA in 1989 and has since decreased by 43% due to earlier diagnosis (SIEGEL et al., 2023). (FDA, 2017) affirms that early detection may make chemotherapy unnecessary.

It is observed that if breast cancer is detected early when it is still localized (confined entirely to the organ of origin), the 5-year survival rate is 99%. If breast cancer is regional, that is, it has spread to nearby tissue, the 5-year survival rate decreases to 85%. When cancer is reported distant or invasive, which means that it has metastasized to distant tissues, the survival rate drops to only 27%, highlighting the importance of medical imaging for early diagnostics. Furthermore, this reduction in survival rate should motivate women to undergo the breast screening process. Hence, tumors found during screening exams are more likely to be smaller and still confined to the breast, i.e., localized. Ordinarily, it becomes an invasive type before signs have begun, increasing the mortality rate. The size of the tumor and the extent to which it has spread are some of the most important factors in predicting the prognosis of a woman with this disease; in addition to its location inside the breast, such as the most common ductal carcinoma, which originates in the milk duct. (ANDRADE, 2014) affirms that a breast tumor can be diagnosed as an initial or localized if its size is less than five centimeters, but it is important to mention that size is only one of several characteristics of the tumor that is analyzed during the screening.

As mentioned above, identifying a tumor involves different analyses and is also

impacted by the tumor position in the breast and its type. Furthermore, breast density has a great impact on tumor identification. Any screening procedure has limitations, regardless of the imaging modality. Thus, there are two metrics that relate to the target correct identification: Sensitivity, which is defined by the number of correct tumor detections versus the number of those missed, is also known as the true positive rate; Specificity, which is the proportion of patients correctly identified as cancer-free when, in fact, they do not have a tumor, is also called the true negative rate (PORTER; O'LOUGHLIN, 2022).

Breast density is frequently classified by BI-RADS ®(Breast Imaging-Reporting and Data System), a factor proportional to the size and number of lactiferous lobules that directly affects the interpretation of imaging exams. This characteristic is determined by genetic factors and is influenced by age, weight, pregnancy, lactation, medications, and breast diseases (D'ORSI et al., 2013).

Currently, different breast cancer detection modalities are available in addition to manual palpation, mammography being the gold standard exam used for medical diagnosis around the world (IRANMAKANI et al., 2020). It is the most common imaging modality due to its high image resolution, the ability to detect microcalcifications, and the affordable procedure that results from the waves of process innovation and the adoption of hospitals. This exam is based on the patient's low energy X-ray exposition (estimated as 20 - 30 keV) while the breast is compressed. The work (MOLONEY et al., 2020) also refers to mammography as the main procedure for detecting a breast tumor, but also discusses Digital Breast Tomosynthesis (DBT), which is an advance in mammography technology, enabling multiple tomographic images to be obtained in any conventional mammographic view, creating a "semi-3D" mammogram. This technique is not indicated for young women or women with dense breasts. Its sensitivity is about 62% in women aged 40 to 49 years, while it varies from 68 to 90% in the breast tissue of women 50 years of age.

Ultrasound appears to be a radiation-free and more inexpensive solution and is currently used in addition to mammography. It is not capable of detecting microcalcifications and has limited spatial resolution, but improves overall sensitivity and specificity. The sensitivity and specificity of ultrasound can reach, respectively, 76% and 84% according to (CHEN et al., 2021). The operator's experience counts during examination, affecting the reproducibility, which is low compared to mammography. The Automated Breast Ultrasound System (ABUS) overcomes handheld ultrasound, reducing operator error-prone dependency and increasing reproducibility, therefore the cancer detection rate, according to (HEJDUK et al., 2022).

Magnetic Resonance Imaging (MRI) and Positron Emission Tomography (PET) are considered high-cost and time-consuming exams, which are associated with low availability for large-scale populations. Therefore, they are recommended for the investigation of breast cancer in younger women with dense breasts and in patients with tumors already detected

by other techniques to characterize a lesion or some undetected carcinoma. (HADEBE et al., 2023) mentioned the use of PET for patients with advanced tumor stage, which showed a sensitivity and specificity that reached 96% and 100%, respectively, depending on the size of the tumor and its histological subtype. Overall, those modalities are very precise and harmless, besides the PET radiation exposure. A drawback of the MRI procedure for breast cancer is its high incidence of false positive results, which causes stress and unnecessary biopsies.

Table 1 summarizes the consolidated medical imaging modalities for breast cancer detection based on the results reported in (IRANMAKANI et al., 2020; WANG, 2017). The sensitivity and specificity values for a specific patient could be increased by combining different modalities.

Table 1 – Imaging techniques summary for breast cancer detection

Imaging Modality	Sensitivity	Specificity	Main Benefits	Main Penalties
Mammography	62% - 90%	82% - 97%	Low cost and high resolution	Ionizing radiation breast compression
Ultrasound	76%	84%	Low cost and accuracy	Spatial resolution operator dependence
MRI	95%	26.4%	Harmless exam high sensitivity	High false positive incidence
PET	96%	99%	High accuracy	High cost and radiation exposure

Recently, a bioimpedance-based apparatus for breast cancer screening has shown impressive results, as reported in (OLAOGUN; AGODIRIN, 2022; MANGO et al., 2022). It is called iBreastExamTM, which is a 5 V battery-powered device, comprised of a handheld compression probe of an array of piezoelectric fingers (CLANAHAN et al., 2020). Its working principle is based on the interactions of low current values passing throughout the breast and affected by a tumor if present.

Each of these modalities has its potential and shortcomings, but none with a full confidence prognosis for a challenging problem such as early detection of breast cancer. Moreover, most of them are cumbersome devices that hinder portability to remote areas or low-income regions. Meanwhile, as engineering is always looking for improvements in people's quality of life, some new approaches have been explored for medical imaging screening. Microwave Imaging (MwI) is a visionary way of using engineering to screen for people's health issues, such as a tumor, in a harmless, secure, and painless way, relying on devices that are easy to set up or even portable. The concept of MwI has been consolidated after almost half a century, but the apparatus to realize such a system is still continuously evolving (FEAR et al., 2002). In addition, many methods for imaging reconstruction have been proposed (REIMER; PISTORIUS, 2023).

MwI is based on the interaction of a non-ionizing electromagnetic (EM) wave at microwave frequencies, typically from a few hundred megahertz (MHz) to gigahertz (GHz), as mentioned by (VORST; ROSEN; KOTSUKA, 2005). The waves are radiated over a body part, e.g. a woman's breast, and the scattered or backscattered signals are acquired. The application and acquisition of the signal are made through antennas, which may act as both transmitter and receiver (i.e., monostatic) or as different antennas for each task (i.e., multistatic). Depending on the dielectric properties of the illuminated body part, medical imaging is generated from the processing of the signals received. According to (SASAKI et al., 2022), conductivity (σ) [S/m] and permittivity (ϵ) [F/m] are the most common physical quantities to represent a tissue dielectric response.

(PAULSEN; MEANEY; GILMAN, 2005) has simulated a two-dimensional EM wave being applied in a zone composed of two different dielectric properties (light area with a dashed border), illuminating it from four different placements, as shown in Figure 1. It is possible to see a significant field variation inside the light area. An image could be created in which a buried target could be revealed by processing the portion of the scattered EM wave collected at the receiving antenna. This is possible because the zone compositions are distinguished in terms of their dielectric properties, resulting in different scattering powers.

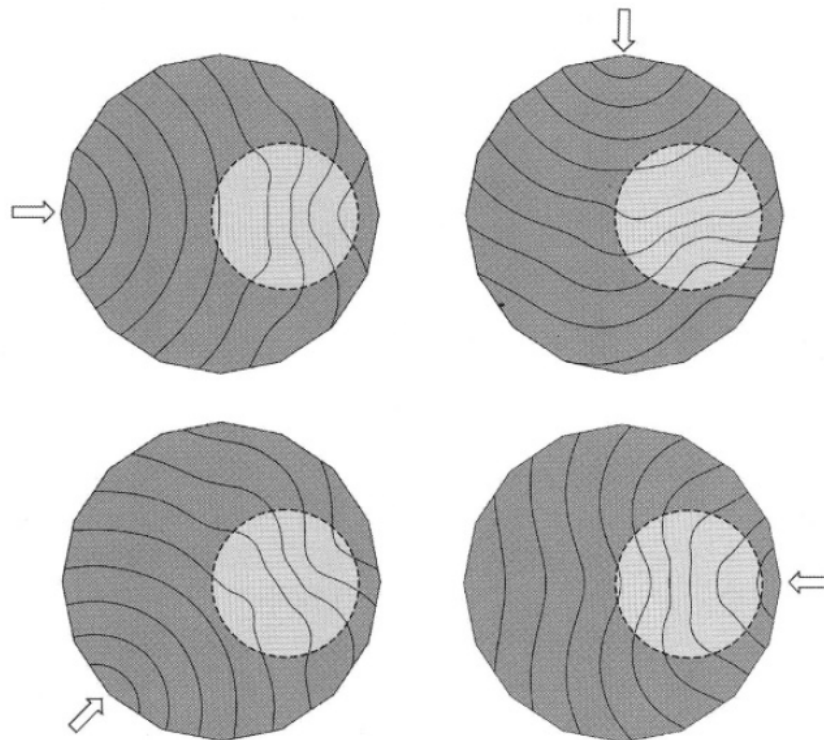


Figure 1 – Simulated electric-field distributions applied over a zone with a target. Source: (PAULSEN; MEANEY; GILMAN, 2005).

This Thesis will analyze the use of MwI in breast screening for early breast cancer detection. This application of MwI has received significant interest over the past decade

(FANG, 2004) and MwI systems have emerged as a new complementary alternative to medical imaging, with several systems reported over the past years, such as (SHERE et al., 2019) and (FASOULA et al., 2018), as non-portable solutions; (ISLAM et al., 2019) as a portable system. All the aforementioned systems were implemented using the Vector Network Analyzer (VNA), which is large and expensive. Also, (SONG et al., 2017) reported a handheld impulse radar detector system that uses only Complementary Metal-Oxide-Semiconductor (CMOS) circuits, but is still not low-cost. Moreover, the Ph.D. Thesis (ARAGÃO, 2021) proposes an affordable and portable radar-based system employing a commercial platform, which reveals promising results.

Looking for to circumvent the VNA usage and concerning portable and low-cost MwI systems, Software-Defined Radio (SDR) has been seen as a technological breakthrough and is the apparatus to be explored and assessed in this Thesis aimed at the realization of frequency-domain systems.

Based on the numerous systems mentioned, it is possible to say that there is no consensus for the best implementation of the MwI system, which motivates researchers to seek this answer. Notwithstanding, Figure 2 illustrates a generic system for MwI, separated into four main parts or concerns, which are further described and some of the challenges raised.

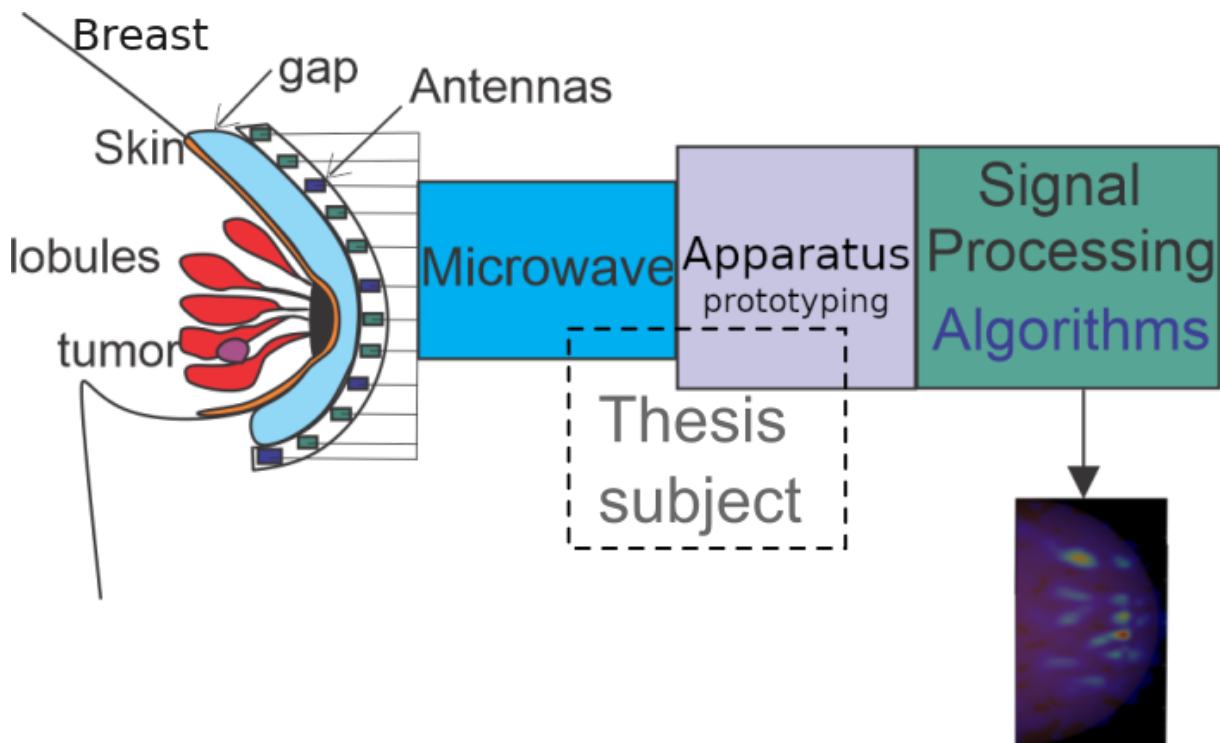


Figure 2 – Generic MwI screening system.

This Thesis can be fitted among the microwave and apparatus concerns that is related how the EM signal is generated and recovered. Besides that, each part is further described and itemized following.

- Breast Features
 - **Heterogeneous breast:** The breast is composed mainly of adipose tissue, with a difference in dielectric properties, i.e. contrast, between normal and malignant breast tissue close to 10 times. However, when considering a heterogeneous breast, with ducts, adipose and fibro-glandular tissues, the difference is much smaller (approximately 10%), as mentioned by (LAZEBNIK et al., 2007);
 - **Dielectric *in vivo* properties:** Most studies suppose a constant breast behavior or dielectric value as normal, once they consider an *ex vivo* or a phantom. However, it is not true for an *in vivo* breast, which deserves concerns about exposure time, temperature, and patient age, as presented by (SANCHEZ-BAYUELA et al., 2022);
 - **Skin impact:** Wherever a microwave pulse in the low gigahertz range radiates the breast, the skin (ε around 30 and σ about 3 S/m) acts as a shield and a strong signal is reflected. This artifact is typically several orders of magnitude greater than the reflections of any tumor present within the breast. If it is not effectively removed, it could easily mask the tumor’s presence;
 - **Phantom:** It is quite complicated to emulate the proper breast features to perform experiments. However, it is crucial to develop a phantom to apply and catch microwave signals;
 - **Patient motion:** The MwI procedure must consider the patient’s motion due to the movement of the breast during breathing, affecting the quality of the image. The patient-prone position is the most indicated to overcome it, used by most of the proposed systems.
 - **Size:** Breast size is considered an important factor for MwI, once its impact the deepest a RF signal must go, and also the system cavity that fits a breast.
- Microwave
 - **Antenna configuration:** The antenna design, type (wide-slot, antipodal Vivaldi, etc.), the array arrangement, or its number definition, is not well established, varying from 1 to 60 antennas, impacting the system cross-range resolution and portability. It is worth mentioning that systems with few antennas use the synthetic array technique;

- **Antenna coupling:** As signal artifacts, antenna coupling must be considered and processed in the same way as skin impact, once it can cause a tumor to be missed;
 - **Calibration:** Some works indicate further research on effective calibration methods of the measured data. Most qualitative systems require calibration to measurement accuracy;
 - **Microwave switch:** In an array arrangement with multiple antennas, a microwave switch is required. As a VNA has limited interfaces, all the systems that use it have implemented a switch. The same is true for advanced SDR-based systems;
 - **Gap between breast and antennas:** A challenge to overcome is the gap between the antennas and the breast, where "coupling liquids" have been employed. Some systems use a mixture of glycerin and water, whereas other systems settle the antenna in contact with the breast;
 - **Penetration:** Even if the microwave power penetrates successfully beyond the skin, several centimeters of tissue along the propagation path suffice to attenuate a 10-GHz signal by more than 80 dB;
 - **Operating frequency:** It is known that the signal penetration increases at lower frequencies. However, the resolution increases at higher frequencies. To overcome this tradeoff, it is important to define the pulse bandwidth that matches the requirements of the system, if the millimetric tumor size is the target;
 - **Power limits:** The application of the microwave signal (illumination) must be in agreement with the power levels of the Federal Communications Commission. Besides, the Specific Absorption Rate (SAR) or the amount of power to be absorbed in the tissue per volume must be carefully considered, which is related to the breast layers. According to (BHARGAVA; RATTANADECHO, 2022), a women aged 51 has maximum value of SAR around 0.59 W/kg in skin, 2.46 W/kg in tumor, and 2.60 W/kg in fat.
 - **Sensitivity:** The weakest signal that can be detected successfully against the background of measurement noise and uncertainties is known as sensitivity. The MwI requires high sensitivity values (larger than 60 dB), making this system more difficult to design.
- Apparatus - Prototyping
 - **System specification:** Several systems have been proposed to perform the MwI. The common approach is to use a VNA to handle the generation and processing of microwave signals. The specifications of each system are generally

not revealed. The system specification is required as input for Integrated Circuit (IC) block implementation;

- **IC Design:** Some IC blocks are recognized as primordial in some circuit topologies, such as Low Noise Amplifier (LNA), Analog to Digital Converter (ADC), Digital to Analog Converter (DAC), Power Amplifier (PA), among others. It is a challenge to design each one. The CMOS IC is developed as an option to replace large and expensive equipment, such as VNA.
 - **Manufacturing:** The IC manufacturing process is challenge and expensive during the prototype stage. The Non-Recurring Engineering is a cost that must be consider for any design, along with the packaging for first level interconnection;
 - **Tests:** To validate any proposed solution and IC blocks, tests and characterizations must be performed. Thus, IC fabrication, test board development along with test benches are necessary that make the design of the MwI system even more complicated.
- Signal Processing
 - **Imaging generation:** Reconstruction algorithms are related to the MwI approach, whether tomography or the confocal imaging method. As mentioned, the tomographic approach is more computationally demanding;
 - **Artifacts suppression:** Several algorithms have been developed for artifacts removal, which are mainly caused by the higher dielectric skin property or artifacts across antenna channels (MEHRANPOUR et al., 2020);
 - **Validation:** To validate an algorithm, it is important to emulate the system and obtain a signal that could be processed in Matlab, for example;
 - **Classification:** Imaging classification is the last step for any MwI. Even mammography has devoted efforts to classification algorithms that could confirm the presence of a tumor. Some works have proposed the usage of Machine learning as Support Vector Machine (SVM) learning classification for breast cancer biopsy.

All of these challenges could be seen as obstacles to finally delivering a system for MwI, along with the physicians' reluctance to adopt disruptive technologies. This Thesis addresses the challenge of defining the hardware apparatus used for signal generation and reception, showing the SDR usage potential and drawbacks.

1.2 Motivation

The public Brazilian health care system, known as SUS (Sistema Único de Saúde), encourages women between 50 - 69 years old to take the mammography screening exam every two years. However, a report by the Sociedade Brasileira de Mastologia (SBM) reveals great concern, where of the 11.5 million mammograms that should have been performed in 2017, only 24,1% or 2.7 million were executed (SBM, 2018). On the one hand, mammography is the most common exam, and on the other hand, it is harmful, incurring a small risk of having a tumor induced by the ionizing properties of radiation; uncomfortable and painful, which discourages periodic examination, as mentioned.

Meanwhile, pioneer comparison (WÖRTGE et al., 2018), which presents a prototype MwI system composed of two bowtie antennas and a VNA, has endorsed the feasibility of MwI screening, identifying tumors of each patient. Recently, many more groups and even startups have focused on MwI for breast cancer, as will be discussed further.

The possibility of a deep, harmless and affordable screening method is a great motivation for this research, which investigates an SDR-based system to realize a MwI for breast cancer early detection. The relatively inexpensive and compact apparatus compared to VNA, the non-ionizing radiation, and the relatively good penetration make microwaves appealing in medical diagnosis breast cancer screening alternatives.

In the whole World, all attempts to develop a system for the detection of breast cancer using MwI have started in universities and very few startups. Brazil has few steps into this field, so, it is intended to make this system real also here.

Integration into the research group at the Laboratório de Sistemas Integráveis (LSI) of the University of São Paulo (USP) is also an unmissable opportunity for the development of my knowledge and skills.

1.3 Objectives

This work aims to contribute to the definition and assessment of an SDR-based system capable of performing the screening using microwaves to detect any abnormality in a woman's breast. The objectives of this work could be summarized as follows:

- To investigate a system able of performing breast screening based on microwave signals;
- To assess an SDR that could be used as an apparatus dealing with microwave signals;

- To perform simulations relating microwave signals and a healthy and unhealthy woman's breast;
- To acquire a strong understanding of RF concepts such as impedance matching, passive circuits, noise, linearity, bandwidth, and stability.

1.4 Contributions

The Ph.D. candidate has contributed in the apparatus definition, which copes with the EM signals, for a MwI system. The methodology for an SDR assessment is demonstrated in this Thesis along with a synthetic pulse realization.

The specific contributions are within the following areas:

- Reviewing the modalities for breast cancer screening, focusing on new approaches;
- Microwave Imaging current systems review, which had driven some choices of this work and others inside the LSI group;
- SDR employment for the MwI, demonstrating its large potential in the health realm;
- Provide a methodology to assess an SDR;
- Synthetic Pulse simulation and working principle demonstration.

It is important to mention that this Ph.D. research has generated several publications in congresses and journals, four of them as the main author and another five as coauthor. Published papers are listed in Appendix A.

1.4.1 Monograph - PECE - USP

Moreover, this research also contributes to a monograph entitled "Business model for a breast cancer detector design based on microwave signals". The Ph.D. candidate coursed a Master Business Administration (MBA) program from 2019 until 2021 in Management and Engineering of Products and Services at Programa de Educação Continuada da Poli (PECE) - USP.

The MBA focused on the development of a new hypothetical product, which is a MwI system, highlighting its development, business model, production chain, and consumption cycle, among others.

1.5 Thesis Organization

This Thesis is divided into five chapters. The first one has presented the context, motivations, objectives, and contributions derivated from this Thesis. Additionally, a discussion of medical imaging modalities for breast cancer detection was conducted.

The second chapter is related to the background knowledge and definitions of dielectric properties of the breast and a tumor, emphasizing EM propagation lossy simulation results; microwave medical imaging approaches, highlighting the generated confocal algorithm image in a radar approach; radar overview and waveforms, distinguishing the time and frequency radar domain; the synthetic pulse concept and steps; the SDR overview, blocks, and frameworks; and scattering parameter or S-Paramater.

Chapter three provides a comprehensive review of the state of the art MwI systems available, showing the different apparatuses to realize them, which includes the SDR device. Potential commercial systems are described along with the clinical acceptance of MwI, which has lasted longer than all other modalities. This chapter concludes with a discussion of the apparatus choices for implementing a MwI system.

Chapter four presents the evaluation methodology and results of the SDR employed, which reveals its ability to deal with the power requirements of EM signals but shows its challenge to implement a radar system. A VNA and Spectral Analyzes were used in the assessment. Moreover, a simulation aimed at synthetic pulse validation will be presented.

Finally, chapter five concludes the Thesis with suggestions for future work.

Chapter 2

Background and Definitions

This Thesis refers to a complex system able to detect and identify an abnormality such as a tumor in a woman's breast employing Radio Frequency (RF) signals. It is based on the dielectric properties of human tissues and on the processing of EM waves in the microwave frequency range. Thus, the chapter starts introducing the dielectric properties of healthy breast tissues and a tumor at the microwave frequency. The EM wave propagation lossy is also discussed, where the simulated results from Advanced Design System (ADS) concerning signal attenuation are shown. The ADS provides an integrated design environment to designers of RF systems.

Moreover, this chapter addresses the topics concerning the challenges and implementation not only of a microwave medical imaging system but also of the radar and the SDR, substantiating each specification that will be used in this work and related published papers. It concludes with a brief discussion of the main concerns and issues.

2.1 Woman breast

2.1.1 Breast classification

During a woman's lifetime, the breast undergoes different stages or BI-RADS classification according to her age or body weight condition (body mass index); the fibroglandular tissues of a younger woman are replaced by fat during the menopause period. Therefore, the breast of a younger woman tends to be firmer and denser than the breasts of older women. However, if a woman takes hormone therapy to relieve signs and symptoms of menopause, the breasts are likely to become denser. Furthermore, women with less body fat are more likely to have more dense breast tissue compared to women who are obese.

The BI-RADS categories for breast density use letters A to D, in place of numbers, to avoid confusion with the BI-RADS abnormality classification (TICE; KERLIKOWSKE, 2016), and categorize breast in the following way:

- A - The breasts are almost entirely fatty,
- B - There are scattered areas of fibroglandular density,
- C - The breasts are heterogeneously dense, which may obscure small masses,
- D - The breasts are extremely dense, which lowers the sensitivity of mammography.

2.1.2 Breast and tumor dielectric properties

Microwave breast imaging is achievable due to the contrast in dielectric properties between malignant and healthy breast tissues, leading to a frequency dispersion of the transmitted microwave signals. (LAZEBNIK et al., 2007) depicted that the relative permittivity of healthy tissues varied between $4 \leq \epsilon_r \leq 51$ for a 3.0 GHz RF signal applied, whereas tumor tissues varied between $50 \leq \epsilon_r \leq 58$ at the same frequency. Moreover, cancerous tumors can present a dielectric constant almost thirteen times higher than the breast adipose region, and the conductivity difference can reach magnitudes seven to nine times larger, leading to stronger backscattering signals. The aforementioned disparity does not reach the same proportion in regions near the skin, pectoral muscle, and glandular lobes. According to (BENNY; ANJIT; MYTHILI, 2020), the higher water content in malignant tumors causes those differences in the values of the dielectric constant. This work also mentions several studies on dielectric quantification and reinforces the MwI viability for tumor detection based on microwave interaction.

The differences in dielectric parameters affect an EM signal radiated over the breast, which affects its loss and velocity throughout the breast. Taking into account the woman's life stage, it is easier to detect a tumor in older ones or with a BI-RADS A classification. This is because the fatty tissues show lower permittivity and conductivity compared to a tumor in a great proportion, resulting in stronger reflections of the RF signals. On the contrary, tumor identification is harder in younger ones or those with breast classification BI-RADS D. This fact is also true for the mammography imaging modality, because a high breast density reduces its sensitivity and specificity (TICE; KERLIKOWSKE, 2016).

Moreover, physiological conditions such as body water percentage or temperature can affect the dielectric properties of the medium, making tumor identification more difficult. (FERNANDEZ-ARANZAMENDI et al., 2022) clarifies that the environmental conditions also impact the measurement results. All these scenarios, such as the age of the woman, the composition of the breast, the size of the tumor, etc., contribute to different investigations and implementations of the MwI system.

Nonetheless, the breast skin acts as a shield to microwave signals due to its higher dielectric properties, reflecting a strong signal back to the receiver, typically several orders of magnitude greater than the reflections from any tumor present in the inner breast. Different characterizations of skin phantoms have been investigated in depth at (KRANOLD et al., 2021), highlighting the importance of reliable tissue mimicking materials. The signal processing to deal with the skin effect is called artifact removal by (FELICIO et al., 2019), which reinforces that if it is not effectively removed, the strong reflection could easily mask the presence of tumors. Moreover, most systems have used some coupling medium to minimize the reflection difference from the breast skin, thereby reducing the propagation loss to ensure the proper system dynamic range.

The dielectric properties of the breast were further analyzed in (NIKOLOVA, 2011), which have carried out experiments with phantoms in the frequency range of 3.0 - 11.0 GHz, as shown in Figure 3. It is possible to observe that above the frequency of ≈ 7.0 GHz the relative permittivity value of the malignant tissue becomes smaller than the fibroglandular one, which affects the reflections of the EM signals. Also, it is shown that the malignant conductivity is greater than the other tissues for the whole frequency range.

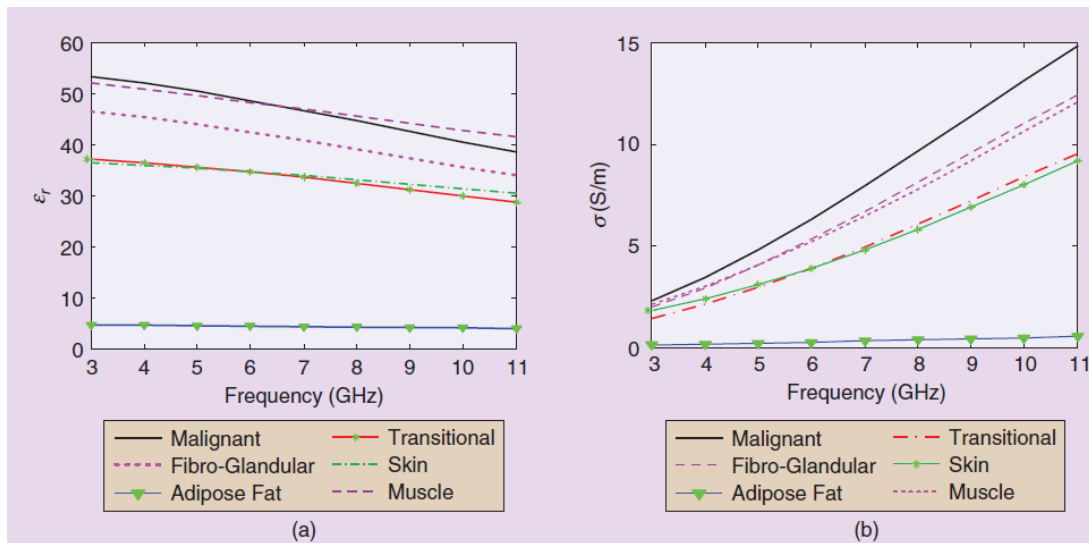


Figure 3 – Phantoms measured values: (a) relative permittivity and (b) conductivity. Source: (NIKOLOVA, 2011).

Breast tumors are most likely to originate in fibroglandular tissues, as described by (BOYD et al., 2010), in which the dielectric properties between them are closer (tumor and fibroglandular tissue) compared to fat tissue (tumor and fat tissue). It makes tumor identification harder and more challenging, especially if its size is on a millimetric scale with the aim of early detection. Nonetheless, it is important to mention that the low contrast between malignant and healthy fibroglandular tissue is not a deterrent for research toward the MwI system, once several different groups have shown practical results. Even X-Ray mammography, considered the gold standard of breast cancer diagnostics, works

with contrasts as low as 4–10%, as reported by (NIKOLOVA, 2011), which reduces its ability to detect a tumor in a dense breast.

A major challenge to be overcome by microwave imaging is the fact that the EM wave may pass through different materials "layers" with different dielectric properties, such as antennas, air or coupling liquid, skin, adipose tissue, glandular tissue, and tumor, which produces a different intensity of the echoes that must be properly treated considering the wave propagation lossy in a medium.

2.1.3 Signal propagation

The propagation of EM signals in a specific medium is governed by Maxwell's equations and the medium's dielectric properties (NGUYEN; PARK, 2016), implying an amount of loss due to non-zero conductivity of any practical medium, known as dielectric loss. Since the woman's breast can be modeled as a dispersive medium for EM waves, the signal is highly attenuated at high frequencies (HIPPEL, 1995).

Propagation or dispersive models have been used to solve Maxwell's equations for the problem of EM waves propagating in the breast. Equation 1 is one of them used to solve the attenuation in a lossy medium as a function of the dielectric constant and conductivity.

$$\alpha = \omega \sqrt{\frac{\mu\epsilon}{2} \left(\sqrt{1 + \left(\frac{\sigma}{\omega\epsilon}\right)^2} - 1 \right)} \quad (1)$$

where α is the attenuation constant, ω is the angular frequency, μ is the permeability, ϵ is the dielectric constant, and σ is the conductivity of the medium.

Cole-Cole or Debye relaxation models are also used to model the dielectric characteristics of the breast over frequency, and are summarized by equations 2 and 3, respectively.

$$\varepsilon^*(\omega) = \varepsilon_\infty + \frac{\varepsilon_s - \varepsilon_\infty}{1 + (i\omega\tau)^{1-\alpha}} \quad (2)$$

$$\varepsilon^*(\omega) = \varepsilon_\infty + \frac{\varepsilon_s - \varepsilon_\infty}{1 + (i\omega\tau)} \quad (3)$$

where ε^* is the complex dielectric constant, ε_s and ε_∞ are the static and infinite frequency dielectric constants and τ is the time constant. Note that the Cole-Cole equation tends to the Debye equation when α tends to zero.

The loss of EM wave propagation reduces its transmitting power and hence the maximum penetration in a breast, also considering its return path for a MwI implementation. To better understand this issue, the work (BRITO; CARVALHO; NOIJE, 2020) has modeled the propagation loss in the ADS, where the transmission block was

responsible for generating the configured inputs of the system, such as a continuous wave transmitter whose output power value P_{TX} was kept constant while the transmitted frequency TX has been increased from 1.0 to 10.0 GHz.

Figure 4 correspond to the testbench, using ADS library components, that simulate an EM wave propagation throughout different media to extract its attenuation.

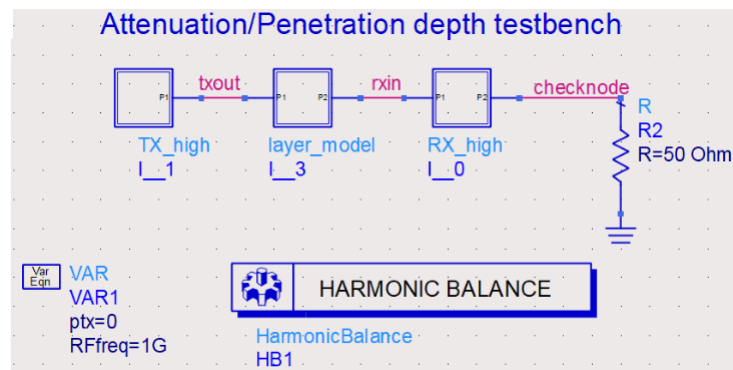


Figure 4 – Testbench for simulations to extract propagation loss and signal penetration. Source: (BRITO; CARVALHO; NOIJE, 2020).

Figure 5 presents the ADS results from different compositions of heterogeneous breast tissues using the ADS library *Layer_model*, in which equations 1 and 3 with parameters from (ZASTROW et al., 2008) was used considering a distance of 1.0 cm between *txout* and *rxin* (Figure 4). Therefore, the power received (P_{RX}) is directly related to attenuation in a 1.0 cm layer of breast tissue.

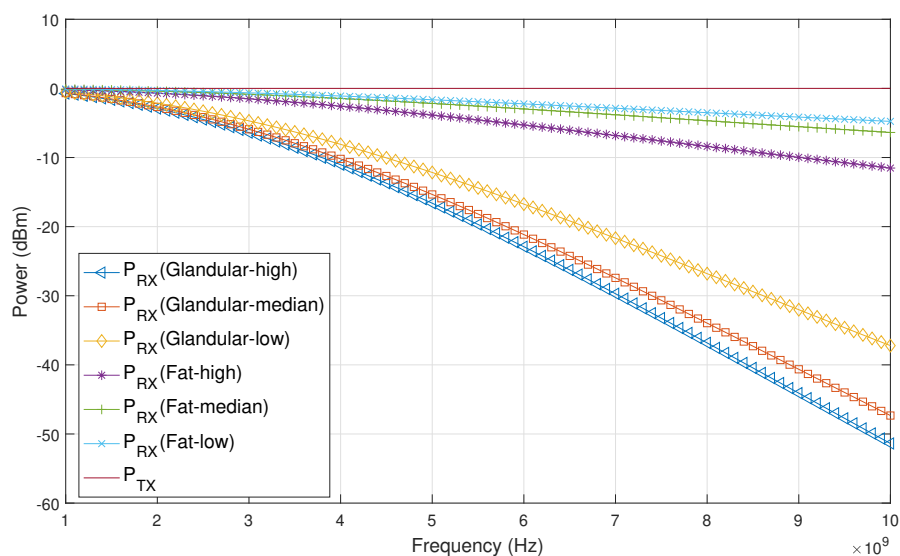


Figure 5 – Attenuation of transmitted signal from TX to RX over frequency for different breast tissue compositions. Source: (BRITO; CARVALHO; NOIJE, 2020).

This simulation illustrates that as the signal frequencies increase, so does its attenuation in a MwI system. Moreover, the different attenuation related to different tissues are depicted. Indeed, this result has been used as input to limit the frequency range in the measurements performed shown in Chapter 4.

2.2 Microwave Medical Imaging

Medical imaging techniques are widely used for the diagnosis of inner structures of tissues, organs, or body members to detect abnormalities. In general, it employs well-established methods, such as ultrasound, X-rays, MRI, and PET scan. MwI has emerged as a potential technique, offering a low-cost complementary option with a low or even zero health risk to a disease screening.

As mentioned in (KOSMAS; CROCCO, 2019), the utilization of microwave technologies in medical imaging and diagnostics is already a reality for the EM engineering community. The interaction of EM fields (e.g. Microwave) with tissues follows three basic mechanisms, as explained by (PAULSEN; MEANEY; GILMAN, 2005):

- displacement of conduction electrons and ions in tissue as a result of the force exerted on them by the applied EM field;
- polarization of atoms and molecules to produce dipoles;
- orientation of permanent dipole molecules in the direction of the applied field.

In response to an applied field, a current is created within the tissue based on its intrinsic electrical conductivity. The current is proportional to the number of free electrons and ions (ionized molecules), which is higher for invasive cancer than for the other tissues in a breast because of the increased volume of water within cancerous tissue. The degree to which it can be polarized, either by creating new dipoles or by co-orientation of permanent dipole molecules, is a measure of its permittivity. Thus, whenever a breast is illuminated by microwave signals, a tumor presence could be identified as a higher energy signal response compared to the original transmitted.

According to (CONCEIÇÃO; MOHR; O'HALLORAN, 2016), the two main approaches historically used for MwI are the Inverse Scattering, e.g. Tomography; and Radar-Based Ultra-WideBand (UWB). Both rely on the application of an EM wave, thus being considered as active imaging methods, and on the dielectric properties of the breast and of the tumor. Image reconstruction algorithms have been developed for different groups and are considered a critical challenge; once a good image is invaluable for finding any signal divergence.

2.2.1 Tomography Approach

MwI tomography is a quantitative analysis that aims to recover the illuminated organ dielectric profile by solving an inverse scattering problem, for which *a priori* information is usually needed (KWON; LEE, 2016). According to (NIKOLOVA, 2017), when linearizing approximations such as Born's and Rytov's cannot be applied, gradient-based non-linear optimization is used to solve the inverse scattering problem. Basically, the breast is illuminated from multiple angles and the collected data is used to reconstruct a cross-sectional image (slice) solving a nonlinear inverse problem, thus creating a breast map of its conductivity and permittivity. In most cases, the algorithms to solve this ill-posed problem (more than one solution satisfies the equation) are based on the iterative Gauss-Newton scheme. Nonetheless, the Jacobian matrix is commonly used to reconstruct the desired image in the iterative reconstruction process (MEANEY; GEIMER; PAULSEN, 2018).

Figure 6 illustrates a possible arrangement for MwI tomography, as seen in (LUI; FHAGER; PERSSON, 2012) but with different antennas setup. It operates by applying electromagnetic waves as narrowband signals (whose bandwidth is much smaller than their carrier frequency), from one antenna (the blue one) and receiving the scattered signals from all activated antenna elements, three antennas (green).

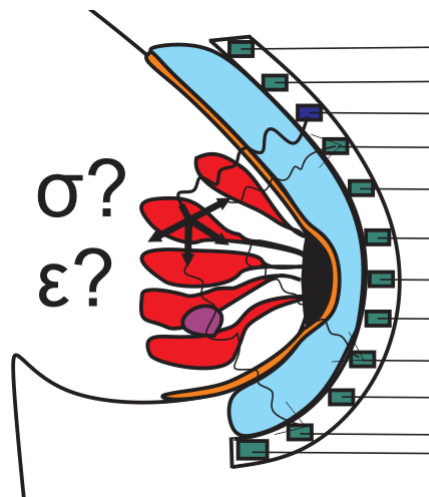


Figure 6 – Microwave signal representation for MwI tomography.

If the antenna operates as bistatic, it is possible to swap the role from transmitter to receiver, thus, views of the illuminated breast from different angles can be obtained. Otherwise, the whole system must rotate in order to get different signals collected from the breast, thus determining its unknown dielectric profile based on these measured projections, as described in (FEAR et al., 2013).

This approach was used in the first MwI system prototype fabricated in 1995 by

Dartmouth College (FANG, 2004). This laboratory-scale prototype operates from 300 MHz to 1.1 GHz frequency with a four-detector monopole antenna array for the receivers. Its features and evolution to the second generation are better described in Section 3.1.1.

The Ph.D. Thesis (MEYER, 2005) discusses the three tomography methods: reflection, diffraction, and iterative. According to this Thesis, reflection tomography imaging analyzes the relationship between the wave reflection coefficient and its dielectric profile, which is based on the solution of the inverse Ricatti nonlinear differential equation; diffraction tomography employs an approximation of the Radon inverse transform: the Fourier diffraction theorem; iterative method is based on the solution of Green's equation, where the same procedure is applied for diffraction tomography and iteration searches for a minimum error function between the calculated result and the received signal. Moreover, such a Thesis concluded that a successful microwave imaging system will incorporate the use of multi-frequency information through the use of many transmitter and receiver positions.

2.2.2 Radar-Based approach

The conception of medical imaging using UWB radar emerged in 1993 with Thomas McEwan, who developed a system named Micropower Impulse Radar(MIR), especially for remote monitoring of vital signs (S. D'Amico et al., 2010). However, for breast cancer detection, this approach was started in 1998 with (HAGNESS; TAFLOVE; BRIDGES, 1998).

MwI radar-based UWB, also known as microwave beamforming, depends on the application of microwave signals that aims at reconstructing the target "energy map", i.e. the position of the strong backscattered signal from the illuminated organ, such as a woman's breast. Based on the non-uniformity of the dielectric properties, a region with increased backscattering could be identified as abnormal tissues or a tumor. According to (AKINCI et al., 2015), this approach is usually easier to implement than tomography once no *a priori* information is needed and it is less computationally demanding.

This approach reveals a tumor as a stronger signal reflection from the inner breast, as discussed above, because of the tumor's dielectric properties. Figure 7 shows a reflection of tumor signal and its identification.

The qualitatively improved confocal algorithm (ARAGAO et al., 2020a) was used for the numerically simulated backscattered signals from a 11.0 cm diameter heterogeneous breast model rounded by 32 antennas. This breast model considers the skin, a glandular region, and a 0.8 cm spherical tumor in its inner part. Additionally, the simulated setup has a signal attenuation factor of 7.1 dB/cm.

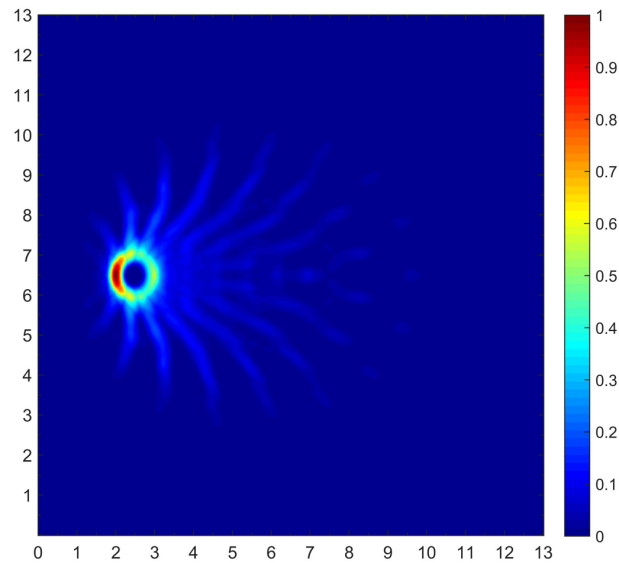


Figure 7 – Target energy map using the improved confocal algorithm. The axes X and Y are in cm.

The confocal imaging algorithm is the most commonly applied algorithm for the radar UWB technique, first developed in 1999 by (FEAR, 2005). It is based on the Delay-And-Sum (DAS) algorithm, which solves a well-posed problem that is less complex than an ill-posed one. This algorithm counts on the signal propagation times calculation between the antennas positions to then reconstructs each image pixel. These data are determined straight by the scattered waveforms.

Nevertheless, other imaging algorithms have been applied by different research groups, such as microwave imaging via space-time beamforming, tissue sensing adaptive radar (TSAR), circular synthetic aperture radar (CSAR), Microwave Imaging via Space-Time (MIST), Delay-Multiply And Sum (DMAS). The list continues, but this latest is suggested as the better choice and the most balanced performed (Shah Karam; O'LOUGHLIN; ASL, 2022).

2.3 Radar Overview

A RADAR, acronym that stands for RAdio Detection And Ranging, is a particular RF system that have countless usage, varying from military to medical applications, all in common designed to detect a target and extract from it some information as its range or speed, shape or even its presence at all. The concept of radar could be considered to take place with the classical experiments on electromagnetic radiation conducted by the German physicist Heinrich Hertz during the late 1880s. A great advantage of radar for medical applications is the fact that no sensor is needed to be attached or connected to a person or patient in order to assist or scrutinize them.

The radar working principle is based on the radiation of EM waves by a directive antenna and then the detection of some of this transmitted signal that is reflected backscatter from a target. Basically, it is considered a range or distance and a medium propagation or environment for radar employment. Hence, a radar calculates a target distance from the round-trip propagation time and wave propagation velocity, which in the free space is equal to the light speed (3×10^8 m/s).

In a long-range radar system, as surveillance, any reflected signal could be considered as a target identification, as an airplane flying above an area, implying less concern about noise from undesirable reflected signals. In a short-range radar system and also static target detection such as MwI for human body screening, the processing of the reflected signal could reveal the presence of an abnormality with a specific size or resolution, in this case, the refraction due to target dielectric properties that have changed the wave response. Here, the interference from reflected signals must be carefully detailed. Many radar functions and types are listed in (CURRY, 2012).

2.3.1 Radar for MwI

Considering the MwI system development based on radar implementation, resolution and penetration are its two most important characteristics to cater for medical devices. The higher the frequency, the higher the imaging resolution, leading to a smaller detectable tumor. However, at high frequencies, microwave signals propagating through the tissue undergo more attenuation, as seen in Subsection 2.1.3, which means that a deep tumor could go undetected. Therefore, there is an inherent tradeoff involved in satisfying both the penetration and resolution requirements dictating the transmitter's power, antenna gain, signal frequency and bandwidth, receiver's gain, noise figure, dynamic range, and sensitivity, as mentioned in (NGUYEN; PARK, 2016).

(YANG et al., 2018) affirms that, for a MwI system, the resolution is one of the main concerns, depending on three factors: Signal-to-Noise Ratio (SNR), signal form, and signal processing method.

The radar's ability to distinguish targets that are closely located is known as range resolution (ΔR), which according to (LI, 2015) reflects the radar specification to resolve multiple targets correctly. For a breast screening exam, these data inform the minimum tumor size that can be detected successfully. It is determined by the equation 4, which is correlated with the speed of the transmitted EM signal v depending on the propagation medium, and inversely proportional to its bandwidth (BW), implying the usage of UWB signals to successfully differentiate targets on a millimetric scale.

$$\Delta R = \frac{v}{2BW} \quad (4)$$

The penetration of an EM pulse from a MwI system depends on its operating frequency and TX power as well as on the dielectric properties of the illuminated object. The TX power is limited by thermal effects due to the microwave radiation absorbed in a living organism, which may cause tissue damage. The choice of the operation frequency should be considered proportionally to the square, as depicted in the Friis equation:

$$\frac{P_r}{P_t} = \frac{G_t \cdot G_r \cdot \lambda^2}{4 \cdot \pi \cdot R^2} \quad (5)$$

where P_t is the power delivered, P_r is the power at the receive antenna terminals, G_t and G_r are the antennas gain, R the distance between the antennas and λ is the wavelength value. The equation 5 corresponds to the relation between the transmitted and received EM signal, which value decreases as the frequency and distance increase.

2.3.2 Radar Waveforms Classification

Radars are commonly classified by the waveform signal applied or transmitted. It is mainly distinguished between Pulsed and Continuous Wave (CW) (NGUYEN; PARK, 2016). The radar waveform not only directly affects its characteristics but also determines the signal processing method between the time or frequency domain. According to (LI, 2015), the choice of frequency or time domain depends on the purpose of the radar. A correct decision on which waveform to use is seen as a cost-effective decision by (JANKIRAMAN, 2007) and impacts the overall MwI system. According to (BENNY; ANJIT; MYTHILI, 2020), time domain systems have recently emerged, motivated by their advantage over time scanning. However, as discussed in Section 3, most of the current MwI systems operate in the frequency domain. A target echo reflectivity is equivalent regardless of the radar domain.

2.3.2.1 Pulsed Radar and Time Domain

As the name suggests, a pulsed radar transmits a pulse signal and keeps waiting for the reflected signal to return to retrieve the target information. Usually, for a UWB MwI system, a short pulse duration is applied due to the limited signal energy (Federal Communications Commission (FCC)); and also due to the high levels of receiver noise, as explained in (TAYLOR, 2016).

The time-domain radar generally transmits a signal modeled as a Gaussian monocycle pulse or its derivative due to the commitment of signal generating circuit complexity and its ability to cope with the whole bandwidth at once, requiring low energy. However, the receiver noise figure is not sustained for the whole bandwidth, which results in decreased sensitivity, affecting the dynamic range and decreasing the penetration, as

mentioned in the Ph.D. Thesis (PARK, 2003). Thus, there is a consensus that pulsed radars cannot achieve high-resolution and deep penetration simultaneously unless the pulse compression technique is used.

Reducing the transmitter complexity has a drawback of a more complex receiver, as shown in Figure 8, which includes the Power Amplifier (PA).

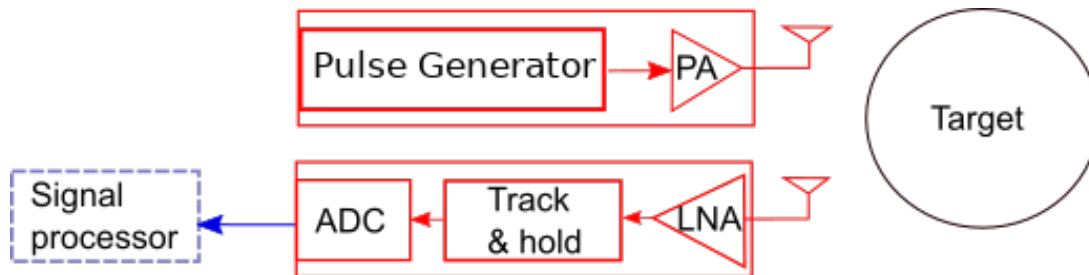


Figure 8 – Typical time domain system blocks.

The pulse generator can be designed by step recovery diodes among other solutions described in (FEGHHI et al., 2022). The LNA is the first receiver building block, which is fed by the RX antenna, improving the SNR and delivering it to the sampler circuit. The track and hold circuit, in most cases, uses the equivalent time sampling technique to translate the signal from the RF range to the baseband. Finally, an ADC converter translates the signal to the digital domain for post-processing image sensing algorithms. In this domain, the DAS confocal algorithm is used due to its robustness, effectiveness, and low computational cost, as already mentioned. Worth mentioning a single antenna could be used, inferring less interference between the transmitter and the receiver.

The LSI group has designed and tested some blocks as part of some master's degrees; publishing their results, such as (MARTINS et al., 2021) for a Class AB Programmable Gain Amplifier; (REYES et al., 2020) for a SAR ADC; (LEOPOLDO; NOIJE, 2022) for an LNA; (ALMEIDA; SANCHES; NOIJE, 2023) for a high-speed sampler.

2.3.2.2 Continuous Wave Radar and Frequency Domain

The CW radar transmits a continuous EM signal and simultaneously receives, ideally, only the backscatter signal. However, since two antennas are required, interference between the transmitter and receiver circuits, known as RF leakage, is always present. To deal with this interference, ultra-high isolation Transmitter/Receiver switch may be used. It is seen as a frequency domain approach for MwI.

Depending on the radar application and objective, its transmission signals can be unmodulated CW, which employ pure sinewaves; and modulated CW, which can be classified as Frequency Modulated (FMCW) and Stepped Frequency (SFCW).

Unmodulated CW radars can accurately measure the target radial velocity based on the phase shift or Doppler shift of the backscattered signal. Sensing applications such as heartbeat or respiration rate, which are important parameters during patient monitoring, are based on this effect, whereby the phase of the reflected signal changes according to the heart or chest movements. However, it is unable to resolve range information due to the narrow spectrum (line spectrum) of its transmitted waveform.

According to (JANKIRAMAN, 2007), frequency modulation of the carrier is one of the most common techniques used to broaden the spectrum and then extract target range information, as required for MwI systems. Also, (TING; OLOUMI; RAMBABU, 2018) refers to the FMCW radar as an alternative to the impulse radar, especially for short-range target detection. Moreover, conversely to the pulsed radar, FMCW and SFCW radars may eliminate the ADC high-speed requirement while still providing the advantage of effective wide bandwidth.

- FMCW - Frequency-modulated continuous-wave

In FMCW radar, the transmitted signal frequency versus time characteristic follows the sawtooth pattern, leading to a linear frequency modulated chirp sequence. Range resolution measurement depends on the frequency sweep rate, which is one of the most important design parameters.

In practice, it is difficult to achieve an accurate and constant frequency sweeping rate over a wide band due to the nonlinearity of the synthesizer, particularly when a voltage-controlled oscillator (VCO) is used in its place. Furthermore, a wide bandwidth degrades the receiver noise figure, resulting in a decreased sensitivity and therefore a decreased dynamic range for the receiver. These drawbacks may prohibit the possible use of FMCW radar sensors for some applications that require wideband operation with very high range accuracy, as mentioned by (NGUYEN; PARK, 2016).

- SFCW - Stepped Frequency Continuous Wave

It is a challenge for a UWB Radar to receive a signal without decreasing sensitivity and hence dynamic range when using pulse or FMCW waveforms. According to (JANKIRAMAN, 2007), a radar technique that avoids the data acquisition problems associated with wide-band signals and has been extensively used in short-range measurements is the SFCW. It consists of the transmission of a burst of narrowband stepwise (Δf) tones until it reaches the effective bandwidth (BW), whose value is defined by equation 6.

$$BW = N * \Delta f \quad (6)$$

where N is the number of steps, as depicted in Figure 9.

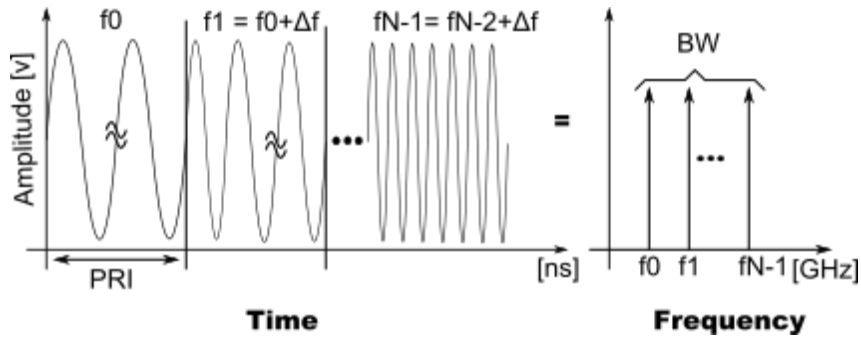


Figure 9 – Time waveform and frequency domain SFCW signals.

The Pulse Repetition Interval (PRI) is the time required for transmitting each tone. These parameters are all strictly related to radar resolution and also operating time. The narrowband signals are processed as complex-valued signals instead of real-valued ones. It consists of both real or In-Phase (I) and imaginary or Quadrature (Q) signals that are 90° different in phase, known as quadrature processing. Each tone is then transformed into a synthetic pulse in the time domain by applying the Inverse Fast Fourier Transform (IFFT), retrieving the target signal information such as magnitude and phase.

(TAKAHASHI; MIWA, 2021) discuss that it is crucial for SFCW radar the coherent amplitude and phase measurements, rising a challenge due to the unknown initial phases of the Local Oscillator (LO) signals. Moreover, (SIPOS; GLEICH, 2021) affirms that the SFCW radar presents better performance compared with FMCW when it is required high resolution with a low noise figure, paying the price for longer time acquisition.

Thus, the frequency domain radar, typically based on the SFCW signal modulation, can be developed as shown in Figure 10.

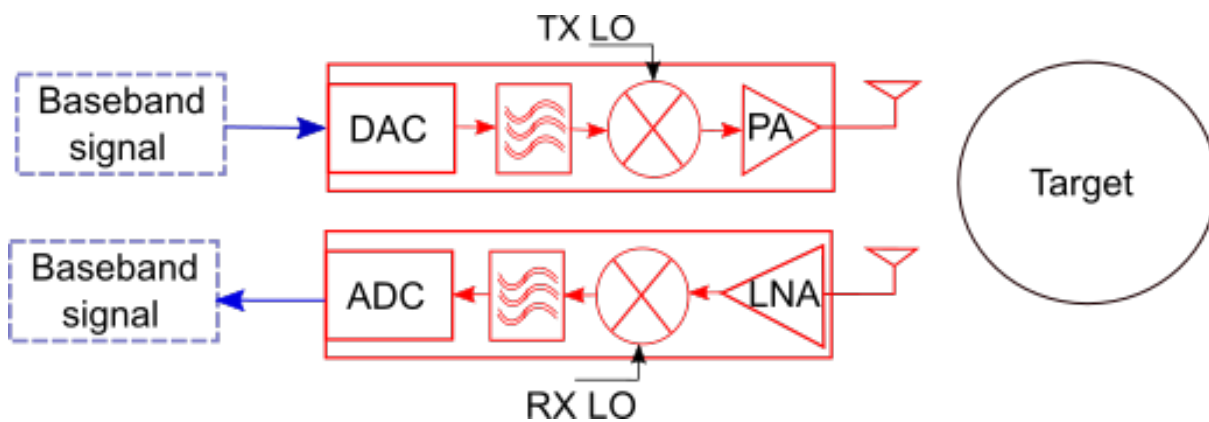


Figure 10 – Typical frequency domain system blocks.

This block diagram is closely related to an SDR apparatus. Thus, each block is better described in Section 2.5.

2.4 Synthetic Pulse

Despite the relatively low range resolution of a narrowband signal, the coherent synthesis of all signals within a range can provide the wide frequency scope, which is required for MWI aiming at breast cancer detection (YANG et al., 2018). Synthetic pulse, also mentioned as Synthetic Range Profiling once the target profile is not measured directly, is a technique whereby high range resolution is obtained by transmitting a series of pulses at different frequencies and then using signal processing to form a high-resolution image of target reflectivity along the range axis.

The concept of generating a synthetic pulse was described in (WEHNER, 1995), which steps are described as follows:

- store the digitized quadrature components (I/Q) of each stepped frequency signals received from its corresponding transmitted pulse burst;
- apply frequency weighting to each burst of data and corrections for target velocity, system phase and amplitude ripple, quadrature sampling bias and imbalance errors;
- perform the IFFT operation of the resulting set of N complex frequency components of each burst to obtain an N-element synthetic range-profile signature of the target from each burst.

According to (YANG et al., 2018), the frequency step affects the time-domain reconstruction once it defines the resolution of synthetic time-domain data, which means the amount of time that can be uniquely resolved through an IFFT before the signal repeats itself.

2.5 Software Defined Radio - SDR

The tradeoff between hardware and software digital processing has driven developers' decisions for a long time, always considering flexibility against performance. Aside from signal processing in the analog world, little could be done but convert it to the digital realm. However, SDR endeavors to deliver high performance while still being flexible to deal with EM waves. Its creator, Joseph Mitola, introduced the SDR concept in the early 90s as a radio that interoperates with any communication service (MITOLA, 1992). According to (COLLINS et al., 2018), the formal SDR definition of the Institute of Electrical and Electronic Engineers (IEEE) is "Radio in which some or all of the physical layer functions are software-defined".

It is possible to say that an SDR is capable of transmitting and receiving RF signals, modulating a baseband to RF signal and demodulating them, converting from analog to digital or digital to analog depending on the signal direction, and processing the baseband signals according to some algorithm running in a Digital Signal Processing (DSP). Its outstanding feature comes from moving as much as possible of the RF system functionalities, typically implemented in hardware, to the software domain. With that, operation, such as frequency translation, is now software-defined. Moreover, its ability to handle waveforms digitally calls attention to radar-based systems, whereas carrier properties, such as frequency, signal bandwidth, modulation, and demodulation, are all defined by software. SDR programmability offers quick and inexpensive development, tests, and further improvements to the Mwi system realization.

SDR is more versatile compared to DSP radio or analog options, as shown in Figure 11, in which the analog modulation parameters as bandwidth and frequency are defined as fixed; the DSP modulation is similar to analog but includes source and channel coding. On the contrary, all of those parameters are programmable through an SDR.

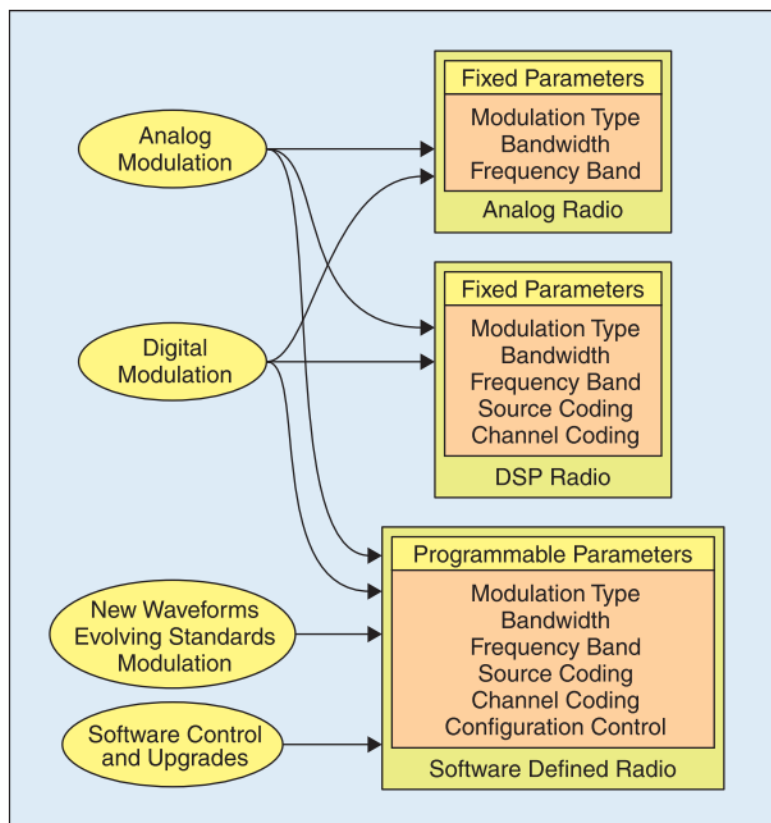


Figure 11 – Radio options: Analog, DSP, and SDR.

Source: (HARRIS; LOWDERMILK, 2010).

SDR, firstly aimed at communication systems, was used to realize those systems back in 2005 as pointed out by (KENINGTON, 2005), which shows its architecture adoption for base-station transceiver systems. Moreover, (AKEELA; DEZFOULI, 2018)

affirms that SDR is a technology for radio communication due to its programmable ability that allows multi-band and multi-functional wireless devices realization, and also (OKADA; KOUSAI, 2011) foresee the need for a reconfigurable radio with the advent of Long Term Evolution or even the 5G. Furthermore, SDR has been seen as a technological breakthrough to implement MmI systems, besides the few systems currently implemented. Indeed, SDR usage for MmI was first indicated by (MARIMUTHU; BIALKOWSKI; ABBOSH, 2016) in 2016 and more recently used by (ZENG; OROZCO; FHAGER, 2019). Another SDR application would be to implement a Ground Penetrating Radar (GPR) system, which has been explored for different groups, aiming at, for example, glacier healthy monitoring.

2.5.1 SDR - Platform Overview

SDR comprises a Radio Frequency (RF) section, coupled with ADC and DAC blocks, Digital Up (DUC) and Down Converters (DDC), all controlled by a glue logic, which interfaces with a computer through a USB or Ethernet connection. Furthermore, it offers SMA connectors to the antenna interface, as shown in Figure 12 with one transmitter and one receiver interface.

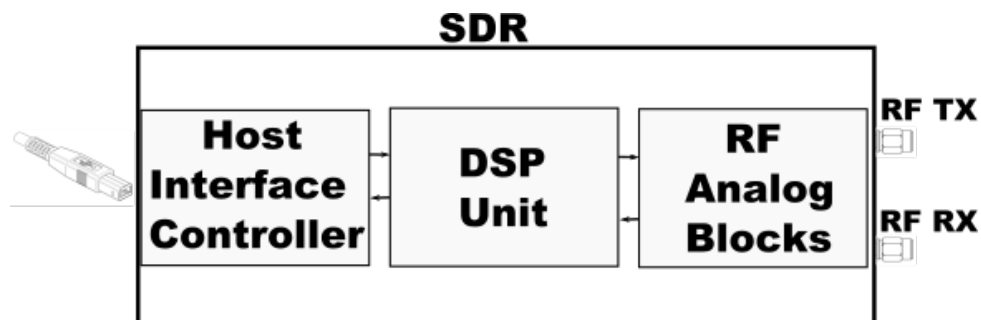


Figure 12 – Typical SDR blocks.

2.5.1.1 Host Interface

The communication between a host and an SDR usually is done by some type of USB or Ethernet interface. This communication intends both to program the SDR and to receive the baseband signals. The former has no need for fast data transfers while the latter is at least at the MHz speed. Thus, Ethernet and USB 3.0 speeds are appropriate for the amount of data that flows between the host and the SDR.

2.5.1.2 DSP Unit

The DSP unit, referred to as the baseband processing block, realizes the digital processing of narrowband signals. It is at the heart of SDR implementation, as mentioned by

(AKEELA; DEZFOULI, 2018). It is on the DSP unit that operations such as modulation, demodulation, operational frequency definition, DUC, and DDC occur. Moreover, this unit is intended to perform both Fast Fourier Transform (FFT) and IFFT as well. Besides, the DSP unit generates the baseband signal to convert the carrier as its function, defining the phase, frequency and amplitude of the RF signal. Within a bandwidth range, any signal can be software generated without changing any hardware. Indeed, this unit can extensively replace analog functions, such as mixers, filters, and oscillators.

Ideally, the DSP unit must be reconfigurable, low power consumption and high performance due to its real time execution and high data throughput. Its requirements leads to a more hardwired processing, ending up with a dedicated hardware like an Application Specific Integrated Circuit (ASIC) or a FPGA, which is a programmable alternative. Nowadays, FPGAs are commonly employed in most of the SDR platform thanks its significantly advanced over the past decade. Furthermore, for reconfiguration delay in milliseconds order, FPGA-based SDRs can change its operation mode or protocol seamlessly.

- I/Q Signals

The same as described for SFCW implementation, the SDR narrowband signals are processed as complex-valued signals based on quadrature processing. In essence, getting that signal involves splitting the incoming signal into two identical copies, mixing one by the carrier and the other by a 90° out-of-phase version of this carrier. According to (CHENEY; BORDEN, 2009), this conversion between real to complex and vice versa has better approximation when the signal is narrowband.

Figure 13 shows the complex time domain of a baseband signal at both stages of RF communication (transmitting and receiving), whereby TX are solid lines and RX are dotted ones.

Those signals have been measured through an SDR in a first experiment carried out for SDR familiarization and published in (CARVALHO et al., 2020), further discussed in Section 4.3. In this test, the TX signal is straightforwardly collected by the RX antenna, which was positioned 15.0 cm distant from each other. The RX attenuation is related to the system loss, which could refer to the antennas and also to the transceiver response, and the air attenuation.

2.5.1.3 RF - Analog blocks

The RF and analog blocks are intended to transmit and receive RF signals, hence leading to a transceiver. Further, the analog blocks convert the signal domain regarding

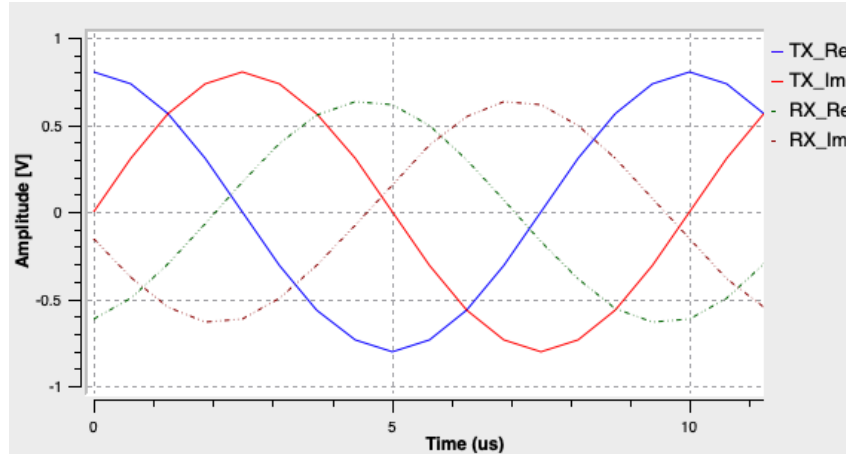


Figure 13 – Baseband signal - Time Domain.

its direction which requires ADC and DAC circuits. It is possible to couple a PA to the TX interface and an LNA to the RX interface to increase the system dynamic range gain.

- PLL Synthesizers

A transceiver requires frequency synthesizers to generate the LO signals for the up-and-down conversion of RF signals with great accuracy, stability, and repeatability. Phase-Locked Loop (PLL) synthesizer is a device with fractional N designs that incorporates VCO and loop filters to synchronize two periodic waveforms creating the required LO signals. Usually, SDR's transceiver contains two PLLs to allow Frequency-Division Duplex (FDD) operation (YUKSEL et al., 2017).

- Transmitter

An SDR transmitter is essentially a signal generator that must be able to take a baseband signal and convert it to an RF signal. Moreover, it must support FDD standards, in which the transmitter is active while receiving. SDR transmitter circuit is based on some form of super-heterodyne or direct conversion architecture.

It is possible to describe an SDR transmitting chain such as: a digital baseband signal that starts at the DSP unit and passes through a DUC circuit to data rate adjustment (interpolation) or transfers the baseband signal to IF (frequency translated) prior to reaching the DAC; which converts the signal from digital to analog; afterward, a filter is used to remove sampling artifacts and then fed a mixer; which under a LO operation converts the incoming signal to higher RF signal to be transmitted; at last, a PA is used to guarantee signal strength before the TX antenna as depicted in the Figure 14.

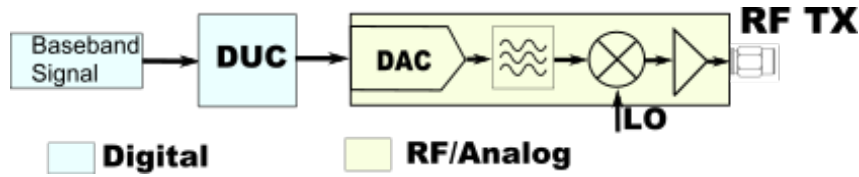


Figure 14 – Transmitter SDR blocks.

According to (OKADA; KOUSAI, 2011), the mixer is the determinant and the key component for successful transmitter operation, once it guarantees stability and coherence to the transmitted signals.

- Receiver

The SDR receiver undoubtedly plays a critical role in any application, receiving unknown but bandwidth-limited RF signals with different levels corrupted by noise, and converting them to the digital data domain. Its circuit is also based on some form of super-heterodyne or direct conversion architecture. The latter is also known as homodyne, synchrodyne, or zero-IF receiver. The most critical function of an RF receiver, whether its architecture, is to fully recover an RF signal without degradation.

It is possible to describe an SDR receiving chain as: a LNA amplifies the incoming RF signal from the RX antenna; the mixer converts the signal from RF to IF or baseband, i.e. frequency translated signal; a filter is used to remove sampling artifacts and then fed an ADC; which converts the signal from analog to digital; the digitized signal pass through a DDC that down-converts to a software-defined output data rate.



Figure 15 – Receiver SDR blocks.

An SDR that employs the direct-conversion architecture, as shown in Figure 15, is more attractive to UWB radar systems due to the receiver's ability to demodulate ultra-wideband RF signals, providing the most efficient use of the data converter bandwidth. However, in this architecture, it is a challenge to maintain the I/Q balance with low levels of image rejection, LO leakage, and dc offset, which limits the receiver dynamic range.

Those challenges have been overcome with digital calibrations according to (Peter Delos, 2016), which rely on the advantages of CMOS technology. Indeed, (ROSOLOWSKI et al., 2016) has successfully obtained a dc offset as below as -85 dBFS by the use of strong capacitive coupling between the mixer's output and the succeeding amplifying stages.

2.5.2 Software Framework

SDRs require a design environment framework providing drivers, interface control, access to the DSP Unit, and so on. Generally, a software framework is compatible with a range of SDR vendors offering a graphical interface that allows designing flowcharts projects. Software framework's major distinctions arise in licensing and source control. National Instruments provides support for Labview and MATLAB® platforms, which are proprietary software.

On the other hand, GNU Radio (GNU Radio, 2021) is a free and open-source software development toolkit able to implement the design of the RF, analog, and digital parts of an SDR. It provides a plethora of processing blocks that are easily connected in order to perform the baseband signal processing, such as low pass filter, high pass filter, data rate conversions, FFT/IFFT operations among others. It is widely used in hobbyist, academic, commercial, and military environments to support wireless communications research, as well as to implement real-world radio systems.

2.6 Scattering parameter

Whatever the approach is used, whether tomography or radar, the scattering parameter could be employed to realize a MwI system. The scattering parameters, also known as S-parameters, are the most common mechanism to evaluate, in the frequency domain, the performance of a microwave device that employs EM signals, as mentioned by (NIKOLOVA, 2017). Moreover, it is suitable to measure signal features such as amplitude and phase in frequency-sweep evaluation systems. As mentioned in (ROOT et al., 2013), it is possible to quantify the reflection and transmission characteristics of devices based on the amplitude and phase information. According to (CASPER, 2011) it is convenient to describe a given RF system in terms of *waves* rather than voltages or currents, mainly for high frequencies such as the microwave range. The two main terms to describe a device with 2-ports are the signal return loss or S_{11} , which is related to the reflected waves that were incident by port 1 terminated by a reference impedance load (usually 50 ohms); and the signal propagation loss or S_{21} , which is related to the forward transmission waves from port 1 to port 2.

The wave quantities are expressed as complex numbers, whose magnitude is the square root of the power carried by the traveling wave. Meanwhile, the phases of the power waves correspond to the phases of their electric fields at the specific port. An S-parameter of unity magnitude indicates full transmission-reflection, whereas zero magnitudes indicate full power absorption by the device. Considering a MwI, the ideal system or device, coupled with the antennas, has zero reflection or $S_{11} = 0$ dB, which indicates an ideal

termination or a perfect match between each component. Moreover, practical experiments have demonstrated that a return loss smaller than -13 dB does not affect the transmitted signal. A full power transmission from one antenna to another one or $S_{21} = 1$, which indicates both system and media without any loss.

The S-parameter could be used to scrutinize a positioned object, once its presence will change the expected received signal power rate. Response sensitivities analysis provides crucial information once it describes the rate at which the response changes. Thus, the well-discussed idea for detecting an inner breast tumor presence is to send an EM wave and then analyze the backscattering received power. The return loss usage has been demonstrated in (KAUR; KAUR, 2020) and (SELVARAJ et al., 2021), whereas the transmission loss is more commonly employed.

2.7 Discussion

MwI aimed at early detection of breast cancer faces the complex nature of EM waves interactions in human tissues. It is due to the heterogeneity of various tissue "layers" and also the tumor, with vastly varying dielectric properties. The image reconstruction method is related to how the EM waves illuminated the breast. (BENNY; ANJIT; MYTHILI, 2020) mention that finding the inverse problem solution is still the main challenge of the approach, with the tendency to replace the original ill-posed problem with a well-posed one, which they call the regularization technique. Thus, as will be described in Section 3, most MwI systems are implemented using a radar-based approach.

The system RF signal operational frequency that copes with penetration and high image resolution is still a challenge, which leads to the SFCW approach dominance. Most systems have employed the VNA apparatus, which already deals with the coherent amplitude and phase measurements of the transmitted and received EM signals. Nevertheless, an SDR-based system is a possibility due to its programmability related to the RF system.

Chapter 3

Microwave Imaging Systems

In the wake of MwI for medical applications, this chapter has explored its vast niche, showing that the best solution is not yet a reality. Research groups are seeking practical and achievable systems as such, using laboratory instruments, e.g. a VNA, a pulse generator, a real-time oscilloscope, etc., for their validation and tests. It still happens even almost 10 years later in the work (CHANDRA et al., 2015) that discusses different imminent opportunities. Some systems were reviewed in (KWON; LEE, 2016), published one year later. Soon after, (O'LOUGHLIN et al., 2018) discussed the same systems, including others, and raised challenges, some of which were already addressed and will be discussed in this chapter. The issues related to the hardware apparatus, the better operating frequency, and antennas are well discussed in (ALDHAEEDI et al., 2020). However, even this recent publication had not considered the use of SDR to implement a MwI system, together with the work (WANG, 2018) previously published.

None of the systems described here are commercially available at the time this text has been elaborated, besides the Micrima company, which has reached a significant milestone with initial presales of its product, described in Section 3.2.1, or the Microwave Vision Group, which looks forward to commercializing its system, described in Section 3.2.4. These spin-offs will be further discussed along with two more. All these systems could be seen as a breakthrough for MwI realization.

It is important to mention that half of the presented systems do not have clinical or patient evaluations, which is a necessary step according to the International Medical Device Regulators Forum (IMDRF, 2019a), to commercialize any medical device. In fact, most of the current research groups could be seen in the clinical investigation stage, which is concerned with the effectiveness of a medical device according to (IMDRF, 2019b).

Figure 16 shows a scheme timeline model for other imaging modalities (ultrasound, MRI, and PET). Usually, a foundational discovery is placed at the start of a new imaging

modality, such as the microwave response in human tissues. On the basis of that, it is possible to affirm that MwI is in the clinical acceptance stage.

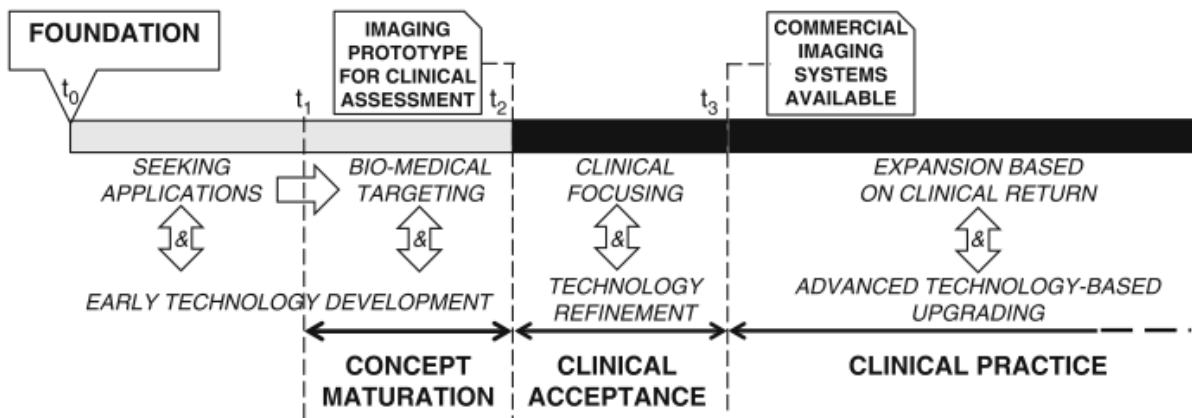


Figure 16 – Medical imaging technology evolutionary timeline.

Source: (BOLOMEY, 2018).

3.1 Tomography approach

Table 2 summarizes the MwI tomography systems presented in this work.

Table 2 – MwI tomography systems review

Origin	Features	Imaging Algorithm	Clinical Stage
Dartmouth College	16 monopole antennas Freq. range: 0.5-2.3 GHz Mechanical Scanning Glycerin/water solution	Log-phase formulation	Clinical trials
	16 monopole antennas Freq. range: 0.5-2.5 GHz Ettus B210 SDR	Log-phase formulation	Clinical investigation
McMaster University	Freq. range: 3.0-8.0 GHz Planar Scanning	SPM QMH	Clinical investigation
Istanbul Technical University	bistatic system Freq. range: 1.4-8.0 GHz Mechanical Scanning VNA usage	LSM FM	Clinical evaluation

3.1.1 Dartmouth College - USA

The microwave imaging group at the Thayer School of Engineering, Dartmouth College (DC) (Dartmouth, 2021), has been studying microwave imaging since the 1990s. The group is led by Prof. Keith Paulsen (PAULSEN, 2021). The first prototype system for

breast cancer detection was fabricated in 1995. It consisted of a four-detector monopole antenna array operating at a frequency between 300 MHz and 1.1 GHz. The system uses the tomographic approach, with the images reconstructed using a Gauss-Newton algorithm. Images were reconstructed after multiple phantom measurement data and results were satisfactory according to (FANG, 2004).

Four years after the laboratory prototype, in 1999, a new system was built based on the previous one, referred to as the "first generation". It consisted of an array of 16 monopole antennas, each capable of transmitting and receiving microwave signals. Additionally, the array can be moved manually up and down through a hydraulic jack. The system also operates at frequencies ranging from 300 MHz to 1.1 GHz, using Newton-based nonlinear inverse scattering to create images. The Dartmouth group conducted the first clinical tests at the Dartmouth-Hitchcock Medical Center, with more than 200 patients participating in the imaging studies.

In 2002, an improved system, known as the "second generation", was fabricated, which is depicted in Figure 17, showing that the patient lies prone atop a measurement table with her breast suspended through an aperture in the table. This first exam patient position proposal is still in use, raising the question whether the woman's breast must be in such a way for a better screening procedure.



Figure 17 – Photograph of the second-generation MWI prototype made up of a cylindrical array of 16 monopole sensors.

Source: (MEANEY et al., 2007).

The major difference was the implementation of the parallel data acquisition strategy instead of the serial approach used in the first generation. The operating frequency range of the system changed to 500 MHz - 3 GHz. The proposal concerning the coupling medium

was to replace the high-attenuation saline with a glycerin/water solution, once this solution had a better match with the breast permittivity and conductivity dispersion. Furthermore, the glycerin solutions are biostatic, which makes them safe for patient examinations. Later, manual control of the antenna array was replaced with an automatic control system, and the antennas are moved vertically through seven different measurement positions, creating images of the breast under the assumption of a 2-D scattering problem.

The Technical University of Denmark, with the cooperation of the DC and inspired by its system, has developed a system for detecting breast cancer using microwaves, as shown in the Ph.D. Thesis (RUBÆK, 2008), which focused on the development of the imaging algorithm and the antenna system. This Thesis mentioned that a key feature in the imaging algorithm applied to DC is the use of the so-called log-phase formulation.

3.1.1.1 SDR-based system

Notwithstanding his pioneering work, Prof. Meaney has recently developed a Mwi system comprising nine Ettus SDR boards (National Instruments, 2021), one of which operates as a dedicated transmitter, while the other eight as receivers (MEANEY et al., 2020). It is also composed of 16 monopole antennas operating from 500 MHz to 2.5 GHz and is able to distinguish signals as low as -140 dBm. Figure 18 shows the fully integrated system composed of the SDRs, groups of eight switch/amplifier modules, digital I/O cards and power supply, keeping bias and control lines as short as possible.

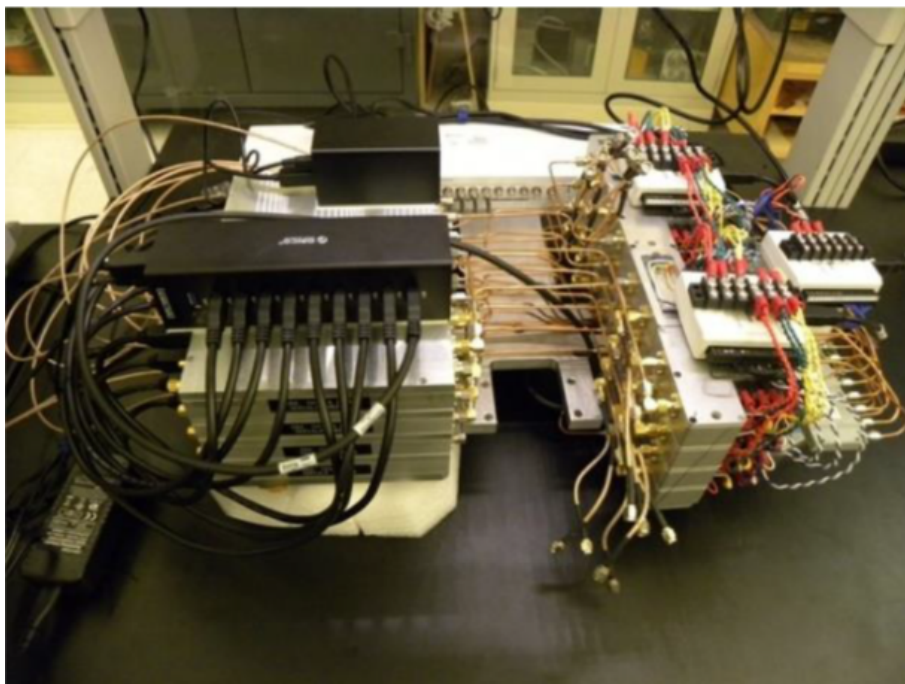


Figure 18 – Photography of the microwave electronic subsystem fully assembled. Source:(MEANEY et al., 2020).

As this system is composed of an antenna array, cross-channel leakage was a great concern and was thoroughly investigated. It also implements a tomographic approach, taking advantage of all the background knowledge accumulated since the 90s.

3.1.2 McMaster University - CA

A McMaster University group, led by Prof. Nikolova (??), is at the forefront of the development of a near field microwave imaging system for early-stage breast cancer detection. She is the author of the book "Introduction to Microwave Imaging" (NIKOLOVA, 2017), which is an introductory-level text about the use of microwaves and millimeter waves in the imaging of optically obscured targets.

The challenges in the development of a MwI system are discussed in the first place in (NIKOLOVA, 2011), bringing to light the model simplifications used for simulations. She also mentioned that the "community" was no longer impressed with the simulation results after more than 20 years of research related to MwI.

Prof. Nikolova has investigated systems for detecting breast cancer using mainly the tomographic approach, proposing new processing methods, such as the Scattered Power Mapping (SPM) demonstrated at (SHUMAKOV; NIKOLOVA, 2018), and Quantitative Microwave Holography (QMH). Both imaging methods utilize linear approximations of scattering that enable real-time image reconstruction. Recently, her group published (TAJIK; TRAC; NIKOLOVA, 2020) discussing the quality of microwave imaging data according to the experimental results protocol, which did not reproduce the idealized system environment. Also, Ph.D. Thesis (TAJIK, 2022) made a difference in image quality based on QMH and SPM algorithms enhancements.

Finally, her group has collaborated with others, such as McGill University (3.2.3) and Galway University (3.2.4), using the radar-based UWB approach. (WORTGE et al., 2018) is one of the results in which practical tests with phantom have been performed.

3.1.3 Istanbul Technical University - TR

The Department of Electronics and Communication Engineering of the Istanbul Technical University (ITU) has investigated the qualitative approach to MwI over the past decade, with remarkable results, as depicted in (AKINCI et al., 2015). Along with other departments, the MwI system called SAFE (Scan and Find Early) was recently launched.

Figure 19 shows the SAFE product and its surround equipment. For a scanning session, the woman lies in a prone position on the table, while one breast is inserted into the coupling medium, necessary for impedance matching. A bistatic system was employed in which one transmitting and one receiving antennas were positioned, touching and circling

the coupling cylinder. Moreover, a mechanical mobile system is required to rotate the antennas. For each transmitter position, 36 receiving points were achieved, generating a total of 1296 measurements for each frequency that illuminates the breast, retrieving the S_{21} parameter, and then identifying any abnormality.



Figure 19 – SAFE design in a clinical surrounding.

Source: (JANJIC et al., 2021).

Looking for a suitable trade-off between absorption rate and resolution, an operating frequency band was applied between 1.4 and 8.0 GHz, with the data acquisition step of 200 MHz.

Concerned about scan time, the SAFE wasted at most fifteen minutes on average for both breasts, which is around the same time spent during a mammography exam. Five more minutes were spent positioning the patient.

Based on the inverse scattering algorithm, such as the linear sampling method (LSM) and the factorization method (FM), image reconstruction was performed after the scan was complete (AKINCI et al., 2015).

3.2 Radar-based UWB approach

Table 3 summarizes the operational MwI radar-based UWB systems presented in this Thesis. It is notable that this Section describes most of the MwI systems. In addition, the results of the LSI group will be presented.

Table 3 – MwI radar-based systems review

Origin	Features	Imaging Algorithm	Clinical Stage
University of Bristol	60 wide-slot antennas Freq. range: 3.0–8.0 GHz VNA usage	Confocal DAS	Clinical evaluation
University of Calgary	1 antenna antipodal Vivaldi Freq. Range:0.05-15.0 GHz Laser for outline Coupling with canola oil VNA usage	TSAR	Clinical investigation
McGill University	16 travelling-wave antennas Freq. Range 2.0-4.0 GHz Coupling with ultrasound gel Pulse Generator and Oscilloscope usage	Confocal DMAS	Clinical investigation
Galway University	18 wideband Vivaldi antennas Coupling liquid Freq. Range: 1.0-4.0 GHz Mechanical Scanning VNA usage	TR-MUSIC	Clinical evaluation
Chalmers University	2 monopole antennas Freq. range: 0.2–3.0 GHz Off-the-shelf components	Confocal DAS	Clinical investigation
	2 antennas Vivaldi Freq. range: 1.0-6.0 GHz Ettus B210 SDR	Without Imaging	Clinical investigation
University of Perugia	1 horn/monopole antennas Freq. range: 1.0–9.0 GHz No coupling liquid VNA usage	Huygens Principle	Clinical evaluation
Hiroshima University	16 Planar UWB antennas Freq. Range 3.1 - 10.6 GHz Coupling with glycerin Mechanical Scanning CMOS implementation	Confocal DAS	Clinical evaluation
University of São Paulo	2 antennas Freq. range: 5.0-7.0 GHz No coupling liquid Xetru Board	Improved Confocal DAS	Clinical investigation
University of Queensland	1 tapered slot antenna Freq. range: 1.2-2.14 GHz Coupling with glycerin Nuand SDR	Confocal DAS	Clinical investigation

3.2.1 University of Bristol - ENG

The University of Bristol unfolded a MwI system, known as MARIA (Multistatic Array Processing for Radiowave Image Acquisition). Its technique uses an innovative radar

system, based on multistatic radar operation, originally proposed for land mine detection by Bristol University's Prof. Ralph Benjamin (PREECE et al., 2016). One of his first publications (KLEMM et al., 2009) shows the development of the 16-element UWB radar system for breast cancer detection.

The Maria M_WI system underwent stages of development, evolving from an initial 16-antenna array to a 31-element UWB slot antenna system (MARIA M₃). To improve imaging performance and reduce scanning time, a new 60-element wide-slot antenna array system was designed known as MARIA M₄ and described in (HENRIKSSON et al., 2011).

The current version of the MARIA system, known as M₆, can scan breasts twice the size of version M₅, addressing a large number of patient exclusions that had to be made due to breast size, as reported in (SHERE et al., 2019). The interface between the antennas and the breast, a well-known issue, was overcome by a coupling medium, comprising beeswax, paraffin oil, aqua, and a preservative.

Figure 20 shows the MARIA M₆ version block diagram with the patient placing her breast through an opening in the table while laying prone. Note that the exam is performed at one breast per time. The prone position has the advantage of reducing the effects of motion due to breathing.

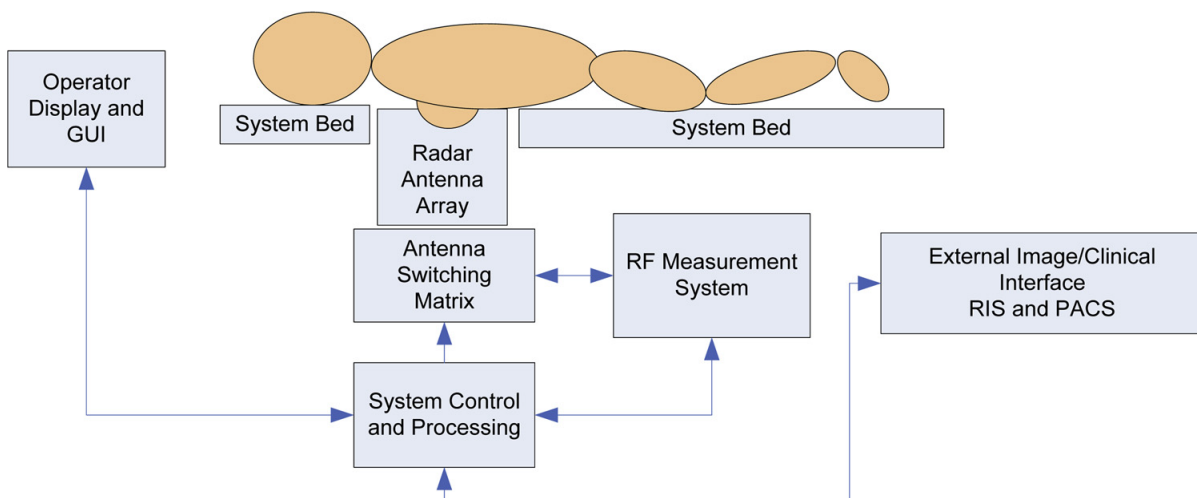


Figure 20 – MARIA M₆ system block diagram.

Source: (SHERE et al., 2019).

The system signal source is the Keysight VNA M9372A (Keysight Technologies, 2020) operating in the frequency range of 3.0 to 8.0 GHz, employing the Stepped Frequency Continuous Wave (SFCW) radar mode at 101 different frequencies. Indeed, each MARIA contains eight of the M9372A, and each one has 16 ports. The antennas operating in the mentioned frequency range are placed in a cavity-loaded slot arrangement. The backscattered collected signals are measured in the frequency domain and transferred to the time domain using the Inverse fast Fourier transform. The signal domains are changed

because the image is reconstructed by a focusing algorithm using the time domain signals. A switch matrix connected to the feed of the antennas swaps the pair of antennas during the measurements. To generate the image, the system uses a modified version of the classical Delay And Sum (DAS) beamforming algorithm.

Each antenna is designed to be coupled to a dielectric constant environment equal to 10. (PREECE et al., 2016) reports some MARIA measurements at 3.2 GHz indicating that the most common relative permittivity values for breast fat were 4 to 4.5, for normal glandular tissue 10 to 25, and for malignant tissues 45 to 60, values in accordance with the ones mentioned in Section 2.1.

3.2.2 University of Calgary - CA

The researchers at the University of Calgary have explored different methods for early cancer detection, including blood test kits and nanoparticles. Elise Fear's team has developed and tested prototype systems for radar-based breast imaging, which includes the design of sensors (antenna and laser), implementation of imaging algorithms, and patient studies to evaluate the technology.

Figure 21 shows the apparatus of the system developed in 2012, where the woman lies prone with her breast hanging through a hole on an examination table.



Figure 21 – Photograph of the system composed of the table, one VNA, and cables. Source: (BOURQUI; SILL; FEAR, 2012).

This prototype is based on a monostatic radar approach that employs a single

antenna to transmit and collect EM signal data, and has been termed the TSAR (Tissue Sensing Adaptive Radar) method. As described in (BOURQUI; SILL; FEAR, 2012) and (FEAR et al., 2013), the system is composed of a table, a tank containing canola oil, a laser, and a VNA. The canola oil fills the gap and works as a coupling liquid, once it exhibits a relative permittivity of 2.5 and a conductivity below 0.04 S/m up to 12.0 GHz, improving the dielectric match between the breast skin and the antenna. The custom UWB antenna, which is an antipodal Vivaldi has a bandwidth (S11 better than -10 dB) from 2.4 to 18.0 GHz. The laser is used to record the breast outline, defining the imaging volume, which provides essential information for enhancing image reconstruction. The system signal source is the Keysight's VNA 8722ES, used to illuminate the breast and retrieve the microwave signals.

As the system has only one antenna, it is necessary to rotate it. For this, the antenna and laser are both attached to an arm, which is used to move the sensors in the vertical direction, and the entire tank rotates. Hence, the breast is scanned all around by the antenna, which sends and receives microwave signals over the frequency range from 50 MHz to 15.0 GHz. The antenna is connected to the VNA via a 3 m-long cable. The recorded data are used to generate 3-D images of the breast using a time-shift and sum approach, with the volume of interest for imaging defined by the laser data and an adaptive algorithm used to reduce the dominant reflections from the skin.

(FEAR et al., 2013) demonstrated satisfactory results of the mentioned TSAR system applied to a phantom and a volunteer. This work affirms that good measurement sensitivity is a key aspect of the system since reflections from internal breast tissues are expected to be very weak. The sensitivity is directly influenced by the measurement noise floor of the VNA receiver. A sensitivity below -90 dBm is achieved over most of the frequency band.

3.2.3 McGill University - CA

The RF Breast Cancer Detection Research Group (McGill University, 2021) at McGill University is part of its Computational Electromagnetics Laboratory. The group has already granted many Ph.D. Theses between 2011 and 2021, such as (PORTER, 2015) and (SANTORELLI, 2017). Besides, they have published dozens of papers in conferences and journals.

Figure 22 illustrates a prototype system developed, which performs detection through multistatic radar using measurements in the time domain. According to (LI et al., 2017), the system consists of sixteen bistatic traveling-wave antennas to transmit and to collect the backscattered signals from the breast, which means that one antenna transmits the EM signal, while all the other fifteen receiving antennas collect.

The system was thoroughly tested in 2017 with phantoms that exhibited reasonable results.

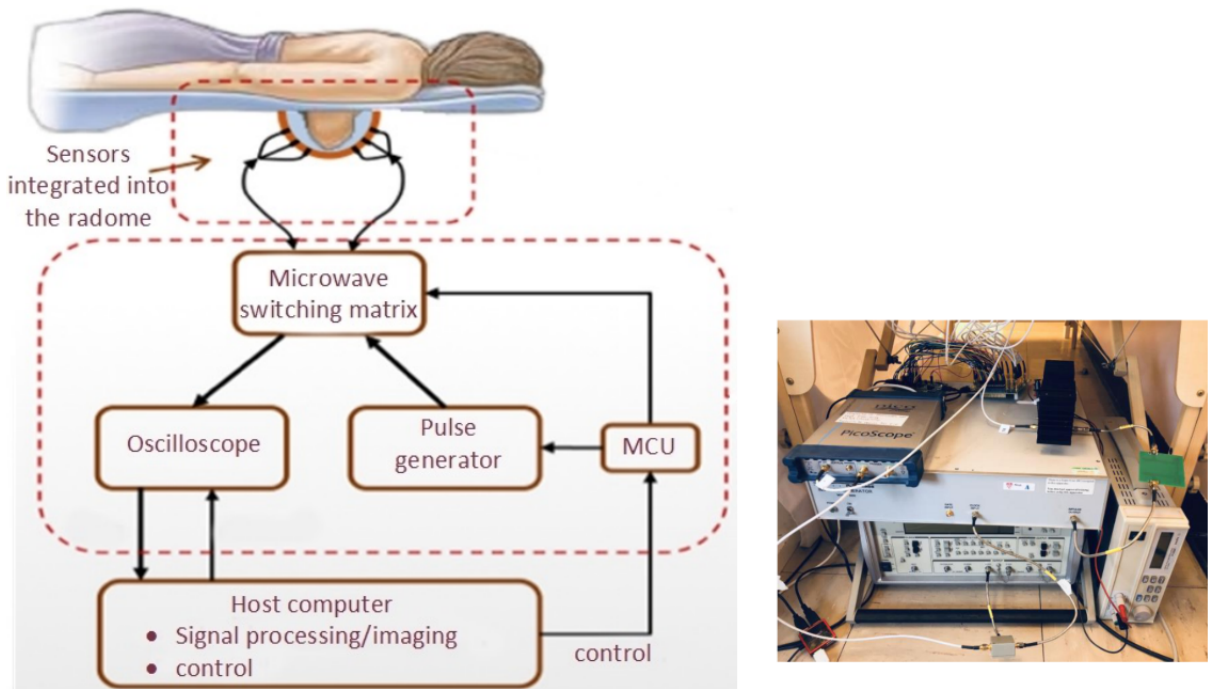


Figure 22 – System prototype illustration and some equipment.
Source: (LI et al., 2017).

A short-duration Gaussian-modulated pulse (2.0-4.0 GHz frequency range) is generated through the Pulse Generator (PG), which is fed into the switching matrix. An equivalent-time sampling oscilloscope (picoScope) records the data collected by the receiving antenna. The antennas are settled in a hemispherical dielectric radome, which is a ceramic dielectric made from alumina (with relative permittivity $\epsilon_r = 9.6$). The antennas and the radome are fixed, and the switching matrix controls the antennas until all possible combinations have been cycled through.

All the mentioned equipment is placed under a table, so a patient lies in the prone position, with her breast in the radome. As it is designed to be the largest possible breast size, a coupling liquid is required to fill the gap between the breast and the radome walls. An ultrasound gel was used, with relative permittivity $\epsilon_r = 68$ and conductivity $\sigma = 3$ S/m at the center frequency of 3.0 GHz.

A second-generation prototype was first proposed in 2016 (PORTER et al., 2016). Its advancement is the wearable patient interface, with no need for the patient exam table; it does not require immersion medium, and, due to a close fit with the fabric hosting the antenna array, the position of the breast relative to the array is known. Differences also include the use of a monopole antenna instead of a traveling wave and the elimination of the ceramic radome as well.

Figure 23 shows this second-generation settled, with the sixteen flexible microwave antennas coupled to a bra.

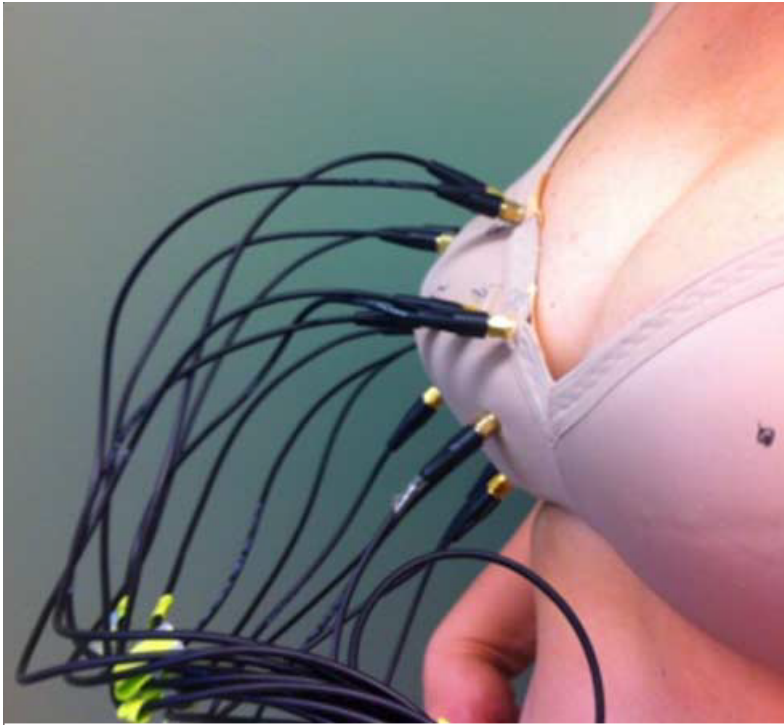


Figure 23 – Wearable prototype fitted to a volunteer.

Source: (PORTER et al., 2016).

For both prototypes, data were collected daily for one month. The inner breast representation was built using the algorithm Delay-Multiply-and-Sum (DMAS) method. Scans with the wearable prototype on a healthy volunteer were performed and the resulting data were compared with those collected with the table-based prototype and demonstrated that the wearable prototype is an improvement over the table-based one. Taking into account this latest solution, (KRANOLD; POPOVIC, 2021) has reported that its multistatic system can detect tumors as small as 1.0 cm in diameter in fat or embedded in the gland, based on phantoms developed.

Recently, (KRANOLD et al., 2021) presented a huge step forward in seeking miniaturization and cost reduction of the system apparatus, replacing both the PG and a clock generator by an Integrated Circuit (IC) of CMOS technology, which generates UWB pulses of bandwidth close to 1.0 GHz with an adjustable center frequency. The IC consists of two oscillators, one of them to generate a 3.0-6.0 GHz RF signal; a narrow-pulse generator; and an RF mixer.

Currently, the group focuses on clinical trials, whose objectives include verifying patient comfort, repeatability of the scan, and how patient movement affects results. The patient position is still a great concern, along with the coupling medium and the need to ensure hygiene.

3.2.4 Galway University - IE

The Translational Medical Device Lab (TMDV, 2021), located at the University College Hospital Galway, Ireland, counts on a diverse team of researchers that bring medicine, science, and engineering together to advance healthcare technologies. Led by Dr. Martin O'Halloran, co-author of the survey (O'LOUGHLIN et al., 2018) and the book (CONCEIÇÃO; MOHR; O'HALLORAN, 2016), the lab has focused on developing medical devices, among which, its remarkable system for breast screening is called Wavelia.

Figure 24 shows the system table. It is made up of two subsystems: microwave breast imaging and optical breast contour detection, which serve to provide the total volume and boundary contour of the breast, prior information for the microwave breast imaging subsystem. Its first in human clinical investigation was conducted in 2018, whereas test were performed with the Wavelia and reported in (FASOULA et al., 2018).



Figure 24 – Photograph of the Wavelia device in a hospital.
Source: (MOLONEY et al., 2022).

Wavelia subsystem employs multistatic radar detection; scanning is performed using a network of eighteen wideband Vivaldi-type antennas. The antennas are positioned in a circular horizontal configuration, performing a vertical motion so that the full breast volume is appropriately illuminated during the scan. As in most reported systems, during

examination, the patient lies in a prone position on the examination table with her breast in a circular opening. Besides, a coupling liquid is used to fill the gap between the breast and the antennas, which was designed to have a real permittivity that well matches the permittivity of the human skin. Wavelia uses a VNA in its front-end implementation, resulting in an emission/reception RF chain with a dynamic range of 75 dB.

The Wavelia validation is further discussed in (MOLONEY et al., 2019), which includes realistic asymmetric tumor shapes and sizes in a breast phantom, which was manufactured by solid mixtures of graphite, carbon black, and urethane. Figure 25 illustrates two acquisition experiments, in which the antenna center positions are depicted with purple dots. The system produced images that can be clearly associated with the unambiguous detection of tumor phantom inclusions within breast molds.

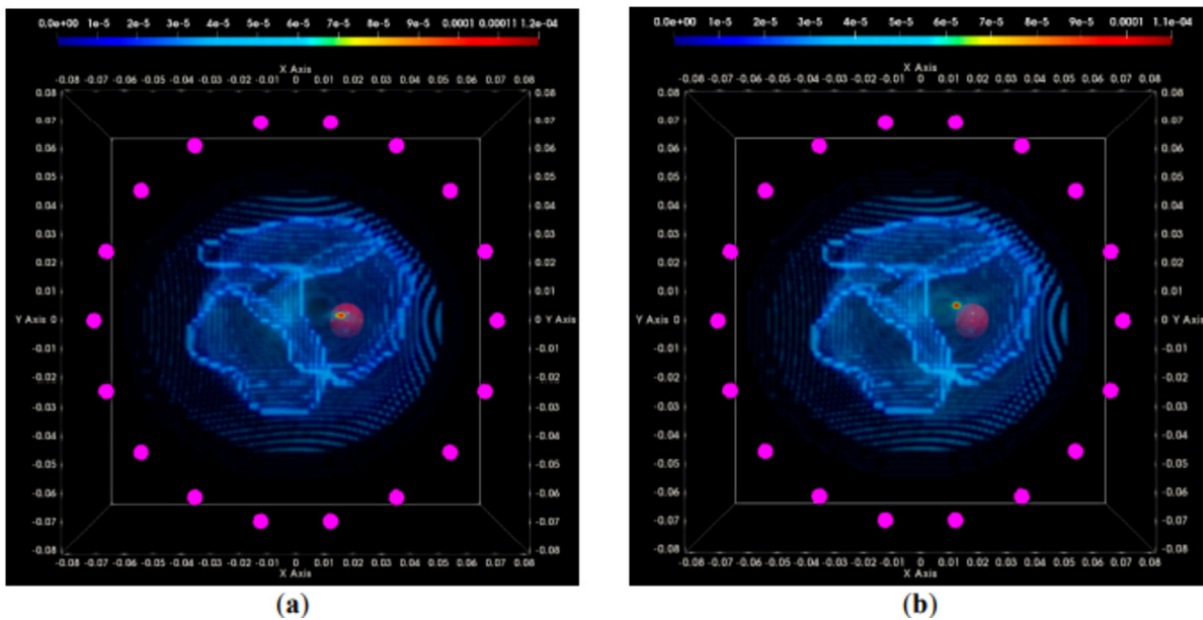


Figure 25 – Results from different acquisition days.

Source: (MOLONEY et al., 2019).

After preprocessing the signals and calibrations, the device uses the Time-Reversal Multiple Signal Classification (TR-MUSIC) algorithm to generate breast interior images.

3.2.5 Chalmers University of Technology - SE

The Chalmers University biomedical electromagnetic research group has made efforts to perform microwave diagnostic imaging systems, mainly with Prof. Xuezhi Zeng (ZENG, 2021) and Andreas Fhager (FHAGER, 2021). Professors believe in the potential of MwI to eventually replace current screening modalities and also to perform imaging examinations to follow up on patients undergoing breast cancer treatment. Figure 26 shows this first solution presented in 2013.

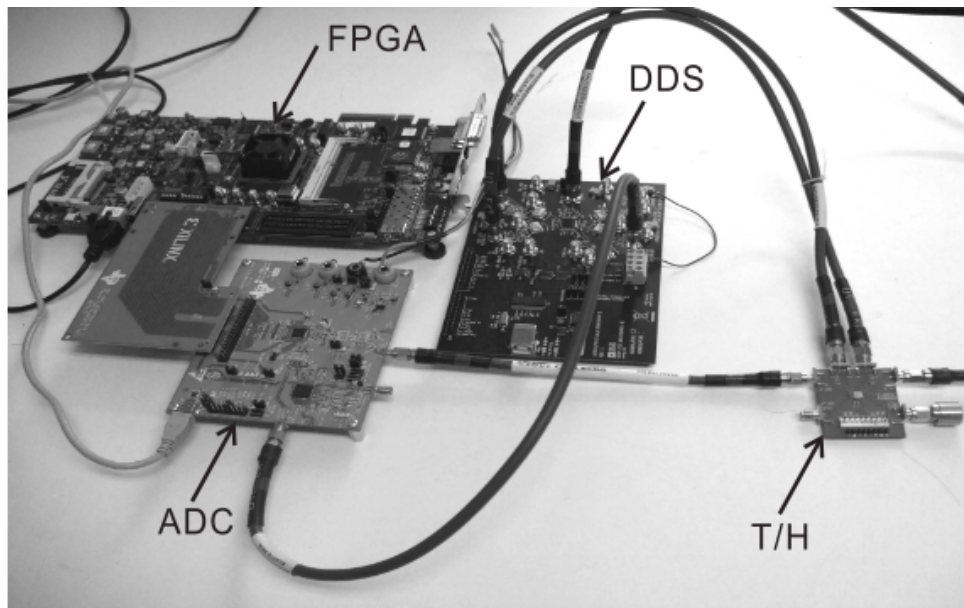


Figure 26 – Photograph of the system prototype devices.

Source: (ZENG, 2013).

Prof. Zeng's Ph.D. Thesis proposed the first-time domain system prototype based on off-the-shelf components such as an Analog-Digital-Converter (ADC), Track and Hold (T/H), Direct Digital Synthesis (DDS), and Field-Programmable Gate Array (FPGA) circuits. As seen in (ZENG, 2013), the system frequency range chosen is from a few hundred megahertz to about 3.0 GHz, and the pulse is generated by an Arbitrary Waveform Generator (AWG). With that, it achieves reasonable signal penetration and resolution.

3.2.5.1 SDR-based system

Similarly to DC, Chalmers University proposed using the Universal Software Radio Peripheral (USRP) SDR instead of the off-the-shelf components, as discussed in a Master Thesis (OROZCO, 2019). Moreover, (ZENG; OROZCO; FHAGER, 2019) proposed two different calibration strategies for proper phase measurements using SDR to implement a MwI system.

The fact that this well-established group has used SDR technology as an apparatus to deal with EM signals reinforces that it is suitable for the development of MwI systems.

3.2.6 University of Perugia - IT

The Physics and the Diagnostic Imaging departments of Perugia University developed a UWB microwave apparatus called MammoWave, from which collected signals are processed by the Huygens Principle (HP), providing images that represent homogeneity

maps of the breast (VISPA et al., 2019).

A horn antenna, operating as a transmitter in the frequency band from 1.0 to 9.0 GHz, is used to strike breast tissue with microwave signals, while a microstrip monopole antenna, operating as a receiver in the same frequency range, is used to collect reflected microwave signals (SANI et al., 2016). To this end, the woman's breast (one per time) fits a hub with a cup when the patient lies in the prone position on the examination table, as depicted in Figure 27 described in (SANI et al., 2017).



Figure 27 – Mammowave system apparatus.

Source: (SANI et al., 2017).

This system does not require any matching liquid. Two arms perform the rotation of the hub with the TX and RX antennas, which are connected to a VNA (Cobalt C1209, Copper Mountain). Thus, the frequency domain system retrieves the S_{21} signals and processes them by the HP.

3.2.7 Hiroshima University - JP

All radar-based systems presented (Sections 3.2.1 to 3.2.6) used a VNA or related instrument, i.e., a commercial pulse generator and oscilloscope, to generate and acquire microwave signals. Besides the system seen in 3.2.3, which has recently replaced its front-end system with an IC. Prof. Takamaro Kikkawa, from Hiroshima University, has been working and publishing on early breast cancer detection for more than 10 years. His last and more complete work results in a hand-held impulse-radar detector, fully described in (SONG et al., 2017), which is the first system implemented using CMOS technology circuits able to detect a malignant breast tumor.

This system does not need any off-the-shelf large and expensive equipment and its functionality is demonstrated in the clinical test at Hiroshima University Hospital. Figure

28 presents the system block diagram, in which the blue parts correspond to receiver blocks, while the red ones correspond to the transmitter blocks.

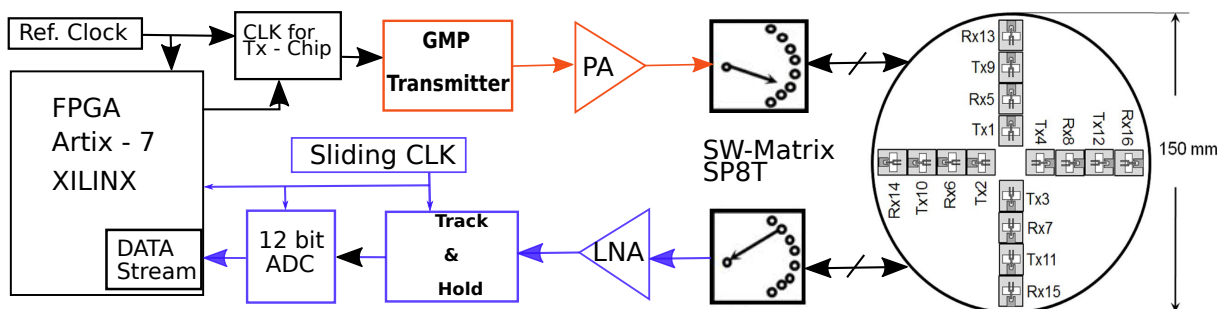


Figure 28 – Architecture system diagram.

Source: (SONG et al., 2017).

The system prototype is designed to be placed on the breast with the patient in the supine position, not prone as in most of the systems presented. It has functional modules such as a Gaussian monocycle pulse (GMP) generation, a switching (SW) matrix, and a receiver. A 4x4 cross-shaped dome planar UWB antenna array, detailed in (SUGITANI et al., 2013), comprises the transmitter and receiver antennas to the microwave signals. This array is placed on the breast with a coupling liquid (glycerin), and a step-motor rotates the array. After collecting the signals, a 12-bit ADC is placed and the data stream is stored in an FPGA for post-processing.

The GPM transmitter, detailed in (KUBOTA et al., 2014), generates a periodic UWB Gaussian pulse with a width of 160 ps with a center frequency of 6.0 GHz, and thus a bandwidth of around 6.7 GHz. Once the pulse is generated, it is placed on a Power Amplifier (PA) and fed into the antenna port by the connector. To change the operating antenna pair, two single poles eight-throw (SP8T) switching matrix modules are employed.

To receive and record the reflected signal from the breast, whose duration is very short, a high-speed sampling circuit is necessary, mainly consisting of a track and hold and a 12-bit ADC block (TOYA et al., 2013). The equivalent time sampling method is employed; by sliding the phase of the clock, the sampling is conducted in a slow-motion-like process. The first circuit to receive the reflected signal is a Low Noise Amplifier (LNA), whose system noise is around -75 dBm. A modified version of the classic DAS algorithm reconstructs the breast image to identify the inner target position.

(ADACHI et al., 2021) reports the ability of the proposed apparatus to detect breast cancer in ten real patients. Images were produced without issues related to the patient's complaint or device malfunction. All patients also underwent a mammography examination. Breast cancers were detected in all patients by microwave imaging, which means a sensitivity of 100%. In contrast, the mammography test has not detected the tumor in two patients with dense breasts, which means a sensitivity of 80%.

3.2.8 University of São Paulo (USP) - BR

The USP, under Prof. Wilhelmus Noije's supervision, is in the process of developing an impulse radar microwave imaging system applied for breast cancer detection. It is focused on the realization of low-cost and portable system prototypes. As described in (ARAGÃO et al., 2023), a built-in antenna and transceiver time-domain UWB hardware platform were chosen, employing a 6.4 GHz operational frequency and 2.17 GHz bandwidth, with signals applied to an equidistant 64-angle. whereas custom firmware, software, and communication protocol were developed from scratch contemplating the hardware control and exam routines. A standalone apparatus on a handheld support that fits in a custom-developed bra allows the handheld system to be rotated around the breast, as depicted in Figure 29a. Meanwhile, the backscattered signals are collected and processed by an improved confocal algorithm, also developed by the USP researchers group (ARAGAO et al., 2020a). An energy map image is then generated after all predefined positions are measured, as shown in Figure 29b.

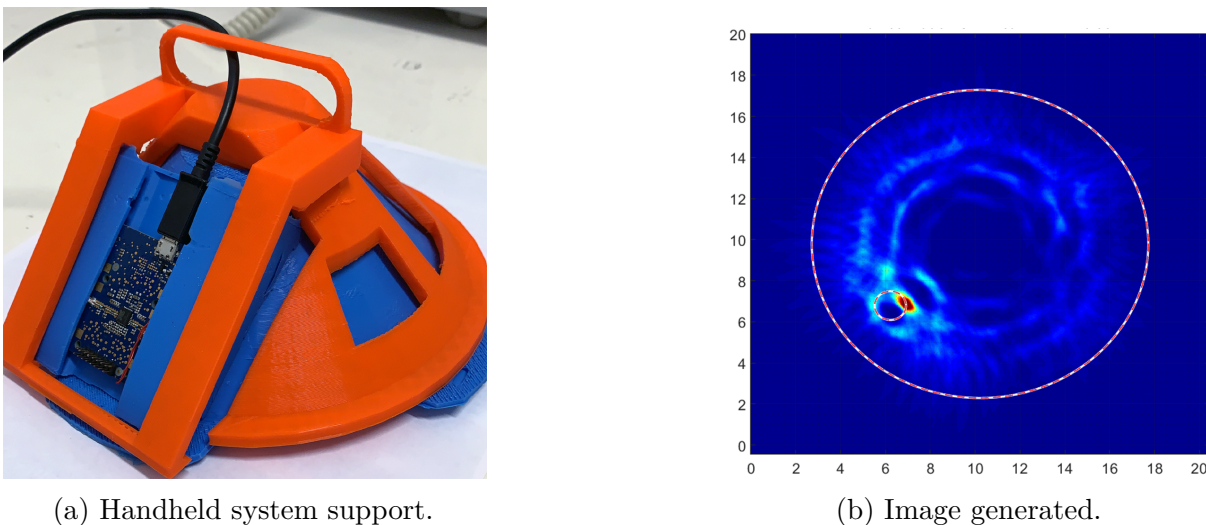


Figure 29 – USP System results.

The entire system cost has been US\$ 175.00, and it was developed focusing on clinical usage. Experimental tests were performed using a breast phantom which employed materials with dielectric constants similar to real breast tissues. The hardware receiver minimum signal was -87.32 dBm with 64.00 dB DR which is compatible with breast cancer MwI detection (calculated and simulated breast tissues total loss for a maximum distance of 5.0 cm depth in the breast was 59.00 dB). The portable apparatus was able to detect a 1.0 cm tumor buried 3.0 cm deep into a 15.0 cm diameter breast, and based on the calculations and simulations results, a 0.6 cm diameter tumor would be detectable by this system proposal, which is detailed in the Ph.D. Thesis (ARAGÃO, 2021).

3.2.9 University of Queensland - AU

Prof. Amin Abbosh (ABBOSH, 2021) and his group supervised several works related to EM medical imaging focusing on breast cancer and brain stroke detection (STANCOMBE; BIALKOWSKI, 2019) for more than a decade. He supervised the Ph.D. Thesis (MARIMUTHU, 2016), with pioneering work relating SDR to a MwI system. It proposes a monostatic tapered slot antenna system that successfully detects small targets embedded in a liquid mimicking different human tissue properties, as depicted in Figure 30.

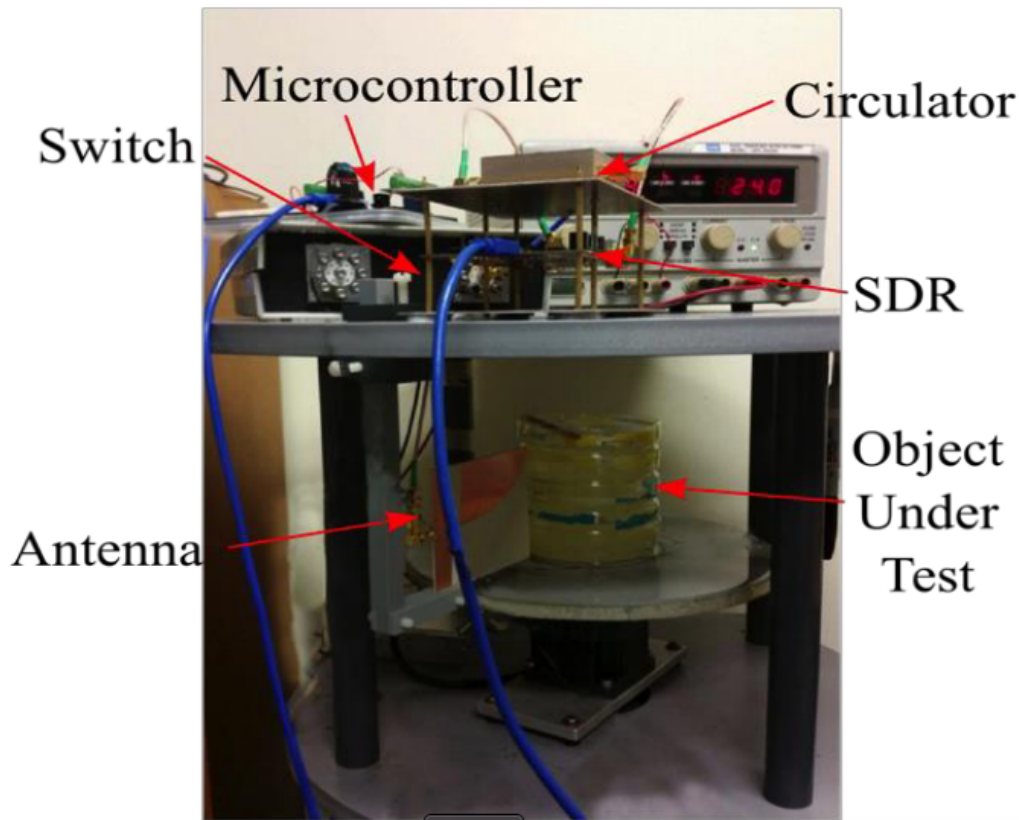


Figure 30 – SDRadar proposed by Marimuthu.

Source:(MARIMUTHU, 2016).

A rotating platform was developed to reach a virtual array of 20 elements with 18° separation. It implements the SFCW radar approach for a frequency band of 1.2 to 2.14 GHz with a constant transmit power of -20 dBm. The SDR is connected to a personal computer via a USB cable, which is also connected to a microcontroller via an ethernet cable. The tapered slot antenna is placed 0.78 cm from the center of the rotating circular platform. The object under test has a ball-metal target of 1.5 cm that was properly identified.

Currently, this group is dedicated to brain imaging aimed at stroke detection. The work (COOK et al., 2021) reports preliminary image results.

3.3 Combined approach

3.3.1 Politecnico di Torino - IT

The research group at Politecnico di Torino University has developed and implemented MwI systems for breast cancer detection. The thesis (GUO et al., 2014) shows a UWB system specification for this application. However, (CASU et al., 2017) have implemented and used a different system, whose blocks are shown in Figure 31. This system approach is based on the Interferometric-Multiple Signal Classification (I-MUSIC), which is not tomography, once belongs to the linear scattering techniques; neither Radar-Based UWB, because I-MUSIC does not require a large bandwidth, using eleven discrete frequencies chosen between 1.4 and 1.6 GHz. Beyond that, I-MUSIC does not require a pre-characterized response of the system antennas, which is a pair operating in bistatic mode (one transmitting and one receiving).

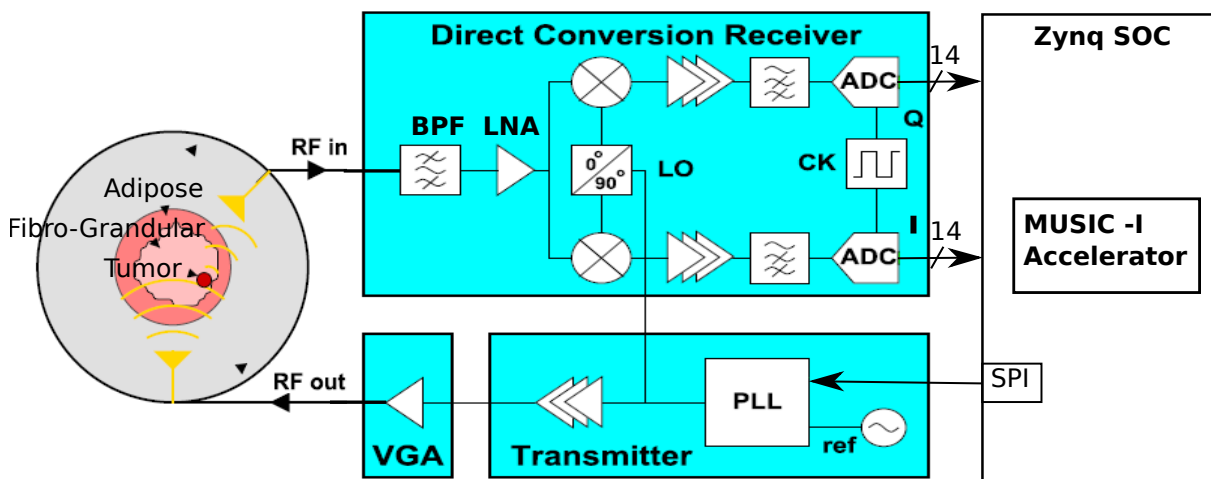


Figure 31 – Architecture system diagram.

Source: (CASU et al., 2017).

The implemented system operation relies on a transmitter to generate a RF signal, whose frequency is defined through an embedded processor in the Zynq System-on-Chip (SoC). The SOC configures, by SPI, the PLL (Phase-Locked Loop) to synthesize an interest frequency. The authors have experience with embedded system co-design, as seen in (CASU et al., 2014). An antenna that radiates a tank with the RF signal out has its signal amplified by a Variable-Gain Amplifier (VGA). The tank contains a coupling liquid (water + glycerin) and a breast phantom with a tumor.

The scattered signal is received by the other antenna, which transmits the RF signal to a direct conversion (DC) receiver. The addition of the band-pass filtering (BPF) receiver path and LNA helps increase the performance of the DC receiver. The in-phase (I) and quadrature (Q) outputs of the DC receiver are digitized into 14-bit words and

sent to the SoC to be processed. The two antennas are rotated by a brushless motor that maintains an angle of 135° between them. The authors discuss that all the RF parts colored in light blue in Figure 31 could be replaced by a conventional VNA.

With the system previously described, it acquired data of the scattered field between 1.4 GHz and 1.6 GHz, which is where the receiver board is best matched, in 20-MHz steps. In addition, with a VNA, data were collected in the same bandwidth for a fair comparison. Nonetheless, it was also scanned between 0.5 and 3.0 GHz. The aim was, first, to evaluate the accuracy of the proposed system compared to the VNA. Secondly, it was assessed whether relevant information is lost when considering only the 1.4–1.6 GHz range. Comparing the results, the authors conclude that I-MUSIC is capable of identifying a tumor in an ideal condition.

3.4 MwI system - Spin-off

Although a public skepticism barrier and medical reluctance must be overcome, some spin-offs have become a tangible reality in the commercialization of a MwI device for breast cancer detection. Following will be described the patient evaluations performed by four systems and their companies.

- Micrima - Maria Device:

Micrima, a spin-off of Bristol University, has already installed the MARIA device in several imaging centers such as Athens (Micrima, 2021). Furthermore, the clinical results reported in (SHERE et al., 2019) are very promising, where 225 patients have been evaluated, 170 cases were classified as a 'hit' and 55 as a 'miss'. Additionally, the smallest recorded lesion size, which was classified as a 'hit' with MARIA, had a diameter of 0.5 cm. The classification 'hit' and 'miss' means, respectively, when there is a good correspondence in the location of an area of high intensity in the MARIA image and the known location of the lesion from the clinical diagnosis; and when it does not identify any areas of high intensity in the target location or identifies an area of high intensity in a different location compared to the clinical notes.

- Microwave Vision Group - Wavelia:

Microwave Vision Group, a spin-off of Galway University that is on its way to commercializing the WaveliaTM device. (FASOULA et al., 2021) has reported the first clinical investigation in 25 patients, the results of which demonstrated the ability to detect and discriminate between palpable malignant and benign breast lumps.

- Umbria Bioengineering Technologies (UBT) - Mammowave:

UBT, a spin-off of the University of Perugia that received a commercial venture for the Mammowave device, which was used for clinical trials in 22 breasts without lesions and 29 having it, results of which were presented in (SANI et al., 2019). Further trials are ongoing at Perugia Hospital, S. Maria Della Misericordia, and Foligno Hospital according to (UBT, 2021).

- MITOS Medical Technologie - SAFE:

MITOS, an ITU spin-off, was created in 2010 to design, develop, and commercialize its MwI system for breast cancer diagnosis. (JANJIC et al., 2022) reported 113 patients evaluated with SAFE for breast cancer early detection, which was approved by an ethics committee. The SAFE efficacy distinguishes benign and malignant breast lesions with an overall 79% sensitivity, 77% specificity, and 78% diagnostic accuracy, concluding that it reaches a correct classification of 79% of breast lesions.

3.5 Discussion

In contrast to the gold standard for breast cancer detection, MwI irradiates harmless levels of microwave energy, which is safe in terms of the Specific Absorption Rate (SAR) (BENNY; ANJIT; MYTHILI, 2020). In addition to that, MwI has the potential to detect a tumor in a dense breast, among other benefits discussed in this work. These facts motivate the interest of different research groups. However, MwI requires a very complex system realization as a result of the patient's idiosyncrasy and dielectric property scenarios. Due to that, several approaches have been taken, as shown in this Chapter 3 and discussed next.

3.5.1 Apparatus

3.5.1.1 VNA based

Regarding the hardware apparatus of MwI systems, the four previously mentioned spin-off devices are VNA-based systems, often used due to its high availability and accuracy, as mentioned in (AKINCI et al., 2015). (SHAO; MCCOLLOUGH, 2020) listed twelve research groups investigating breast microwave medical imaging, out of which five have used a VNA as the main apparatus to deal with EM waves. Moreover, according to (MEANEY et al., 2019), the attractiveness of VNA for MwI measurements is due to its ability to collect coherent data that illuminate a breast for image generation in both amplitude and phase information.

In conclusion, it is possible to say that the VNA simplifies a MwI system development, allowing to focus on algorithms to deal with the retrieved signals to imaging generation, or in the antenna design along with its operational band. However, in the observed systems implemented, the VNA is an expensive and bulk instrument, with more functionalities than MwI requires, which makes it not indicated for portable and low-income MwI development groups. Besides that, there is a cheaper and portable VNA, known as NanoRFE VNA6000 from HCXQS group (NanoRFE/HCXQS, 2024), which was not analyze in this Thesis once there is no MwI system employing such VNA.

3.5.1.2 IC based

Very few systems have been dedicated to implement a MwI based on ICs besides its portability potential, such as those shown in Sections 3.2.8, 3.2.7, and 3.2.3, which have employed an IC that replaces some blocks or instruments while developing a MwI system.

Notably, IC block employment requires its development and tests efforts; also production and validation stages. As these stages are also expensive, the usage of IC is more indicated in the high-scale product volume because of its manufacturing cost being diluted per product.

3.5.1.3 SDR based

Finally, seeking a low-cost and portable platform for prototyping and research, the SDR-based system has evolved for medical imaging, due to its reconfigurability and high range resolution, as shown in Sections 3.1.1 and 3.2.5. Due to that, this Ph.D. Thesis follows with an SDR assessment aiming at microwave breast cancer detection, which is detailed in Chapter 4.

3.5.1.4 Antenna

The antenna plays a crucial role in transmitting microwave signals into the breast tissue and receiving scattered signals for image reconstruction. It is important to mention that the choice of antenna type, array arrangement, and design depends on various factors, including imaging technique, system requirements, frequency range, and desired performance characteristics. Although the multistatic configuration is more complex than the monostatic configuration, it can provide more information about the illuminated target, making the parallel data acquisition strategy dominant among the reported systems. Moreover, wearable breast cancer detection is a target that more concerns antenna design, as seen in (ELSHEAKH et al., 2023).

It should be mentioned that most systems employ the same antenna type for transmitting and receiving, once the same antenna may operate in both functions. However, the Mammowave system, from the University of Perugia, has employed two different types of antenna, one for transmitting and the other for receiving the RF signals. This is the only observed MwI system with this antenna arrangement, and it is worth raising the pros and cons of such an approach.

3.5.2 Clinical Acceptance

It is possible to assert that MwI systems have not yet been found to meet all the requirements between academia and industry, since they are not yet commercially available and no exam procedure is offered to patients seeking breast cancer. This affirmation is supported by (PORTER; O'LOUGHLIN, 2022), which shows the efficacy of the MwI system, but also raises the fact that no system has achieved clinical acceptance or usage to date. One possible reason for this is the fact that the market for medical diagnosis is driven much more by incremental innovations in existing characteristics, such as digital breast tomosynthesis (DBT) and digital mammography, which reduces the exposure to ionizing mammography.

In light of available information, MwI can be seen as a disruptive innovation that requires a different approach to the way medical imaging is performed, which may cause some resilience. Furthermore, as noted in (UTTERBACK, 1995), as products and industry become more specific, greater resilience is placed on new full products. Thus, hard clinical acceptance was verified more often by physicians than by product development, according to (BOLOMEY, 2018), which also mentioned that MwI for medical applications has been developed for more than 30 years, exceeding any other modality.

Chapter 4

SDR Assessment

MwI system is designed to reveal a woman's breast tumor in a completely harmless and painless examination throughout EM signals, which enables early tumor detection even in a dense breast. The most advanced systems have incorporated a VNA to transmit and receive microwave signals while measuring the scattering parameters (s-parameter). Typically, it employs the SFCW waveform to perform its measurements in the frequency domain. The received signals are normalized and then transformed into a synthetic pulse in the time domain using the IFFT, which corresponds to an impulse-based UWB, retrieving the target signal information.

Considering MwI systems operating in the frequency domain, a VNA is the most common equipment due to its high availability and accuracy, as already mentioned, beyond the support of large companies such as Keysight; however, it is expensive, bulky and has more functionalities that are not required for MwI, noted by (TAKAHASHI; MIWA, 2019), making it unsuitable for research and prototyping. Furthermore, the VNA calibration procedure typically requires additional components provided by the manufacturer, often referred to as the calibration kit.

In turn, SDR, a promising low-cost programmable platform development, is tailored to measure the s-parameter dealing with the SFCW radar implementation, as described in Section 2.5. An SDR advantage is that its calibration procedure could be inserted as an intern routine, which does not require a calibration kit. Moreover, the SDR is also supported by large companies, such as National Instruments.

This Chapter reports on the experiments performed to evaluate the vvin both: radio power ability and programmability to realize a synthetic pulse. The former shows to be versatile while meeting the requirements for finding a breast tumor using EM waves. The latter rises to expose the challenges of implementing an SDR as a VNA. To measure BladeRF 2.0 in terms of power, a PA and an LNA were coupled to its SMA interface.

A breast phantom mimicking a heterogeneous breast was used as the signal propagation medium instead of the air. It is better discussed and shown further in this Section and was first employed in (ARAGAO et al., 2020b) where a 11.0 cm silicone rubber base acted as a coupling medium and the skin was simulated through a sorbitol layer. Sand was used as fatty tissue, and the glandular area was mimicked with liquid glycerin. This phantom was also considered in the Simulia CST Studio Suite® (CST) simulation aiming at synthetic pulse implementation to an inside target identification. The simulation results will be presented in this Chapter 4.

4.1 Nuand - BladeRF 2.0

BladeRF 2.0 was developed by Nuand™ to be a versatile SDR device that provides full duplex operation of up to 40 MSPS with an instantaneous bandwidth of 56.0 MHz. As shown in Figure 32, the Cyclone V FPGA is at its heart, performing, for example, Automatic Gain Control (AGC) or providing an embedded waveform, and interfacing with both the Cypress FX3 peripheral controller and the AD9361 RF transceiver (Analog AD9361, 2016). The latter is composed of ADCs and DACs featuring 12-bit resolution, delivering a native DR of 74 dB, which can be increased by averaging techniques, the same as used in most of the VNAs.

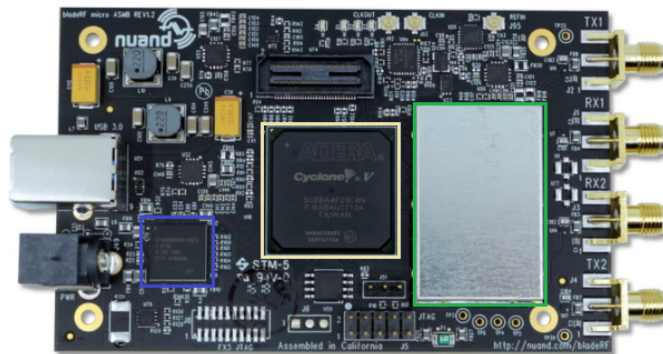


Figure 32 – BladeRF2.0 board. FX3-blue square, FPGA-yellow square, Transceiver-green square.

BladeRF 2.0 also provides two TX and two RX SubMiniature version A (SMA) interfaces, allowing performing multi-input multi-output. This is useful when a system is running with multiple antennas. Moreover, it is possible to use one channel (TX-RX) to have a reference of the transmitted signal waveform to perform system compensation or calibration. It is known that the feed-through nulling reduces the bleed-through signal.

Both the TX and RX signal strength can be increased by the means of coupling a PA and an LNA, respectively. The former, known as BT-100, increases the output signal

power by at least 10 dB; while the latter, called as BT-200, increases the gain by at least 16 dB. The use of these amplifiers will depend on the BladeRF 2.0 application.

4.1.1 Transceiver AD9361

The Analog Devices[®] AD9361 transceiver block diagram is depicted in Figure 33. The TX band ranges from 47.0 MHz to 6.0 GHz, while its RX band ranges from 70.0 MHz to 6.0 GHz, covering most of the operational frequency for Mwi system implementation. Each RX subsystem includes independent automatic gain control (AGC), dc offset correction, quadrature correction, and digital filtering, thus eliminating the need for these functions in the digital baseband according to (Analog AD9361, 2016). Moreover, it also provides self-calibration to maintain a high-performance level under temperature and input signal varying conditions, which is a crucial feature of Mwi systems. Both channels were assessed with the BladeRF 2.0, once this transceiver is incorporated on the board.

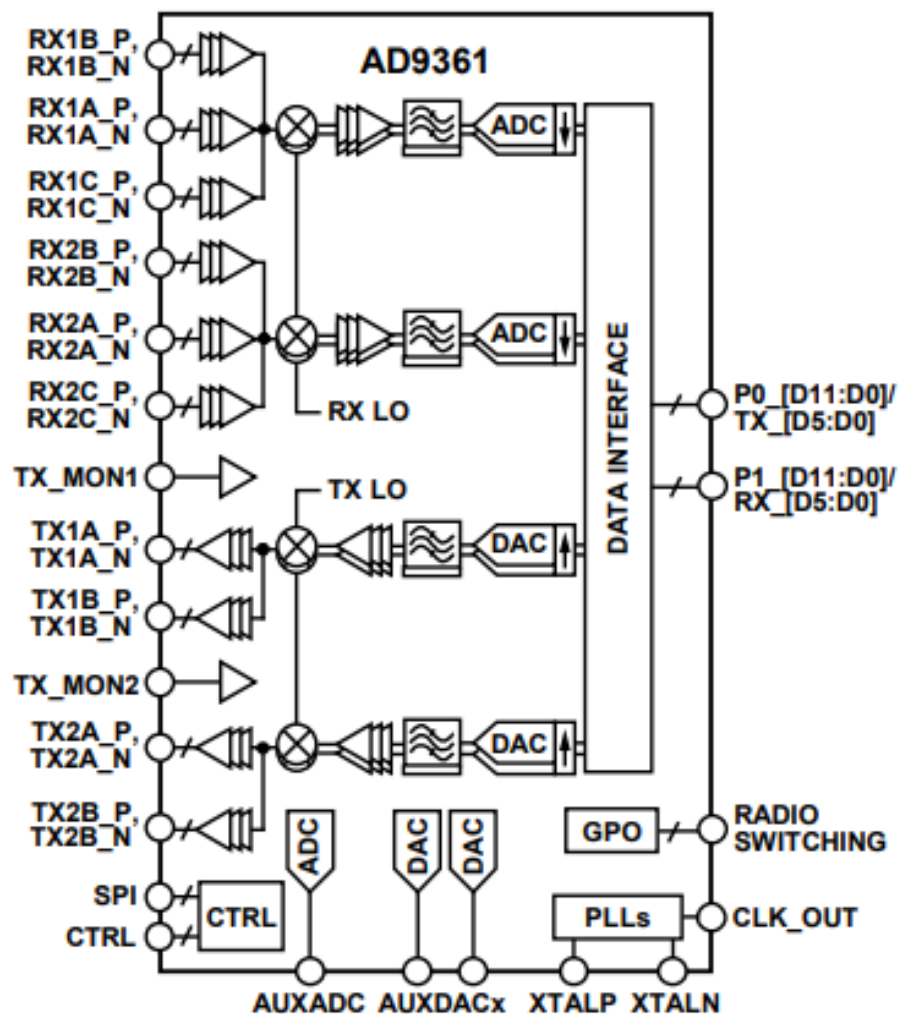


Figure 33 – Transceiver block diagram.

Source: (Analog AD9361, 2016).

4.2 Vivaldi Antennas

Important factors to be considered during antenna selection for a radar-based Mwi system are its UWB range capability, high signal fidelity, stable radiation patterns, compact size, and gain. There is a tradeoff between the antenna gain and beamwidth that implies how the signals reach the target, which means that the higher the gain the narrower the beam. Vivaldi antennas (and their variations) have some advantages, such as improved bandwidth, radiation patterns, high fidelity, and low cost, according to (MISILMANI et al., 2020). In addition, the high fidelity with a tapered slot antipodal Vivaldi antenna is reinforced in (SAMSUZZAMAN et al., 2019). Therefore, they have been widely used since the Vivaldi antennas effectively meet most of the requirements of a UWB antenna for a radar-based Mwi system.

The TX and RX Vivaldi antennas used in the performed experiment were described in the Ph.D. Thesis (ASCAMA, 2010), which proposes its usage for people buried detection considering a frequency range from 2.0 GHz to 4.0 GHz. The antennas were manufactured with the R03003 substrate; connected with the SMA microstrip transmission line whose impedance matches 50Ω . These antennas were used motivated by their availability, once they were at USP, and tailored UWB response.

Unlike its original operating frequency region, the Vivaldi antennas will operate in a frequency range from 1.0 to 6.0 GHz. Therefore, the CST has simulated to predict their behavior on those frequencies. A higher gain was observed at higher frequencies, such as 8.64 dBi at 6.0 GHz, as shown in Figure 34, against 4.0 dBi at 1.0 GHz.

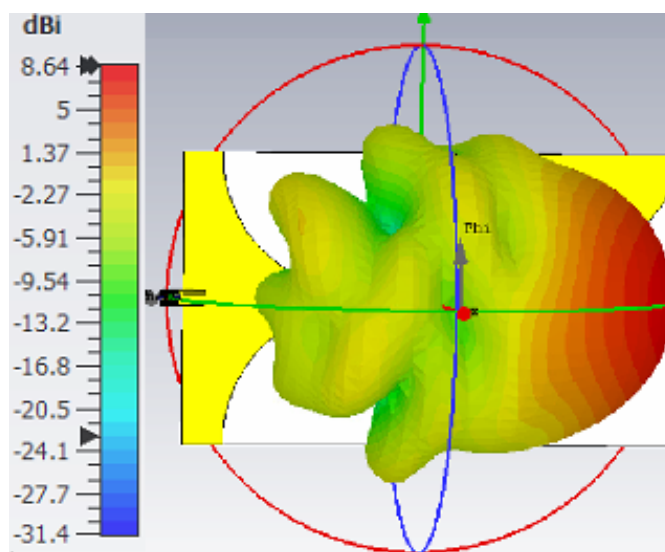


Figure 34 – Simulated radiation pattern of the Vivaldi antenna at 6.0 GHz.

A drawback of the Vivaldi antenna is its size, which makes a wearable solution impractical. The current antenna, shown in Figure 35, is large and impossible to be

embedded in a bra as those one shown in Figure 23. Nonetheless, these antennas were functional to assess the BladeRF 2.0 SDR.



Figure 35 – Picture of the employed vivaldi antenna.

4.2.1 Simulation with Phantom

A further CST simulation was performed considering the mentioned phantom properties and the Vivaldi antennas for propagation loss reference, which blocks diagram is shown in Figure 36. This simulation calculated the S-parameter (S_{21}) between the Vivaldi antennas (TX and RX) with and without the breast phantom. The frequency varies from 1.0 to 6.0 GHz. The results of these two simulations are presented in Figure 37.

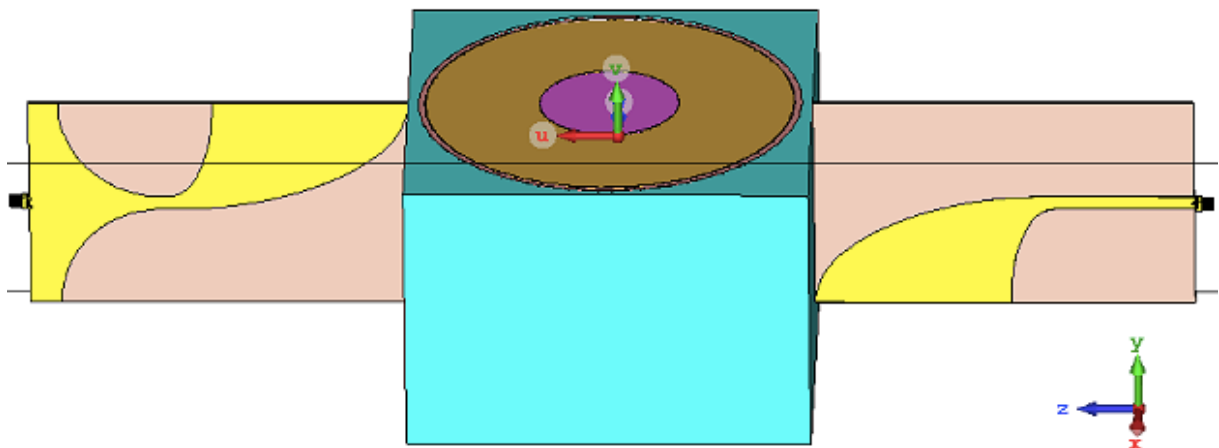


Figure 36 – Simulation scenario with the breast phantom between TX and RX Vivaldi antennas.

In Figure 37 a higher propagation loss is seen with the breast phantom medium, once its dielectric properties induce higher attenuation. A similar result was observed in (KAUR; KAUR, 2020), including the noted lack of a huge attenuation at higher frequencies.

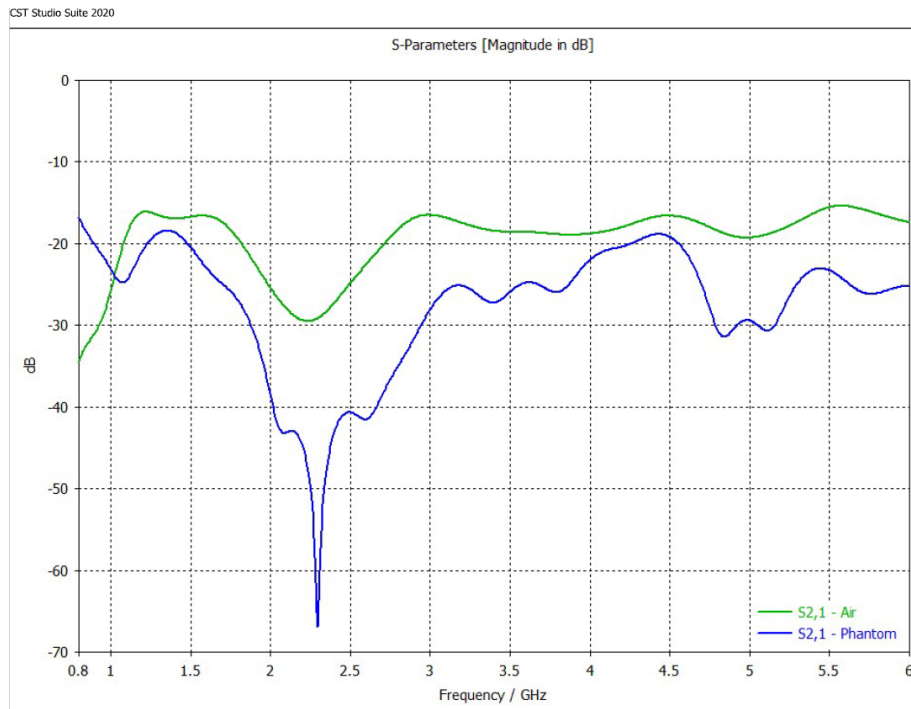


Figure 37 – S_{21} (dB) x frequency curves considering the Vivaldi antennas and different propagation media.

The observed higher attenuation between 2.0 and 2.5 GHz was not investigated but is not determinant in bladeRF assessment process, once it is likely to be an antenna feature due to its design. Worth to mention that this attenuation was not observed while measuring the manufactured antennas, as shown in Section 4.5.

4.3 BladeRF 2.0 - First Steps Programming

As a programmable device, BladeRF 2.0 supports different platforms. As the first approach aiming at familiarization, it was used the GNU Radio toolkit to perform an RF communication, which the main blocks are depicted in Figure 38.

It is composed of the signal source, providing a single frequency tone waveform; the osmocomb sink and source, which powers the BladeRF 2.0 TX and RX respectively; and a GUI interface. The osmocomb sink first assignment is to modulate the baseband to the RF signal, while the osmocomb source's first stage is to extract this baseband from the RF signal. The results of this first test were presented in Figure 13. It was an initial step useful to familiarize myself with the BladeRF 2.0.

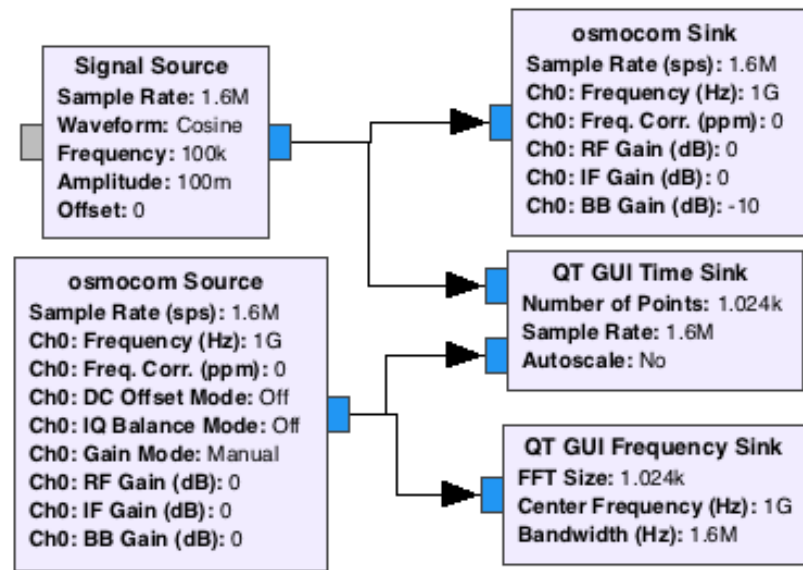


Figure 38 – GNU radio blocks for BladeRF 2.0 RF communication.

This first experiment consists of a baseband signal of 100 kHz modulated at an IF, which has been increased from 1.0 GHz up to 6.0 GHz by a 25.0 MHz step. The TX signal is straightforwardly collected by the RX antenna, while the antennas are positioned 15.0 cm away from each other with the radiation direction aligned. The IF value corresponds to the Ch0 frequency at Osmocom blocks in Figure 38.

This evaluation shows a native SNR close to 80.0 dB at 1.0 GHz and a reduction to around 63.0 dB at 5.0 GHz, as depicted on Figure 39. The results of this first experiment were published in (CARVALHO et al., 2020).

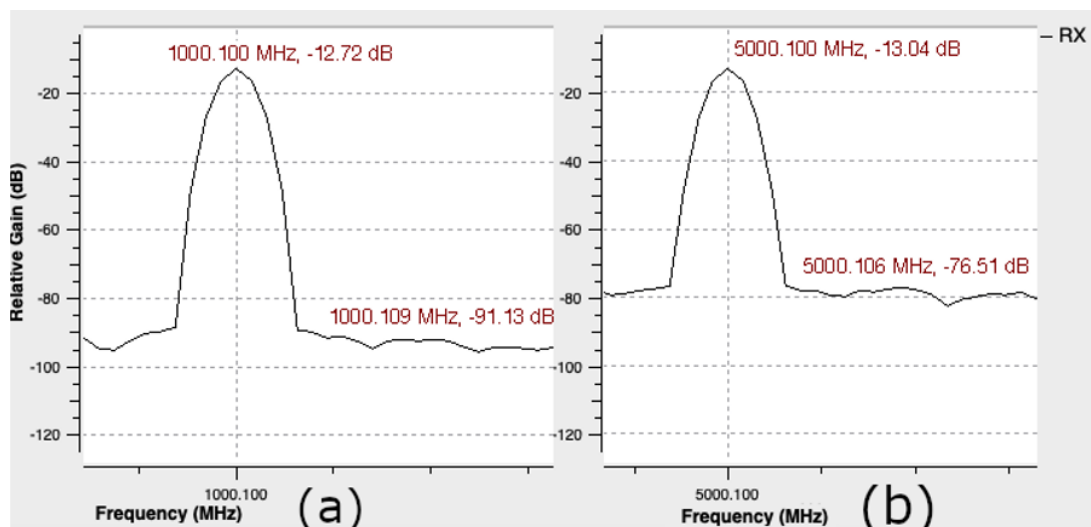


Figure 39 – SNR of RF signal at: (a) 1.0 GHz and (b) 5.0 GHz.

4.4 Assessment Setup

To carry out further BladeRF 2.0 evaluation, its transmission and reception power abilities were measured in two different media: the air and the developed breast phantom (ARAGAO et al., 2020b) that mimics the dispersive dielectric properties of breast tissues. Different from the first step described, its signals were coped with the BladeRF-cli (Command-Line Interface), a program built atop the BladeRF 2.0 library.

The VNA ZVA24 from Rohde&Schwarz[®] and the Spectrum Analyzer (SA) E4404B from Agilent[®] were employed to extract the BladeRF 2.0 figure of merit, along with the two Vivaldi antenna behaviors, which were mentioned in Subsection 4.2.

Moreover, a target resolution of 1.0 cm was defined once it is likely to be a localized tumor, leading to a synthetic bandwidth specification of the SFCW radar of 5.0 GHz. Thus, the BladeRF 2.0 carrier frequency increased stepwise from 1.0 GHz to 6.0 GHz (i.e., band of interest), implementing the SFCW approach. This frequency range deals with the attenuation issue and was utmost motivated by the results reported in Section 2.1.3. Moreover, these frequencies will almost explored the full board frequency range. Finally, it was used a 25 MHz step that was automatically increased while the results were saved.

4.4.1 Tests Procedure Over the Air

This Section will describe the steps taken to accomplish the BladeRF 2.0 and the vivaldi antennas assessment using the VNA and SA for measurements, considering the air as a propagation medium. The results of each experiment is demosntrated and discussed in the Section 4.5.

- First, the VNA measured the antennas S_{21} parameter in the band of interest. One cable connected to the RX SMA antenna interface was set on VNA port 1, while other cable connected the TX antenna to the VNA port 2. The antennas were positioned 11.0 cm spaced from each and the TX signal was straightforwardly collected, in accordance to the radiation patter, by the RX antenna. This distance, kept for all the other measurements, is related to the diameter of the bra model considered.
- Secondly, BladeRF 2.0 transmitter output power, coupled with BT-100, was measured throughout the SA for different TX gains along with the band of interest, as depicted in Figure 40.

It transmitted a baseband signal of 500 kHz over the carrier, whose frequency was increased. Thus, the TX signal was collected by the RX antenna and the transmitted power was measured.

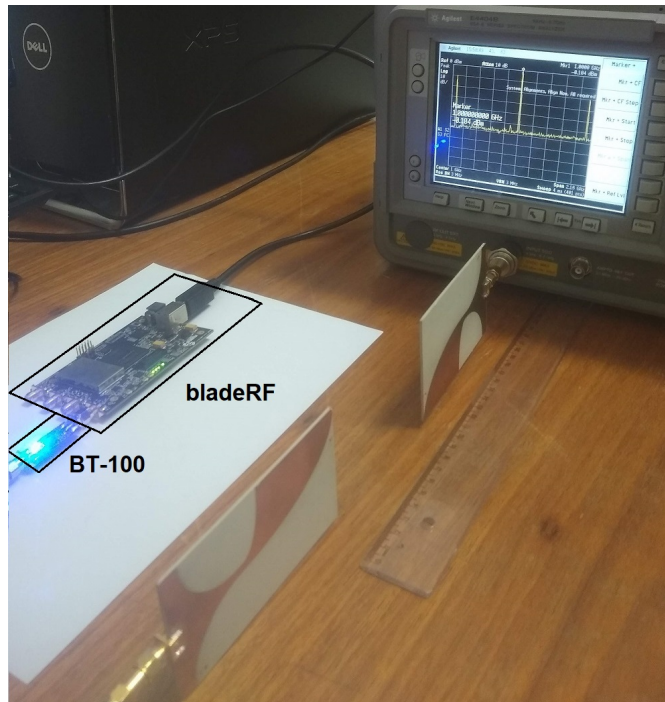


Figure 40 – BladeRF 2.0 transmitting RF signal to SA-E4404B.

- Thirdly, the BladeRF 2.0 receiver noise floor, coupled with the BT-200 but without the Vivaldi antenna or a load, was measured considering the LNA firstly operating (turned on), and then turned off, which means, not operation but still connected.
- Finally, the VNA was employed to transmit pulsed CW signals to the BladeRF 2.0, which was coupled with the BT-200, covering the band of interest, as depicted in Figure 41.

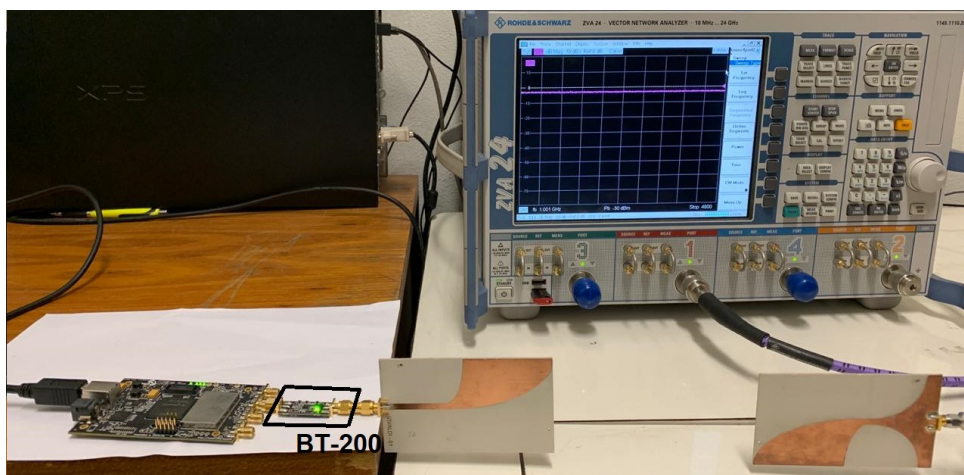


Figure 41 – BladeRF 2.0 receiving RF signal from VNA-ZVA24.

4.4.2 Tests Procedure Over the Breast Phantom

Considering now the breast phantom as a propagation medium instead of the air, the BladeRF 2.0 transmitted and received the microwave signals that go through that, as depicted in Figure 42. It is expected higher attenuation in this medium and so it is important to verify the SDR ability to measure the RF signals that cross the phantom. It is possible to notice that the BT-100 is connected to the TX SMA port and the antenna is directly connected to this interface, while the BT-200 is connected to the RX SMA port that connect the antenna by a cable.



Figure 42 – BladeRF 2.0 coupled with the PA and LNA illuminating the breast phantom through the Vivaldi antennas.

The SDR operates as the transmitter and receiver simultaneously based on a program that executes the frequency sweep and also store the received signals. After that, the captured signals SNR were calculated based on the strength signals difference. The input impedance match of 50Ω is considered on the antennas and also in the amplifiers circuits.

4.5 Power Measurements

4.5.1 Over the Air

The Sections from 4.5.1.1 to 4.5.1.4 reports the RF signals strength transmitted over the air by the VNA when related to the antenna and also by the BladeRF 2.0 while its assessment.

4.5.1.1 Antennas S-parameter

Figure 43 shows the antennas VNA measured S_{21} (magnitude) results over the air, which were connected by a cable. It shows some higher insertion loss measured at lower

frequencies, mainly between 1.5 through 2.5 GHz. It was observed in the simulated results shown in Figure 34. This could be explained by the antenna gain behavior. Nonetheless, the VNA measured result shows a relatively flat S_{21} magnitude response over the whole band of interest. Hence, both antenna's impedance match shows its response in accordance with their value around 50Ω .

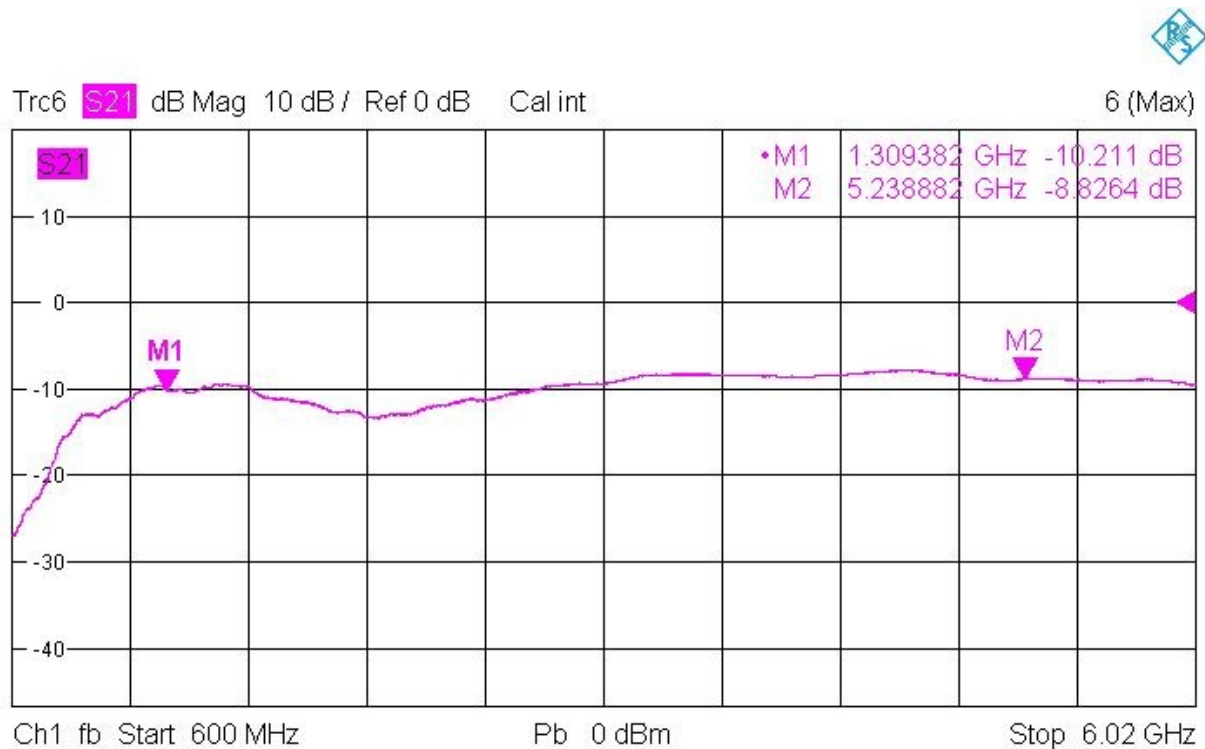


Figure 43 – S_{21} (dB) x frequency of air link using two Vivaldi antennas.

Worth to mention that the VNA first underwent its calibration procedure with its calibration kit for better accuracy.

4.5.1.2 Transmitted Power

BladeRF 2.0 transmitted an RF signal strength up to +15 dBm at 1.0 GHz, which was achieved using the BT-100 and a TX gain set to 60.0 dB, as seen in Figure 44. The figure also shows the BladeRF 2.0 output power along with increasing the carrier frequency for three TX gain configurations: 40, 50 and 60 dB, in which a power variation around 28 dBm was observed and minimum value at 5.0 GHz frequency carrier.

These results demonstrate that to keep the same relation of RF power transmission along the frequency sweep during a possible exam, the RF strength at around 5.0 GHz should be at least ten times higher than around 1.0 GHz, which is possible thanks to the TX circuit gain configuration.

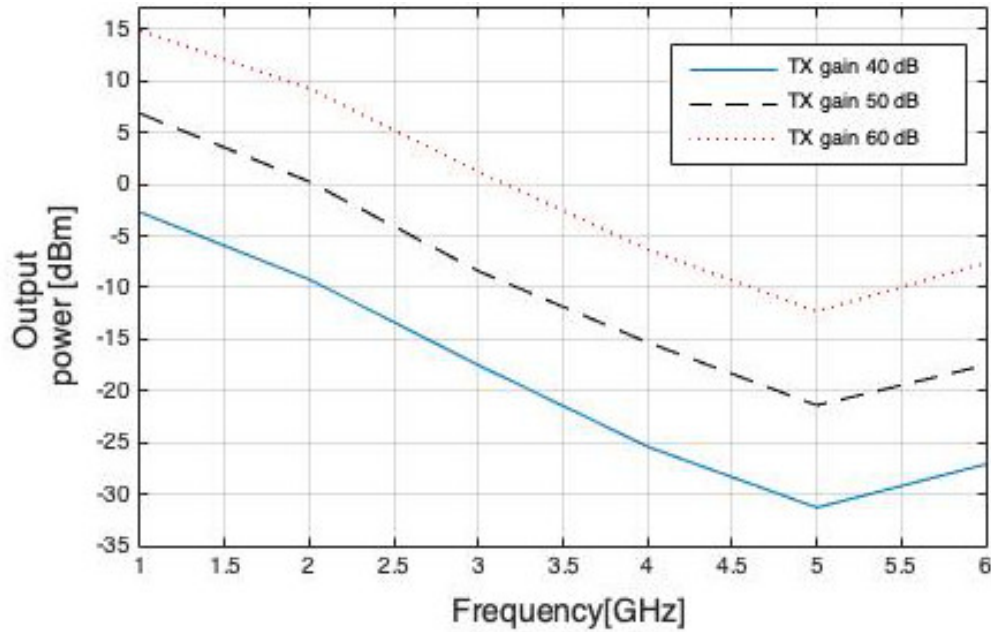


Figure 44 – BladeRF 2.0 output power for different TX gains.

Figure 45 depicts the SA measured power values of the transmitted RF signal from the BladeRF 2.0 antenna, which set the TX gain to + 60dB and was coupled with the BT-100.

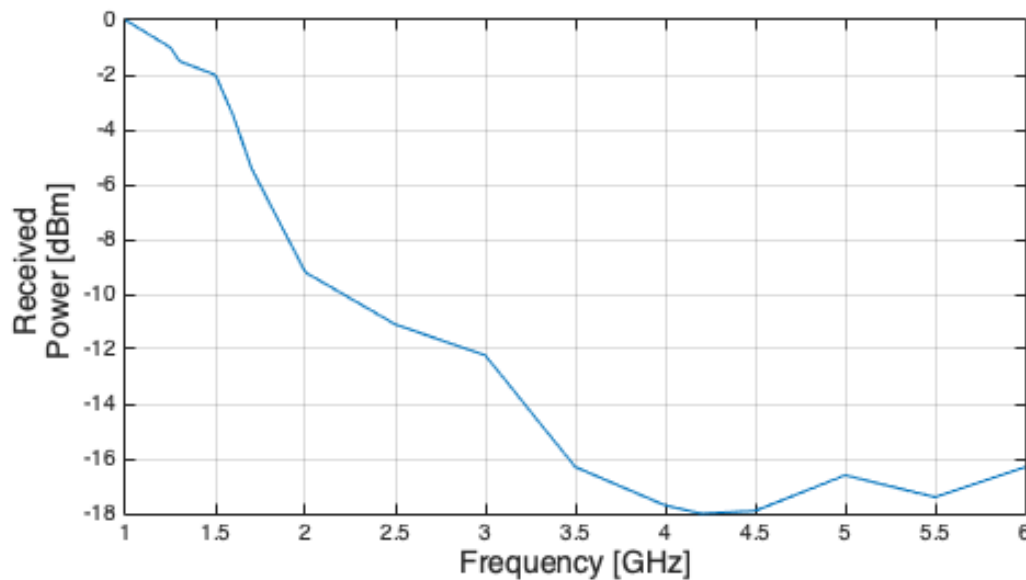


Figure 45 – Measured RF power vs. TX Carrier Frequency.

The SA has measured a RF received signal strength variation of 18 dBm for the whole frequency range, which indicates the smallest power around 4.5 GHz. Based on that, to pursuit a flat transmission power, it is indicated to reduce the power transmission at lower frequencies.

4.5.1.3 Receiver - Noise Floor

Figure 46 shows the BladeRF 2.0 receiver noise floor coupled to the BT-200, comparing the results between the LNA turned on or operating, and off or not operating but still connected. It is possible to see a noise floor increment of around 5.0 dB due to the LNA, which promotes a typical gain of 20.0 dB, increasing the overall dynamic range.

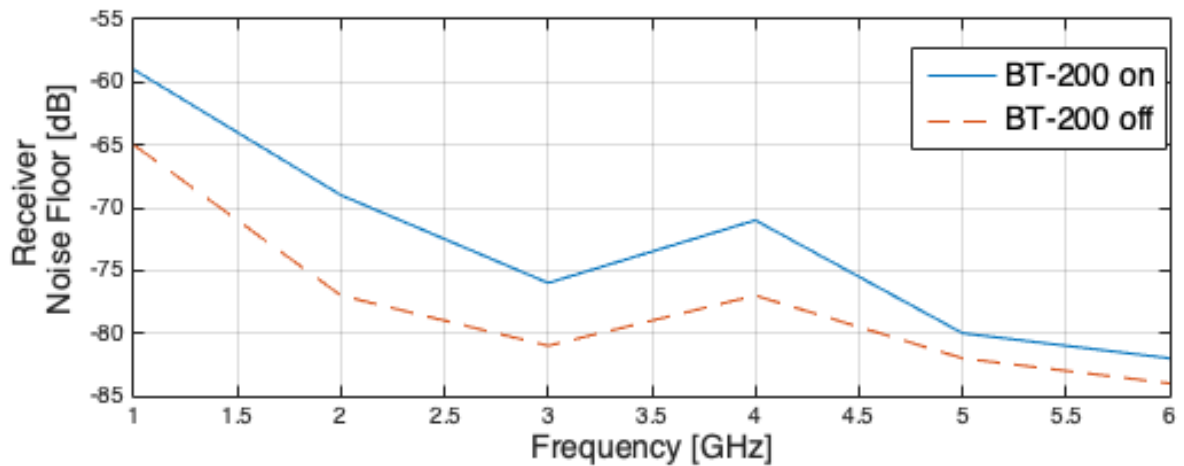


Figure 46 – Measured noise floor with RX carrier frequency varying from 1 GHz to 6 GHz.

The dynamic range can reach a value of 120 dB for M_wI system, as discussed in (ZHURBENKO, 2011), and it is one of the main concerns while implementing a system for breast cancer detection. Based on that, this results endorses the LNA uses pursuing its higher value.

The bladeRF2.0 incorporates the AD9361 RF transceiver, which according to Analog AD9361 (2016), when RF gain is very small, its noise floor is dominated by the 12-bits ADC noise floor.

4.5.1.4 Received Power

Figure 47 corresponds to the time and frequency response of a -40 dBm pulsed CW RF signal irradiated by the antenna connected to the VNA at 6.0 GHz. This signal was collected by the antenna coupled to the bladeRF2.0 that was positioned according the setup described in the Section 4.4.1. The BladeRF 2.0 receiver carrier frequency was set to 6.0 GHz; the peak is thus shown at 0 MHz in the baseband. Besides, the measurement was made with the AGC receiver enabled.

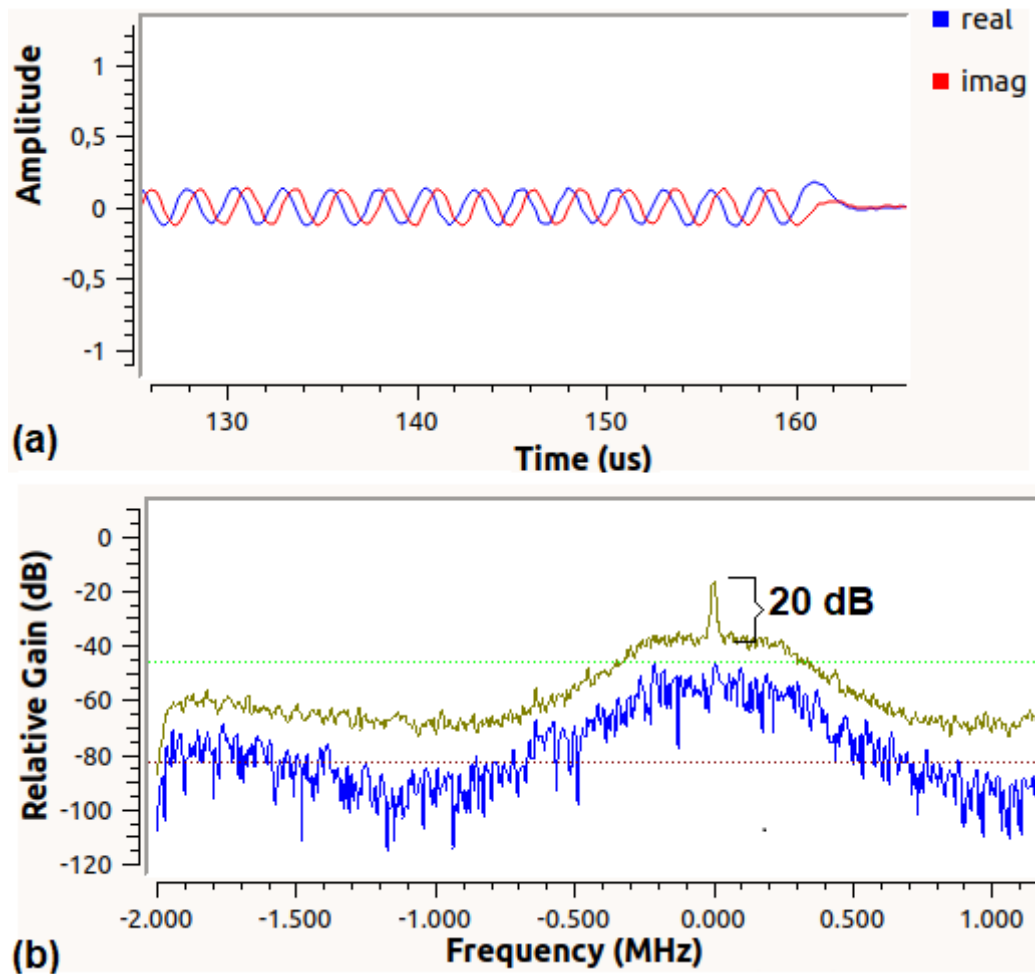


Figure 47 – BladeRF 2.0 time (a) and frequency (b) responses to the transmitted -40 dBm VNA signal at 6.0 GHz.

The frequency domain response (Figure 47 (b)) reveals a noise floor (blue signal) around -60 dB, without the VNA pulse signal but considering the signals from the environment once the tests are not in an anechoic chamber; and then a signal-to-noise of 20 dB (gold signal) is calculated after the pulse.

The results show its ability to successfully measure signal strength as low as -40 dBm based on the VNA transmitted RF signals from 1.0 GHz to 6.0 GHz traveling over the air. Interesting to mention that, by a cable connecting the VNA to the BladeRF 2.0, thus eliminating the antenna influence, it was possible to receive signals as low as -130 dBm for the whole band of interest.

4.5.2 Over the Phantom

Figure 48 shows the measured SNR of the BladeRF 2.0 collected signals along with the whole band of interest. Those signals were generated by the BladeRF 2.0, transmitted by the Vivaldi antenna, and passed throughout the breast phantom. Besides, these measurements were performed with the BT-100, BT-200 and AGC enabled.

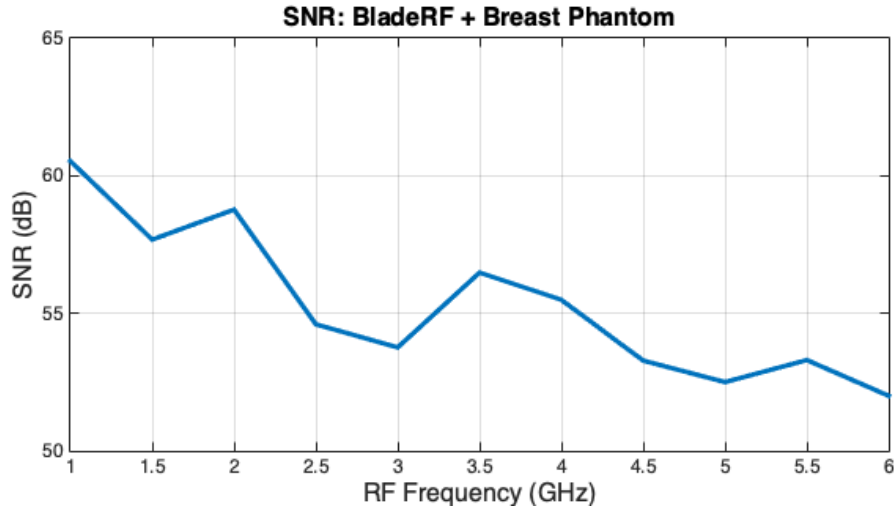


Figure 48 – SNR plot related to BladeRF 2.0 transmission.

It is possible to notice a variation close to 10 dB while measuring SNR, which could be related to low signal strength already reported at higher frequencies. One possibility to increase the SNR is to perform an average measuring which implies in longer signal acquisition.

4.5.3 Discussion

Section 4.5 is based on the published work (CARVALHO et al., 2021). It showed the BladeRF 2.0 assessment using two UWB Vivaldi antennas and different propagation media. CST simulation verified that at higher frequencies, the transmitted power has the benefit of the higher used Vivaldi antenna gain. Thus, the S-parameter simulation does not show higher attenuation at higher frequencies.

Table 4 summarizes the main specifications for the proposed system designed to perform breast cancer screening based on microwaves. It also shows BladeRF 2.0 (coupled to the BT-100 and BT-200) and the VNA ZVA24 evaluation.

From Table 4, it is possible to conclude that BladeRF 2.0 meets the specifications for operating in a MwI system, which motivates its use as an apparatus together with the bias tee (LNA and PA) and Vivaldi antennas. As shown, the BladeRF 2.0 RF signal power measurements for the transmitter and receiver meet the system requirements and are close to the VNA performance. Moreover, its cost is less than a tenth of the ZVA24, even considering the amplifiers (BT-100 and BT-200). Another cost reference would be the work (KRANOLD et al., 2021), which mentions that its developed system, including the IC manufacture, costs around US\$ 23,000.00. Again, BladeRF 2.0 is much cheaper than this solution (the BladeRF 2.0 value in 2023 was around US\$ 540.00).

Table 4 – Summary of MwI requirements and SDR - VNA performance over the air.

Performance	MwI Required	BladeRF 2.0 Provide	ZVA24 Provide
Bandwidth (GHz)	5.0	5.93	Up to 24
Receiver Sensitivity (dBm)	- 60	$\geq - 66$	$\geq - 60$
Dynamic Range (dB)	70	> 74	> 90
Transmitter Power (dBm)	< 0	< 15	< 18
Receiver Power (dBm)	$> - 60$	$> - 80$	$> - 100$
SNR (dB)	> 60	> 52	> 80
Price (US\$)	-	$< 1,000$	$> 10,000$

Nonetheless, there are some options for cheaper LNAs with reduced frequency range, as the NanoRFE VNA6000, but this comparison is outside this Thesis.

Concerning the microwave propagation loss on a breast phantom, the BladeRF 2.0 shows to be tailored to deal with the RF signals, in addition to the usage of PA and LNA circuits. An SNR higher than 52 dB was measured for the whole band of interest. Signal cross-talk was observed between the RF input/output on the board, which causes detrimental effects, such as linearity reduction (NGUYEN; PARK, 2016). As a strategy to mitigate this effect, the RF power transmitter was adjusted to lower levels, which could implies on the elimination of the PA, which is not necessary. It is suggested to keep the LNA due to its dynamic range contribution.

4.6 Synthetic Pulse Simulation and Measurement

A synthetic pulse based on SFCW signal modulation was simulated using the CST. A woman's breast was emulated with the same features that was used in the prior experiments. The steps involved and the results of that will be shown in this Subsection and were published in (CARVALHO; ARAGAO; NOIJE, 2022).

4.6.1 Simulation Setup

Table 5 and Figure 49 detail the baseband and SFCW signals in the simulation setup, with a range resolution of around 1.5 cm, leading to a BW of around 4.0 GHz. The modulated RF signal (red wave) feeds the TX antenna. It is not considered a PA in this simulation, with the output power settled at 0 dBm for all the signals transmitted. A step

frequency of 100 MHz was defined, which implies in an ambiguous range specification in the limit of the target size. Smaller step frequency would requires longer simulation time.

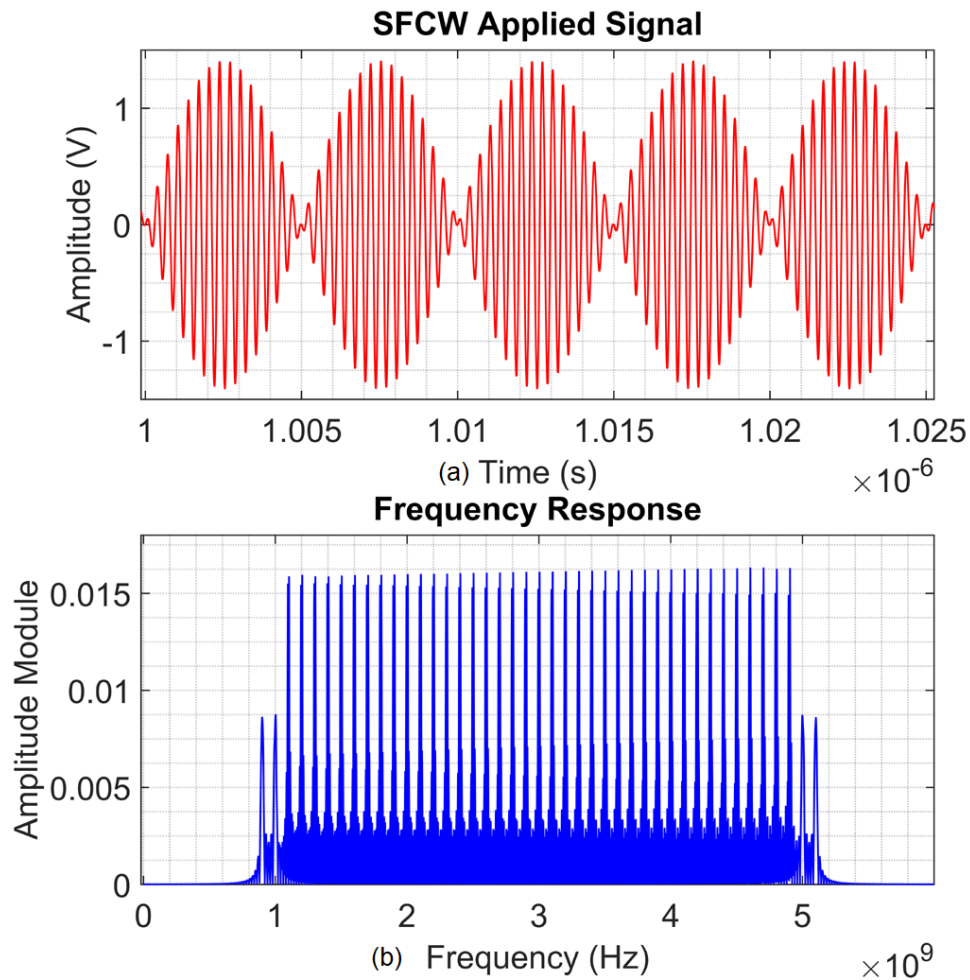


Figure 49 – SFCW applied signal (a), and its respective frequency response (b).

Table 5 – Characteristics of the SFCW signal applied in the simulation setup

Start Frequency	1.0 GHz
Stop Frequency	5.0 GHz
Step Frequency	100 MHz
Output Power	0 dBm
Line Impedance	50 Ohms
Baseband Frequency	100 MHz
Stepped Pulse Duration	50 ns

The simulations were performed in two different scenarios. First, a breast with a tumor of 1.4 cm diameter that was placed 3.5 cm deep or away from the antenna's direction, as depicted in Figure 50, a 3D cross section of the heterogeneous breast model scenario. Second, the same configuration was performed, but without the tumor inside the breast. The reflected signals were collected in both cases and then processed using a

stretch processing technique that was explained in Subsection 2.4. Thus, after the signals were processed, a synthetic range profile of the illuminated mimic breast was generated, revealing the inside target.

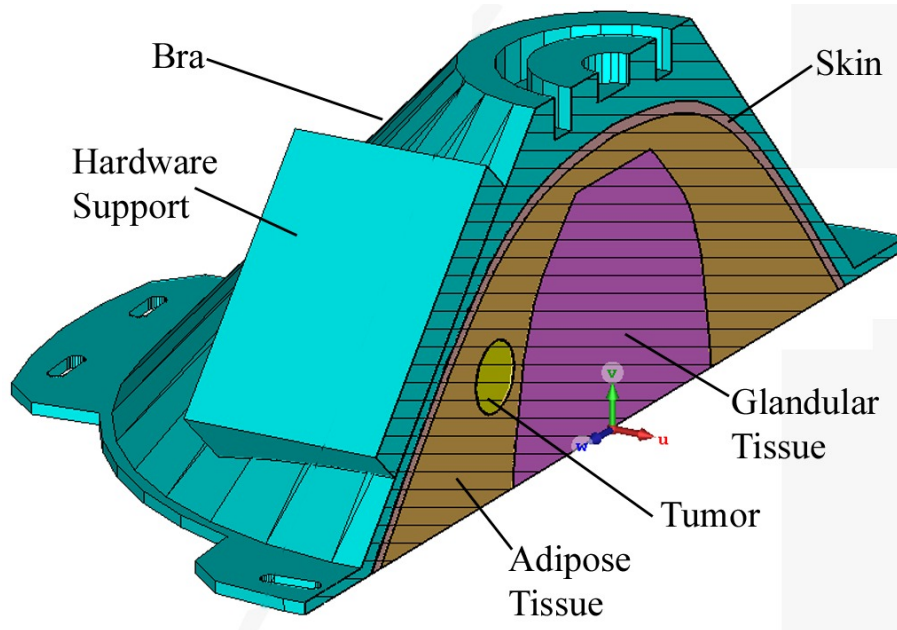


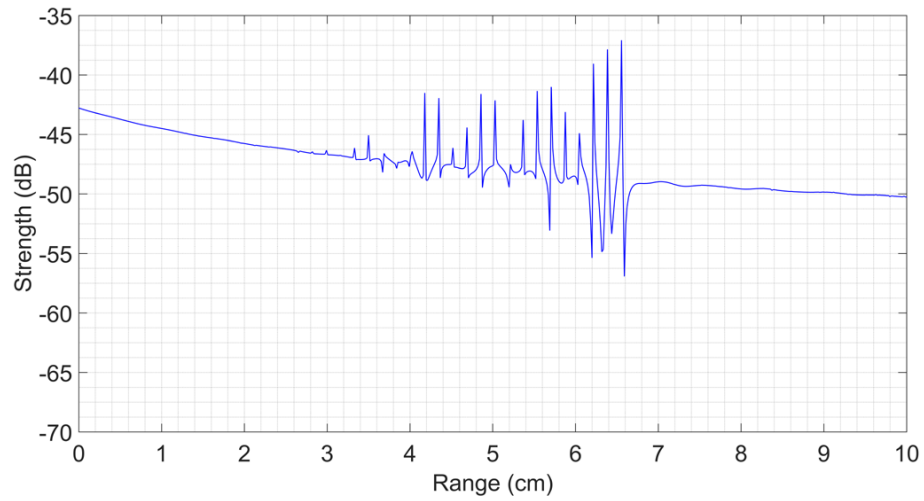
Figure 50 – CST setup of a bra model mimicking a breast.

4.6.2 Simulation Results

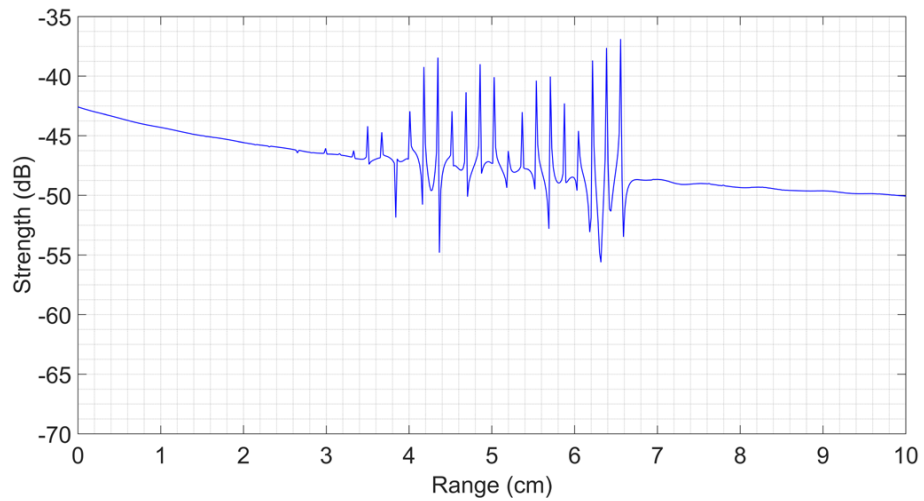
Figure 51 shows the calculated range profile from collected SFCW signals achieved from the simulated platform. The Y-axis corresponds to the signal strength in dB, and the X-axis corresponds to the range in cm.

Figure 51a shows the response to the profile of the emulated breast range without tumor. The response considering the presence of the tumor in the emulated breast is depicted in Figure 51b. Subtracting both signals, it is possible to notice a 16.0 dB strength amplitude peak difference, which is closely related to tumor position. This difference is emphasized in Figure 51c.

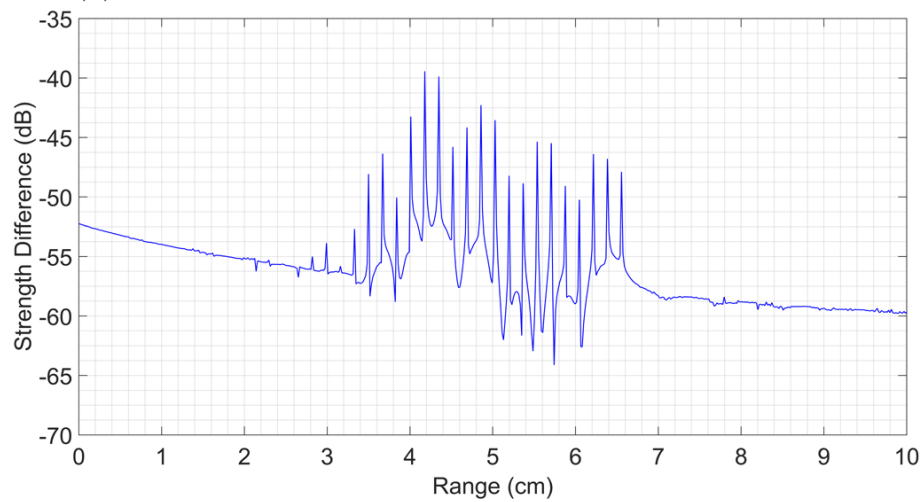
Most M_wI systems deliver a breast energy map, which corresponds to its reflectivity, as medical imaging for diagnoses. As discussed in this Thesis, it corresponds to the radar approach instead of the tomography. The simulated results illustrate the reflectivity ability based on SFCW signals, in spite of a single position being simulated. As long as the signals illuminate a breast in several positions, a DAS confocal algorithm could generate an energy map that reveals the presence of a tumor and also estimates its location and size. More advanced systems and algorithms mention the ability to characterize the tumor between malignant and nonmalignant.



(a) Emulated breast without tumor.



(b) 14.0 mm tumor depth 35.0 mm into the emulated breast.



(c) Calculated difference between both signals.

Figure 51 – Calculated range profile of the SFCW collected signals from the simulated platform.

4.6.3 BladeRF 2.0 Programming

Aiming at BladeRF 2.0 assessment and expecting to validate the simulations performed and discussed previously, a C code was developed and compiled to implement an SFCW radar, whose frequency was automatically swept from 1.0 to 5.0 GHz, with a step of 50 MHz. Figure 52 is a short sample of this C code related to the transmission and reception routine. Also, some comments about the SDR configuration were inserted. The entire C code is available in the Appendix B.

```
// ----- Main Function declared above

sdr_config(); //Function that configure the SDR as below:
//sdr_channel.config.channel      =  BLADERF_CHANNEL_TX(0);
//sdr_channel.config.frequency   =  sdr_resources[1].frequency;
//sdr_channel.config.bandwidth   =  sdr_resources[1].bandwidth;
//sdr_channel.config.samplerate  =  sdr_resources[1].samplerate;
//sdr_channel.config.gain        =  sdr_resources[1].tx1_gain;

for(uint64_t step_counter = 0 ; step_counter <= FREQ_STEP ; step_counter++ )
{
sdr_channel.config.frequency     =  FREQ_INIT + (step_counter*FREQ_SIZE);
sdr_channel.config.channel       =  BLADERF_CHANNEL_TX(0);
status = configure_channel_frequency_tx(sdr_channel.dev, &sdr_channel.config);
sdr_channel.config.channel       =  BLADERF_CHANNEL_RX(0);
status = configure_channel_frequency_rx(sdr_channel.dev, &sdr_channel.config);
{
    status = sync_rx(sdr_channel.dev);
    usleep(10000); // T=1/PRF => T = 10e-3 segundos
}
}
}
```

Figure 52 – C code sample developed aiming at SFCW radar implementation.

BladeRF 2.0 has loaded both the compiled code that executes an SFCW radar and an FPGA bitstream that contains an embedded baseband signal of 100 kHz. The idea to store the baseband in the FPGA is to reduce the data throughput from the CPU. Thus, from the transmitter's perspective, the main task has been to sweep the RF signal along with the whole band of interest (from 1.0 to 5.0 GHz).

Due to the absence of a proper UWB antenna, the first approach was to perform a cable loop-back to retrieve the transmitted signals and thus process them. It should be noted that the BladeRF 2.0 receiver AGC was kept on. This feature is a challenge to overcome since, in a practical radar experiment, the receiver signals strength information is used, for instance, to remove the skin reflection.

4.6.4 BladeRF 2.0 operation

Everything that occurs between the FPGA and the RF modules adds some group delay, as pointed out by (KOHLS, 2021). Thus, the digital up and down conversion chains and buffering impact the ability to properly synchronize transmitted and received signals, leading to reception issues, which is demonstrated in Figure 53, where the in-phase and quadrature (I/Q) signals components are plotted. The Y-axis corresponds to the signal magnitude, and the X-axis corresponds the received sample. The I/Q components were stored and processed, but the 100 kHz signal was not reconstructed, even after several approaches had been attempted. It was not possible then to fully recover the baseband signal transmitted over an SFCW signal modulation.

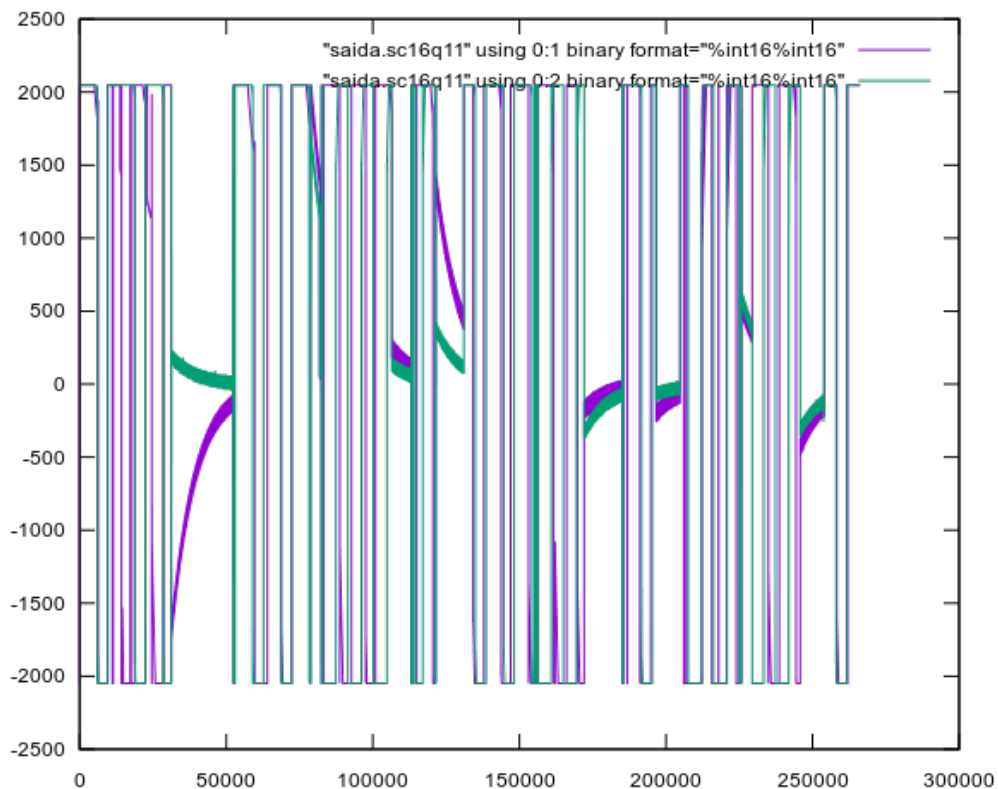


Figure 53 – BladeRF 2.0 loopback measurement (Magnitude x Sample).

Besides missing coherence operation, it is possible to notice the signal saturation, most of all due to the AGC operation, but this may also be due to the signal representation, which is an SC16Q11 (signed-complex, 16-bit Q11) format. Both must be further investigated in order to recover the signal with minimal interference. Moreover, correcting any imbalances in the I/Q components of the received signals is crucial, as imbalances can also lead to phase errors. None algorithms, such as digital compensation, was used to address I/Q imbalance in this experiment.

4.6.5 Discussion

A synthetic pulse aimed at the UWB SFCW radar has been implemented and simulated looking for short-range microwave imaging. The simulation results have endorsed the frequency domain system realization, in which the UWB synthetic pulse is accomplished based on SFCW signal modulation. Mwi system in the frequency domain is predominant due to VNA usage and also for reasons described in Subsection 2.3.2.1, such as receiver noise figure. However, the frequency domain spatial resolution is typically lower than that of time domain systems due to variations in signal amplitude and phase to generate an image, as explained in (NAGHIBI; ATTARI, 2021).

The implementation of a SFCW radar does not require complex modulation of the transmitting signal. Nonetheless, synthetic pulse generation demands post-processing to compose then, conversely to a Gaussian pulse. Moreover, there is a concern of the transmitted and correlated received signal phase coherence.

Considering the BladeRF 2.0 usage, transmitting and receiving continuously with antennas next to each other result in the received signal being saturated by the signal propagated from the transmitter. This signal is known as the bleed-through signal and is a prevalent issue in short-range radars (KOHLS, 2021). This experimental result exposes the challenges while implementing an SDR as a VNA, but does not deter its usage since the signals were properly transmitted and received. A key issue to overcome is the synchronization of transmitted and received signals. Moreover, it is necessary to master the AGC operation to handle the received signals.

Chapter 5

Conclusions and Suggestions for Future Works

This Chapter presents the main conclusions and suggestions for further research that focus on the SDR usage aiming at breast cancer detection. It is evident that the detection of breast cancer in women is a health issue that requires more investment, research, and new solutions that addresses screening exams.

5.1 Conclusions

Microwave imaging for breast cancer detection employing the SDR is an emerging, innovative, and low-cost approach that leverages the flexibility and reconfigurability of SDR platforms for medical imaging applications. SDR allows for the manipulation of microwave signals and the extraction of meaningful information from the scattered signals after its interaction with breast tissues and an inside target, such as a tumor. This Thesis presented an SDR assessment aimed at breast cancer detection based on microwave signal interactions. A bladeRF 2.0 transmitter and receiver system, coupled with its respective bias tee circuit PA and LNA was used, which met the requirements for a MWI system considering both air and a phantom as a microwave propagation medium. For the measurements, a frequency range of 1.0 to 6.0 GHz was considered, which aims at a target resolution (tumor size) of around 10 mm. BladeRF 2.0 RF circuits vary within this range, dealing with the SFCW approach in a software-defined way. RF signals received from the VNA ZVA24 with a transmitted power as low as -80 dBm were successfully measured. Furthermore, the bladeRF 2.0 transmitter shows the ability to provide up to +18 dBm at 1.0 GHz and close to -10 dBm at 6.0 GHz, whose transmitted signals power were measured by the spectrum analyzer E4404B. Finally, BladeRF2.0 achieved an SNR higher than 52.0 dB operating as a transceiver, transmitting and receiving the microwave signals over a breast phantom, for the whole band of interest.

A synthetic pulse aimed at the UWB SFCW radar has been implemented and simulated looking for short-range microwave imaging. The simulation results have endorsed the realization of the frequency domain system, in which the UWB synthetic pulse is accomplished based on SFCW signal modulation. A difference of 16.0 dB has been noticed due to the presence of a 14.0 mm tumor inserted in an emulated heterogeneous woman's breast. The experimental result exposes the challenges while implementing bladeRF 2.0 as a VNA, which means transmitting and receiving the microwave signals for s-parameter characterization. During the loopback measurements, high RF leakage was faced on the SDR board. As a strategy to deal with this effect, the RF power transmitter was adjusted to low levels. It is possible to say that due to the absence of a digital compensation routine, the I/Q imbalance also compromises the measurements, in addition to the lack of phase coherence.

BladeRF 2.0 shows to be suitable, in terms of power requirements, to replace a VNA while measuring the s-parameter (S_{21}) for the implementation of a MwI system in the frequency domain. It would be more indicated for rapid prototyping and the investigation of the features and solutions of a system. However, this Thesis concludes that using only one SDR is impracticable due to RF leakage and the challenge while programming the SDR. Compared to a VNA, SDRs are more susceptible to noise and interference, which can degrade measurement accuracy, especially in noisy RF environments. Due to this, shielding and filtering techniques must be employed to mitigate these effects. Another challenge is phase coherence and stability, which are critical for measuring phase-sensitive information, such as group delay and phase response. SDRs, being software-driven, may face challenges in maintaining long-term phase stability and coherence, especially in harsh or variable environments.

In addition, this Thesis has consolidated the most advanced MwI systems to detect breast cancer, showing their unfolded devices and reconstruction image methods. The most important publications in the MwI field were reviewed and presented. Indeed, the effort of several research groups was demonstrated to emphasize the benefits of this non-ionizing medical imaging modality. Despite of the still lack of clinical acceptance, different research groups have been implemented practical MwI systems, based mainly on the use of VNAs to deal with EM signals, making MwI available. Low-cost devices have been sought, and an SDR-based system has been thoroughly investigated. Paving the way for MwI implementation and clinical practice, this Thesis reported some spin-offs that presented patients diagnosed with their devices, showing high precision in revealing a breast tumor. The difficulty of clinical acceptance of MwI can be reduced as more successful clinical trials and new technologies are added to this research niche.

There are many screening modalities, as described in this work, concerning breast cancer detection. Nonetheless, breast and breast cancer have several characteristics that

imply the choice of the best method, such as tumor type, location, and breast BI-RADS classification (which is related to the patient's age and body weight). In some cases, the better option is only the one available. Therefore, it is crucial to realize the cooperation between the different modalities, to develop harmless and affordable screening modalities, and the commitment of physicians to succeed with early breast cancer detection.

5.2 Future works suggestion

The following future works that can be derivated from this Thesis:

- a) Further investigation of SDR programming to deal with the RF leakage, to implement the I/Q digital compensation, and also how to cope with AGC feature;
- b) Further simulation of the synthetic pulse considering more antenna positions and then to develop a SFCW UWB radar system employing the BladeRF 2.0. Also, apply the confocal algorithm on the received signals aiming at imaging generation, as proposed by (ARAGÃO, 2021);
- c) To assess the BladeRF 2.0 performance with other antennas;
- d) To implement a system employing one BladeRF 2.0 as a transmitter and other one or multiple as receiver.

Bibliography

ABBOSH, A. M. *UQ researchers*. 2021. Available from Internet: <<https://researchers.uq.edu.au/researcher/1576>>. Cited once at page 79.

ACS. *Breast Cancer Facts & Figures 2019-2020*. 2019. Available from Internet: <<https://www.cancer.org/content/dam/cancer-org/research/cancer-facts-and-statistics/breast-cancer-facts-and-figures/breast-cancer-facts-and-figures-2019-2020.pdf>>. Cited once at page 28.

ADACHI, M. et al. Feasibility of Portable Microwave Imaging Device for Breast Cancer Detection. *Diagnostics*, v. 12, n. 1, p. 27, 12 2021. ISSN 2075-4418. Available from Internet: <<https://www.mdpi.com/2075-4418/12/1/27>>. Cited once at page 77.

AKEELA, R.; DEZFOULI, B. Software-defined Radios: Architecture, State-of-the-art, and Challenges. *Computer Communications*, Elsevier B.V., v. 128, p. 106–125, 4 2018. Available from Internet: <<http://arxiv.org/abs/1804.06564>>. Cited 2 times at pages 54 and 56.

AKINCI, M. N. et al. Qualitative Microwave Imaging With Scattering Parameters Measurements. *IEEE Transactions on Microwave Theory and Techniques*, v. 63, n. 9, p. 2730–2740, 9 2015. ISSN 0018-9480. Available from Internet: <<http://ieeexplore.ieee.org/document/7161412/>>. Cited 4 times at pages 46, 65, 66, and 82.

ALDHAEEBI, M. A. et al. Review of Microwaves Techniques for Breast Cancer Detection. *Sensors*, v. 20, n. 8, p. 2390, 4 2020. ISSN 1424-8220. Available from Internet: <<https://www.mdpi.com/1424-8220/20/8/2390>>. Cited once at page 61.

ALMEIDA, L. M. M. D.; SANCHES, B.; NOIJE, W. A. M. V. High-Speed Sampler for UWB Breast Cancer Detection System. In: *2023 IEEE 14th Latin America Symposium on Circuits and Systems (LASCAS)*. IEEE, 2023. p. 1–4. ISBN 978-1-6654-5705-7. Available from Internet: <<https://ieeexplore.ieee.org/document/10108279/>>. Cited once at page 50.

Analog AD9361. RF Agile Transceiver Datasheet. *Datasheet*, 2016. Available from Internet: <www.analog.com>. Cited 3 times at pages 86, 87, and 97.

ANDRADE, W. P. *Performance do PET/CT pré-operatório na predição de resposta patológica após tratamento com quimioterapia neoadjuvante para pacientes com câncer de mama*. Thesis (Doctoral) — Fundação Antônio Prudente, 2014. Cited once at page 28.

ARAGÃO, A. d. J. *Low-cost microwave imaging portable device for breast cancer detection*. Thesis (Doctoral) — Universidade de São Paulo, São Paulo, 10 2021. Available from Internet: <<https://www.teses.usp.br/teses/disponiveis/3/3140/tde-18012022-163306/>>. Cited 3 times at pages 32, 78, and 109.

ARAGÃO, A. de J. et al. Low-cost device for breast cancer screening: A dry setup IR-UWB proposal. *Biomedical Signal Processing and Control*, v. 79, p. 104078, 1 2023. ISSN 17468094. Available from Internet: <<https://linkinghub.elsevier.com/retrieve/pii/S1746809422005390>>. Cited once at page 78.

ARAGAO, A. de J. et al. An improved confocal algorithm for breast cancer detection using UWB signals. In: *2020 IEEE 11th Latin American Symposium on Circuits & Systems (LASCAS)*. IEEE, 2020. p. 1–4. ISBN 978-1-7281-3427-7. Available from Internet: <<https://ieeexplore.ieee.org/document/9069034/>>. Cited 2 times at pages 46 and 78.

ARAGAO, A. de J. et al. Low-cost portable system prototype for breast cancer detection using UWB signals. In: *2020 13th International Congress on Image and Signal Processing, BioMedical Engineering and Informatics (CISP-BMEI)*. IEEE, 2020. p. 715–720. ISBN 978-0-7381-0545-1. Available from Internet: <<https://ieeexplore.ieee.org/document/9263688/>>. Cited 2 times at pages 86 and 92.

ASCAMA, H. D. O. *Antena E Mecanismo Para Detecção De Pessoas Radar Uwb : Antena E Mecanismo Para Detecção De Pessoas*. 122 p. Thesis (Doctoral) — Universidade de São Paulo, 2010. Cited once at page 88.

BENNY, R.; ANJIT, T. A.; MYTHILI, P. An Overview of Microwave Imaging for Breast Tumor Detection. *Progress In Electromagnetics Research B*, v. 87, n. April, p. 61–91, 2020. ISSN 1937-6472. Cited 4 times at pages 40, 49, 60, and 82.

BHARGAVA, D.; RATTANADECHO, P. Microwave imaging of breast cancer: Simulation analysis of SAR and temperature in tumors for different age and type. *Case Studies in Thermal Engineering*, Elsevier Ltd, v. 31, p. 101843, 2022. ISSN 2214157X. Available from Internet: <<https://doi.org/10.1016/j.csite.2022.101843>>. Cited once at page 34.

BOLOMEY, J.-C. Crossed Viewpoints on Microwave-Based Imaging for Medical Diagnosis: From Genesis to Earliest Clinical Outcomes. In: *The World of Applied Electromagnetics*. Cham: Springer International Publishing, 2018. p. 369–414. Available from Internet: <http://link.springer.com/10.1007/978-3-319-58403-4_16>. Cited 2 times at pages 62 and 84.

BOURQUI, J.; SILL, J. M.; FEAR, E. C. A Prototype System for Measuring Microwave Frequency Reflections from the Breast. *International Journal of Biomedical Imaging*, v. 2012, p. 1–12, 2012. ISSN 1687-4188. Available from Internet: <<http://www.hindawi.com/journals/ijbi/2012/851234/>>. Cited 2 times at pages 69 and 70.

BOYD, N. F. et al. *Breast tissue composition and susceptibility to breast cancer*. Oxford University Press, 2010. 1224–1237 p. Available from Internet: </pmc/articles/PMC2923218/?report=abstract<https://www.ncbi.nlm.nih.gov/pmc/articles/PMC2923218/https://academic.oup.com/jnci/article-lookup/doi/10.1093/jnci/djq239>>. Cited once at page 41.

BRITO, F.; CARVALHO, D.; NOIJE, W. Near Field Radar System Modeling for Microwave Imaging and Breast Cancer Detection Applications. In: BASTOS-FILHO, T. F.; CALDEIRA, E. M. de O.; FRIZERA-NETO, A. (Ed.). *XXVII Brazilian Congress on Biomedical Engineering*. [S.l.]: IFMBE Proceedings - Springer, 2020. p. 338–343. Cited 2 times at pages 42 and 43.

CARVALHO, D.; ARAGAO, A. de J.; NOIJE, W. Synthetic Pulse based on SFCW Modulation: a Proposition for Microwave Imaging. In: *2022 IEEE Sixth Ecuador Technical Chapters Meeting (ETCM)*. IEEE, 2022. p. 1–6. ISBN 978-1-6654-8744-3. Available from Internet: <<https://ieeexplore.ieee.org/document/9935767/>>. Cited once at page 100.

CARVALHO, D. et al. Analysis of Breast Cancer Detection Based on Software-Defined Radio Technology. In: BASTOS-FILHO, T. F.; CALDEIRA, E. M. de O.; FRIZERA-NETO, A. (Ed.). *XXVII Brazilian Congress on Biomedical Engineering*. Vitória - ES: IFMBE Proceedings - Springer, 2020. p. 439–444. Available from Internet: <<https://link.springer.com/book/9783030706005>>. Cited 2 times at pages 56 and 91.

CARVALHO, D. et al. Experimental evaluation of a Software-Defined Radio through a Breast Phantom aiming at Microwave Medical Imaging. *Microprocessors and Microsystems*, Elsevier B.V., n. April, p. 104381, 11 2021. ISSN 01419331. Available from Internet: <<https://doi.org/10.1016/j.micpro.2021.104381><https://linkinghub.elsevier.com/retrieve/pii/S0141933121005305>>. Cited once at page 99.

CASPERS, F. RF engineering basic concepts: S-parameters. *CAS 2010 - CERN Accelerator School: RF for Accelerators, Proceedings*, p. 67–93, 2011. Cited once at page 59.

CASU, M. R. et al. UWB microwave imaging for breast cancer detection. *ACM Transactions on Embedded Computing Systems*, Association for Computing Machinery, v. 13, n. 3s, p. 1–22, 3 2014. ISSN 1539-9087. Available from Internet: <<https://dl.acm.org/doi/10.1145/2530534><http://dl.acm.org/citation.cfm?doid=2597868.2530534>>. Cited once at page 80.

CASU, M. R. et al. A COTS-Based Microwave Imaging System for Breast-Cancer Detection. *IEEE Transactions on Biomedical Circuits and Systems*, Institute of Electrical and Electronics Engineers Inc., v. 11, n. 4, p. 804–814, 8 2017. ISSN 1932-4545. Available from Internet: <<http://ieeexplore.ieee.org/document/7983454/>>. Cited once at page 80.

CHANDRA, R. et al. On the Opportunities and Challenges in Microwave Medical Sensing and Imaging. *IEEE Transactions on Biomedical Engineering*, v. 62, n. 7, p. 1667–1682, 2015. ISSN 15582531. Cited once at page 61.

CHEN, H.-l. et al. Comparison of the sensitivity of mammography, ultrasound, magnetic resonance imaging and combinations of these imaging modalities for the detection of small (<2 cm) breast cancer. *Medicine*, v. 100, n. 26, p. e26531, 7 2021. ISSN 0025-7974. Available from Internet: <<https://journals.lww.com/10.1097/MD.00000000000026531>>. Cited once at page 29.

CHENEY, M.; BORDEN, B. *Fundamentals of Radar Imaging*. Society for Industrial and Applied Mathematics, 2009. ISBN 978-0-89871-677-1. Available from Internet: <<http://epubs.siam.org/doi/book/10.1137/1.9780898719291>>. Cited once at page 56.

CLANAHAN, J. M. et al. Clinical utility of a hand-held scanner for breast cancer early detection and patient triage. *Journal of Global Oncology*, v. 2020, n. 6, p. 27–34, 2020. ISSN 23789506. Cited once at page 30.

COLLINS, T. F. et al. *Software-Defined Radio for Engineers, 2018 | Education | Analog Devices*. [s.n.], 2018. Available from Internet: <<https://www.analog.com/en/education/education-library/software-defined-radio-for-engineers.html>>. Cited once at page 53.

CONCEIÇÃO, R. C.; MOHR, J. J.; O'HALLORAN, M. *An Introduction to Microwave Imaging for Breast Cancer Detection*. Cham: Springer International Publishing, 2016. (Biological and Medical Physics, Biomedical Engineering). ISBN 978-3-319-27865-0. Available from Internet: <<http://www.springer.com/series/3740http://link.springer.com/10.1007/978-3-319-27866-7>>. Cited 2 times at pages 44 and 73.

COOK, D. et al. Case Report: Preliminary Images From an Electromagnetic Portable Brain Scanner for Diagnosis and Monitoring of Acute Stroke. *Frontiers in Neurology*, v. 12, n. October, p. 1–7, 10 2021. ISSN 1664-2295. Available from Internet: <<https://www.frontiersin.org/articles/10.3389/fneur.2021.765412/full>>. Cited once at page 79.

CURRY, G. R. *Radar essentials: A concise handbook for radar design and performance analysis*. Institution of Engineering and Technology, 2012. 1–134 p. ISBN 9781613531563. Available from Internet: <<https://digital-library.theiet.org/content/books/ra/sbra029e>>. Cited once at page 48.

Dartmouth. *Dartmouth Engineering | Biomedical*. 2021. Available from Internet: <<https://engineering.dartmouth.edu/research/biomedical#imaging-physics>>. Cited once at page 62.

D'ORSI, C. et al. *Acr BI-RADS[®] Atlas*. [S.l.], 2013. Cited once at page 29.

ELSHEAKH, D. N. et al. Complete Breast Cancer Detection and Monitoring System by Using Microwave Textile Based Antenna Sensors. *Biosensors*, v. 13, n. 1, 2023. ISSN 20796374. Cited once at page 83.

FANG, Q. *Computational methods for microwave medical imaging*. 391 p. Thesis (Doctoral) — Dartmouth College, 2004. Available from Internet: <<http://scholar.google.com/scholar?hl=en&btnG=Search&q=intitle:Computational+Methods+for+Microwave+Medical+Imaging#0>>. Cited 3 times at pages 32, 46, and 63.

FASOULA, A. et al. Automated Breast Lesion Detection and Characterization with the Wavelia Microwave Breast Imaging System: Methodological Proof-of-Concept on First-in-Human Patient Data. *Applied Sciences*, v. 11, n. 21, p. 9998, 10 2021. ISSN 2076-3417. Available from Internet: <<https://www.mdpi.com/2076-3417/11/21/9998>>. Cited once at page 81.

FASOULA, A. et al. On-Site Validation of a Microwave Breast Imaging System, before First Patient Study. *Diagnostics*, MDPI AG, v. 8, n. 3, p. 53, 8 2018. ISSN 2075-4418. Available from Internet: <<http://www.mdpi.com/2075-4418/8/3/53>>. Cited 2 times at pages 32 and 73.

- FDA. *Mammography*. 2017. Available from Internet: <<https://www.fda.gov/radiation-emitting-products/medical-x-ray-imaging/mammography>>. Cited once at page 28.
- FEAR, E. et al. Microwave system for breast tumor detection: experimental concept evaluation. In: *IEEE Antennas and Propagation Society International Symposium*. [S.l.: s.n.], 2002. v. 1, p. 819–822 vol.1. Cited once at page 30.
- FEAR, E. C. Microwave imaging of the breast. *Technology in Cancer Research and Treatment*, v. 4, n. 1, p. 69–82, 2005. ISSN 15330346. Cited once at page 47.
- FEAR, E. C. et al. Microwave Breast Imaging With a Monostatic Radar-Based System: A Study of Application to Patients. *IEEE Transactions on Microwave Theory and Techniques*, v. 61, n. 5, p. 2119–2128, 5 2013. ISSN 0018-9480. Available from Internet: <<http://ieeexplore.ieee.org/document/6502279/>>. Cited 2 times at pages 45 and 70.
- FEGHHI, R. et al. Design of a Low-Cost UWB Time-Domain Radar System for Subcentimeter Image Resolution. *IEEE Transactions on Microwave Theory and Techniques*, IEEE, p. 1–1, 2022. ISSN 0018-9480. Available from Internet: <<https://ieeexplore.ieee.org/document/9772737/>>. Cited once at page 50.
- FELICIO, J. M. et al. Antenna Design and Near-Field Characterization for Medical Microwave Imaging Applications. *IEEE Transactions on Antennas and Propagation*, v. 67, n. 7, p. 4811–4824, 7 2019. ISSN 0018-926X. Available from Internet: <<https://ieeexplore.ieee.org/document/8668512/>>. Cited once at page 41.
- FERNANDEZ-ARANZAMENDI, E. et al. Breast tumor classification by age and size based on analysis of dielectric properties performed on in vivo and ex vivo measurements. In: *2022 International Workshop on Antenna Technology (iWAT)*. IEEE, 2022. p. 192–195. ISBN 978-1-6654-9449-6. Available from Internet: <<https://ieeexplore.ieee.org/document/9811011/>>. Cited once at page 40.
- FHAGER, A. *Andreas Fhager | Chalmers*. 2021. Available from Internet: <<https://www.chalmers.se/en/staff/Pages/andreas-fhager.aspx>>. Cited once at page 74.
- GENTILINI, O. D.; PARTRIDGE, A.; PAGANI, O. *Breast Cancer in Young Women*. Cham: Springer International Publishing, 2020. v. 1. 494 p. ISSN 00071447. ISBN 978-3-030-24761-4. Available from Internet: <<http://link.springer.com/10.1007/978-3-030-24762-1>>. Cited once at page 27.
- GNU Radio. *GNU Radio - The Free & Open Source Radio Ecosystem*. 2021. Available from Internet: <<https://www.gnuradio.org/>>. Cited once at page 59.
- GUO, X. et al. *Simulation and Design of an UWB Imaging System for Breast Cancer Detection*. Thesis (Doctoral) — Politecnico di Torino, 2014. Available from Internet: <<http://www.sciencedirect.com/science/article/pii/S016792601400011X>>. Cited once at page 80.
- HADEBE, B. et al. The Role of PET/CT in Breast Cancer. *Diagnostics*, v. 13, n. 4, 2023. ISSN 20754418. Cited once at page 30.

HAGNESS, S. C.; TAFLOVE, A.; BRIDGES, J. E. Two-dimensional FDTD analysis of a pulsed microwave confocal system for breast cancer detection: Fixed-focus and antenna-array sensors. *IEEE Transactions on Biomedical Engineering*, v. 45, n. 12, p. 1470–1479, 1998. ISSN 00189294. Cited once at page 46.

HARRIS, F.; LOWDERMILK, W. Software defined radio: Part 22 in a series of tutorials on instrumentation and measurement. *IEEE Instrumentation and Measurement Magazine*, v. 13, n. 1, p. 23–32, 2 2010. ISSN 10946969. Cited once at page 54.

HEJDUK, P. et al. Fully automatic classification of automated breast ultrasound (ABUS) imaging according to BI-RADS using a deep convolutional neural network. *European Radiology*, *European Radiology*, v. 32, n. 7, p. 4868–4878, 7 2022. ISSN 1432-1084. Available from Internet: <<https://link.springer.com/10.1007/s00330-022-08558-0>>. Cited once at page 29.

HENRIKSSON, T. et al. Clinical trials of a multistatic UWB radar for breast imaging. In: *2011 Loughborough Antennas & Propagation Conference*. IEEE, 2011. p. 1–4. ISBN 978-1-4577-1016-2. Available from Internet: <<http://ieeexplore.ieee.org/document/6114004/>>. Cited once at page 68.

HIPPEL, A. R. V. *Dielectrics and Waves*. 1. ed. [S.l.]: Artech House Publishers, 1995. 304 p. ISBN 1580531229. Cited once at page 42.

IMDRF. *Clinical Evaluation*. [S.l.], 2019. Cited once at page 61.

IMDRF. *Clinical Investigation*. [S.l.], 2019. Cited once at page 61.

INCA. *Estimativa 2020: incidência de câncer no Brasil*. [S.l.], 2020. v. 1, n. 1. Cited once at page 28.

INCA. *Estimativa 2023: incidência do Câncer no Brasil*. 2022. Available from Internet: <<https://www.gov.br/inca/pt-br/assuntos/cancer/numeros/estimativa>>. Cited once at page 28.

IRANMAKANI, S. et al. A review of various modalities in breast imaging: technical aspects and clinical outcomes. *Egyptian Journal of Radiology and Nuclear Medicine*, *Egyptian Journal of Radiology and Nuclear Medicine*, v. 51, n. 1, p. 57, 12 2020. ISSN 2090-4762. Available from Internet: <<https://ejrnm.springeropen.com/articles/10.1186/s43055-020-00175-5>>. Cited 2 times at pages 29 and 30.

ISLAM, M. T. et al. A Low Cost and Portable Microwave Imaging System for Breast Tumor Detection Using UWB Directional Antenna array. *Scientific Reports*, Nature Publishing Group, v. 9, n. 1, p. 1–13, 12 2019. ISSN 20452322. Available from Internet: <<https://doi.org/10.1038/s41598-019-51620-z>>. Cited once at page 32.

JANJIC, A. et al. Microwave Breast Lesion Classification – Results from Clinical Investigation of the SAFE Microwave Breast Cancer System. *Academic Radiology*, Elsevier Inc., n. 11, p. 1–8, 12 2022. ISSN 10766332. Available from Internet: <<https://linkinghub.elsevier.com/retrieve/pii/S1076633222006419>>. Cited once at page 82.

JANJIC, A. et al. SAFE: A Novel Microwave Imaging System Design for Breast Cancer Screening and Early Detection—Clinical Evaluation. *Diagnostics*, v. 11, n. 3, p. 533, 3 2021. ISSN 2075-4418. Available from Internet: <<https://www.mdpi.com/2075-4418/11/3/533>>. Cited once at page 66.

JANKIRAMAN, M. *Design of Multi-Frequency CW Radars*. 1. ed. Institution of Engineering and Technology, 2007. 1–352 p. ISBN 9781891121562. Available from Internet: <<https://digital-library.theiet.org/content/books/ra/sbra004e>>. Cited 2 times at pages 49 and 51.

KAUR, G.; KAUR, A. Breast tissue tumor detection using “ S ” parameter analysis with an UWB stacked aperture coupled microstrip patch antenna having a “ + ” shaped defected ground structure. *International Journal of Microwave and Wireless Technologies*, v. 12, n. 7, p. 635–651, 9 2020. ISSN 1759-0787. Available from Internet: <https://www.cambridge.org/core/product/identifier/S1759078719001442/type/journal_article>. Cited 2 times at pages 60 and 90.

KENINGTON, P. B. *RF and baseband techniques for software defined radio*. 1. ed. [S.l.: s.n.], 2005. Cited once at page 54.

Keysight Technologies. *First-to-Market Radio-Wave Breast Imaging System Achieved with Network Analyzer The Key Issues : Improve Breast Cancer Detection and*. [S.l.], 2020. 1–4 p. Cited once at page 68.

KLEMM, M. et al. Radar-Based Breast Cancer Detection Using a Hemispherical Antenna Array—Experimental Results. *IEEE Transactions on Antennas and Propagation*, v. 57, n. 6, p. 1692–1704, 6 2009. ISSN 0018-926X. Available from Internet: <<http://ieeexplore.ieee.org/document/5062515/>>. Cited once at page 68.

KOHL, N. E. *Software Defined Radio Short Range Radar*. 75 p. Thesis (Doctoral) — Department of Electrical and Computer Engineering, BYU, 2021. Cited 2 times at pages 105 and 106.

KOSMAS, P.; CROCCO, L. Introduction to Special Issue on “Electromagnetic Technologies for Medical Diagnostics: Fundamental Issues, Clinical Applications and Perspectives”. *Diagnostics*, v. 9, n. 1, p. 19, 2 2019. ISSN 2075-4418. Available from Internet: <<http://www.mdpi.com/2075-4418/9/1/19>>. Cited once at page 44.

KRANOLD, L. et al. Skin Phantoms for Microwave Breast Cancer Detection: A Comparative Study. *IEEE Journal of Electromagnetics, RF and Microwaves in Medicine and Biology*, p. 1–1, 2021. ISSN 2469-7249. Available from Internet: <<https://ieeexplore.ieee.org/document/9442302/>>. Cited once at page 41.

KRANOLD, L.; POPOVIC, M. RF Radar Breast Health Monitoring: System Evaluation With Post-Biopsy Marker. *IEEE Journal of Electromagnetics, RF and Microwaves in Medicine and Biology*, v. 5, n. 2, p. 148–154, 6 2021. ISSN 2469-7249. Available from Internet: <<https://ieeexplore.ieee.org/document/9195122/>>. Cited once at page 72.

KRANOLD, L. et al. Microwave Breast Screening Prototype: System Miniaturization With IC Pulse Radio. *IEEE Journal of Electromagnetics, RF and Microwaves in Medicine and Biology*, v. 5, n. 2, p. 168–178, 6 2021. ISSN 2469-7249. Available from Internet: <<https://ieeexplore.ieee.org/document/9216473/>>. Cited 2 times at pages 72 and 99.

KUBOTA, S. et al. 5-Gb/s and 10-GHz Center-Frequency Gaussian Monocycle Pulse Transmission Using 65-nm Logic CMOS With On-Chip Dipole Antenna and High-k Interposer. *IEEE Transactions on Components, Packaging and Manufacturing Technology*, Institute of Electrical and Electronics Engineers Inc., v. 4, n. 7, p. 1193–1200, 7 2014. ISSN 2156-3950. Available from Internet: <<http://ieeexplore.ieee.org/document/6822529/>>. Cited once at page 77.

KWON, S.; LEE, S. Recent Advances in Microwave Imaging for Breast Cancer Detection. *International Journal of Biomedical Imaging*, v. 2016, p. 1–26, 2016. ISSN 1687-4188. Available from Internet: <<https://www.hindawi.com/journals/ijbi/2016/5054912/>>. Cited 2 times at pages 45 and 61.

LAZEBNIK, M. et al. A large-scale study of the ultrawideband microwave dielectric properties of normal, benign and malignant breast tissues obtained from cancer surgeries. *Physics in Medicine and Biology*, v. 52, n. 20, p. 6093–6115, 2007. ISSN 00319155. Cited 2 times at pages 33 and 40.

LEOPOLDO, L. R.; NOIJE, W. A. M. V. Low Noise Broadband Amplifier for Breast Cancer System. In: *2022 35th SBC/SBMicro/IEEE/ACM Symposium on Integrated Circuits and Systems Design (SBCCI)*. IEEE, 2022. p. 1–5. ISBN 978-1-6654-8128-1. Available from Internet: <<https://ieeexplore.ieee.org/document/9893241/>>. Cited once at page 50.

LI, L. *The analysis of UWB Radar System for Microwave Imaging Application*. Thesis (Doctoral) — Queen Mary, University of London, 2015. Cited 2 times at pages 48 and 49.

LI, Y. et al. Microwave breast cancer detection via cost-sensitive ensemble classifiers: Phantom and patient investigation. *Biomedical Signal Processing and Control*, Elsevier Ltd, v. 31, p. 366–376, 1 2017. ISSN 17468094. Available from Internet: <<https://linkinghub.elsevier.com/retrieve/pii/S174680941630129X>>. Cited 2 times at pages 70 and 71.

LUI, H. S.; FHAGER, A.; PERSSON, M. On the forward scattering of microwave breast imaging. *International Journal of Biomedical Imaging*, v. 2012, 2012. ISSN 16874188. Cited once at page 45.

MANGO, V. L. et al. The iBreastExam versus clinical breast examination for breast evaluation in high risk and symptomatic Nigerian women: a prospective study. *The Lancet Global Health*, The Author(s). Published by Elsevier Ltd. This is an Open Access article under the CC BY-NC-ND 4.0 license, v. 10, n. 4, p. e555–e563, 2022. ISSN 2214109X. Available from Internet: <[http://dx.doi.org/10.1016/S2214-109X\(22\)00030-4](http://dx.doi.org/10.1016/S2214-109X(22)00030-4)>. Cited once at page 30.

MARIMUTHU, J. *Design of Wideband Microwave Frontend for Microwave-Based Imaging Systems*. Thesis (Doctoral) — The University of Queensland - Australia, 2016. Cited once at page 79.

MARIMUTHU, J.; BIALKOWSKI, K. S.; ABBOSH, A. M. Software-Defined Radar for Medical Imaging. *IEEE Transactions on Microwave Theory and Techniques*, p. 1–10, 2016. ISSN 0018-9480. Available from Internet: <<http://ieeexplore.ieee.org/document/7378332/>>. Cited once at page 55.

MARTINS, T. A. et al. A Class AB Programmable Gain Amplifier for an UWB Breast Cancer Detection System. In: *2021 28th IEEE International Conference on Electronics, Circuits, and Systems (ICECS)*. IEEE, 2021. p. 1–4. ISBN 978-1-7281-8281-0. Available from Internet: <<https://ieeexplore.ieee.org/document/9665475/>>. Cited once at page 50.

McGill University. *RF Breast Cancer Detection Research Group*. 2021. Available from Internet: <<http://www.compem.ece.mcgill.ca/breast-cancer-detection/index.html>>. Cited once at page 70.

MEANEY, P.; GEIMER, S.; PAULSEN, K. Examination of the sensitivity matrix during the iterative reconstruction process for microwave tomography. In: *2018 IEEE Conference on Antenna Measurements and Applications, CAMA 2018*. [S.l.]: Institute of Electrical and Electronics Engineers Inc., 2018. ISBN 9781538657959. Cited once at page 45.

MEANEY, P. et al. A 4-channel, vector network analyzer microwave imaging prototype based on software defined radio technology. *Review of Scientific Instruments*, v. 90, n. 4, p. 044708, 4 2019. ISSN 0034-6748. Available from Internet: <<http://dx.doi.org/10.1063/1.5083842><http://aip.scitation.org/doi/10.1063/1.5083842>>. Cited once at page 82.

MEANEY, P. et al. Low Cost, High Performance, 16-Channel Microwave Measurement System for Tomographic Applications. *Sensors*, v. 20, n. 18, p. 5436, 9 2020. ISSN 1424-8220. Available from Internet: <<https://www.mdpi.com/1424-8220/20/18/5436>>. Cited once at page 64.

MEANEY, P. M. et al. Initial Clinical Experience with Microwave Breast Imaging in Women with Normal Mammography. *Academic Radiology*, v. 14, n. 2, p. 207–218, 2007. ISSN 1076-6332. Available from Internet: <<https://www.sciencedirect.com/science/article/pii/S1076633206006301>>. Cited once at page 63.

MEHRANPOUR, M. et al. Robust Breast Cancer Imaging Based on a Hybrid Artifact Suppression Method for Early-Stage Tumor Detection. *IEEE Access*, v. 8, p. 206790–206805, 2020. ISSN 2169-3536. Available from Internet: <<https://ieeexplore.ieee.org/document/9257357/>>. Cited once at page 35.

MEYER, T. *Microwave Imaging of High-Contrast Objects*. Thesis (Doctoral) — Magdeburg, 2005. Cited once at page 46.

Micrima. *MARIA installed in Athens for Data collection*. 2021. Available from Internet: <<https://www.micrima.com/news/aria-installed-in-athens-for-data-collection>>. Cited once at page 81.

MISILMANI, H. M. E. et al. A Survey on Antenna Designs for Breast Cancer Detection Using Microwave Imaging. *IEEE Access*, v. 8, p. 102570–102594, 2020. ISSN 2169-3536. Available from Internet: <<https://ieeexplore.ieee.org/document/9104688/>>. Cited once at page 88.

MITOLA, J. Software radios-survey, critical evaluation and future directions. In: *[Proceedings] NTC-92: National Telesystems Conference*. IEEE, 1992. p. 13–23. ISBN 0-7803-0554-X. Available from Internet: <<http://ieeexplore.ieee.org/document/267870/>>. Cited once at page 53.

MOLONEY, B. et al. The validation of a Microwave Breast Imaging System Prior to a First-In-Human Trial. *European Society of Radiology*, n. April, 2019. Available from Internet: <<https://dx.doi.org/10.26044/ecr2019/C-3539>>. Cited once at page 74.

MOLONEY, B. M. et al. Microwave Imaging in Breast Cancer – Results from the First-In-Human Clinical Investigation of the Wavelia System. *Academic Radiology*, Elsevier Inc., v. 29, n. 3, p. S211–S222, 1 2022. ISSN 10766332. Available from Internet: <<https://linkinghub.elsevier.com/retrieve/pii/S1076633221002993>>. Cited once at page 73.

MOLONEY, B. M. et al. Breast Cancer Detection—A Synopsis of Conventional Modalities and the Potential Role of Microwave Imaging. *Diagnostics*, MDPI AG, v. 10, n. 2, p. 103, 2 2020. ISSN 2075-4418. Available from Internet: <<https://www.mdpi.com/2075-4418/10/2/103>>. Cited once at page 29.

NAGHIBI, A.; ATTARI, A. R. Near-Field Radar-Based Microwave Imaging for Breast Cancer Detection: A Study on Resolution and Image Quality. *IEEE Transactions on Antennas and Propagation*, v. 69, n. 3, p. 1670–1680, 2021. ISSN 15582221. Cited once at page 106.

NanoRFE/HCXQS. *NanoRFE VNA6000*. 2024. Available from Internet: <<https://nanorfe.com/vna6000.html>>. Cited once at page 83.

National Instruments. *Ettus Research - The leader in Software Defined Radio (SDR) | Ettus Research, a National Instruments Brand | The leader in Software Defined Radio (SDR)*. 2021. Available from Internet: <<https://www.ettus.com/>>. Cited once at page 64.

NGUYEN, C.; PARK, J. *Stepped-Frequency Radar Sensors*. Cham: Springer International Publishing, 2016. (SpringerBriefs in Electrical and Computer Engineering). ISBN 978-3-319-12270-0. Available from Internet: <<http://link.springer.com/10.1007/978-3-319-12271-7>>. Cited 5 times at pages 42, 48, 49, 51, and 100.

NIKOLOVA, N. Microwave Imaging for Breast Cancer. *IEEE Microwave Magazine*, v. 12, n. 7, p. 78–94, 12 2011. ISSN 1527-3342. Available from Internet: <<http://ieeexplore.ieee.org/document/6031961/>>. Cited 3 times at pages 41, 42, and 65.

NIKOLOVA, N. K. *Introduction to Microwave Imaging*. Cambridge: Cambridge University Press, 2017. 1–362 p. ISBN 9781316084267. Cited 3 times at pages 45, 59, and 65.

Nuand. *libbladeRF*. 2023. Available from Internet: <<https://nuand.com/libbladeRF-doc/v2.5.0/>>. Cited once at page 133.

OKADA, K.; KOUSAI, S. *Digitally-Assisted Analog and RF CMOS Circuit Design for Software-Defined Radio*. New York, NY: Springer New York, 2011. ISBN 978-1-4419-8513-2. Available from Internet: <<http://link.springer.com/10.1007/978-1-4419-8514-9>>. Cited 2 times at pages 55 and 58.

OLAOGUN, J. G.; AGODIRIN, O. S. Breast cancer screening: can the iBreastExam bridge the gap? *The Lancet Global Health*, The Author(s). Published by Elsevier Ltd. This is an Open Access article under the CC BY-NC-ND 4.0 license, v. 10, n. 4, p. e461–e462, 2022. ISSN 2214109X. Available from Internet:

<[http://dx.doi.org/10.1016/S2214-109X\(22\)00078-X](http://dx.doi.org/10.1016/S2214-109X(22)00078-X)>. Cited once at page 30.

O'LOUGHLIN, D. et al. Microwave Breast Imaging: Clinical Advances and Remaining Challenges. *IEEE Transactions on Biomedical Engineering*, IEEE Computer Society, v. 65, n. 11, p. 2580–2590, 11 2018. ISSN 0018-9294. Available from Internet: <<https://ieeexplore.ieee.org/document/8302576/>>. Cited 2 times at pages 61 and 73.

OROZCO, L. G. *Software defined radio for medical applications*. 1–46 p. Thesis (Doctoral) — Chalmers University of Technology, 2019. Cited once at page 75.

PARK, J. *Development of Microwave and Millimeter-Wave Integrated-Circuit Stepped-Frequency Radar Sensors for Surface and Subsurface Profiling*. Thesis (Doctoral) — Texas A&M University, 2003. Cited once at page 50.

PAULSEN, K. *Keith Paulsen, PhD | The Center for Surgical Innovation | Health Care Professionals | Dartmouth-Hitchcock*. 2021. Available from Internet: <<https://med.dartmouth-hitchcock.org/csi/keith-paulsen.html>>. Cited once at page 62.

PAULSEN, K. D.; MEANEY, P. M.; GILMAN, L. C. *Alternative Breast Imaging*. Boston, MA: Springer US, 2005. v. 1. 1–270 p. (The Kluwer International Series in Engineering and Computer Science, 1). ISSN 0893-3405. ISBN 978-0-387-23363-5. Available from Internet: <<http://link.springer.com/10.1007/b101336>>. Cited 2 times at pages 31 and 44.

Peter Delos. *A Review of Wideband RF Receiver Architecture Options*. 2016. Available from Internet: <<https://www.analog.com/en/technical-articles/a-review-of-wideband-rf-receiver-architecture-options.html>>. Cited once at page 58.

PORTER, E. *Microwave time-domain radar for monitoring breast health: development and testing of an early prototype*. 1–142 p. Thesis (Doctoral) — McGill University, 2015. Cited once at page 70.

PORTER, E. et al. A Wearable Microwave Antenna Array for Time-Domain Breast Tumor Screening. *IEEE Transactions on Medical Imaging*, Institute of Electrical and Electronics Engineers Inc., v. 35, n. 6, p. 1501–1509, 6 2016. ISSN 0278-0062. Available from Internet: <<http://ieeexplore.ieee.org/document/7384493/>>. Cited 2 times at pages 71 and 72.

PORTER, E.; O'LOUGHLIN, D. Pathway to Demonstrating Clinical Efficacy of Microwave Breast Imaging: Qualitative and Quantitative Performance Assessment. *IEEE Journal of Electromagnetics, RF and Microwaves in Medicine and Biology*, IEEE, v. 6, n. 4, p. 439–448, 12 2022. ISSN 2469-7249. Available from Internet: <<https://ieeexplore.ieee.org/document/9944184/>>. Cited 2 times at pages 29 and 84.

PREECE, A. W. et al. MARIA M4: clinical evaluation of a prototype ultrawideband radar scanner for breast cancer detection. *Journal of Medical Imaging*, SPIE-Intl Soc Optical Eng, v. 3, n. 3, p. 033502, 7 2016. ISSN 2329-4302. Available from Internet: <<https://pubmed.ncbi.nlm.nih.gov/27446970/http://medicalimaging.spiedigitallibrary.org/article.aspx?doi=10.1117/1.JMI.3.3.033502>>. Cited 2 times at pages 68 and 69.

- REIMER, T.; PISTORIUS, S. Review and Analysis of Tumour Detection and Image Quality Analysis in Experimental Breast Microwave Sensing. *Sensors*, v. 23, n. 11, p. 5123, 5 2023. ISSN 1424-8220. Available from Internet: <<https://www.mdpi.com/1424-8220/23/11/5123>>. Cited once at page 30.
- REYES, D. et al. A 10.75-ENOB 20 MS/s SAR ADC for an UWB Transceiver Applied in Breast Cancer Detection in 180 nm CMOS. In: *2020 IEEE 63rd International Midwest Symposium on Circuits and Systems (MWSCAS)*. IEEE, 2020. p. 357–360. ISBN 978-1-7281-8058-8. Available from Internet: <<https://ieeexplore.ieee.org/document/9184488/>>. Cited once at page 50.
- ROOT, D. et al. *S-Parameter Measurements Basics for High Speed Digital Engineers*. [S.l.], 2013. 88–111 p. Cited once at page 59.
- ROSOLOWSKI, D. et al. An ultrawideband 1 to 6 GHz 0-IF radio receiver with 500 MHz of instantaneous bandwidth. *2016 21st International Conference on Microwave, Radar and Wireless Communications, MIKON 2016*, p. 2–5, 2016. Cited once at page 58.
- RUBÆK, T. *Microwave Imaging for Breast-Cancer Screening*. Thesis (Doctoral) — Technical University of Denmark, 2008. Cited once at page 64.
- S. D'Amico et al. *Advances in Biomedical Sensing, Measurements, Instrumentation and Systems*. Berlin, Heidelberg: Springer Berlin Heidelberg, 2010. v. 55. 1–27 p. (Lecture Notes in Electrical Engineering, v. 55). ISBN 978-3-642-05166-1. Available from Internet: <<http://link.springer.com/10.1007/978-3-642-05167-8>>. Cited once at page 46.
- SAMSUZZAMAN, M. et al. A 16-modified antipodal Vivaldi antenna array for microwave-based breast tumor imaging applications. *Microwave and Optical Technology Letters*, v. 61, n. 9, p. 2110–2118, 9 2019. ISSN 0895-2477. Available from Internet: <<https://onlinelibrary.wiley.com/doi/abs/10.1002/mop.31873><https://onlinelibrary.wiley.com/doi/10.1002/mop.31873>>. Cited once at page 88.
- SANCHEZ-BAYUELA, D. A. et al. Breast Biopsy Characterization Through Microwave Imaging Using MammoWave® Apparatus. In: *2022 IEEE International Symposium on Antennas and Propagation and USNC-URSI Radio Science Meeting (AP-S/URSI)*. IEEE, 2022. p. 874–875. ISBN 978-1-6654-9658-2. Available from Internet: <<https://ieeexplore.ieee.org/document/9886646/>>. Cited once at page 33.
- SANI, L. et al. Novel microwave apparatus for breast lesions detection: Preliminary clinical results. *Biomedical Signal Processing and Control*, v. 52, p. 257–263, 7 2019. ISSN 17468094. Available from Internet: <<https://linkinghub.elsevier.com/retrieve/pii/S1746809419301223>>. Cited once at page 82.
- SANI, L. et al. Initial Clinical Validation of a Novel Microwave Apparatus for Testing Breast Integrity. *IST 2016 - 2016 IEEE International Conference on Imaging Systems and Techniques, Proceedings*, IEEE, p. 278–282, 2016. Cited once at page 76.
- SANI, L. et al. Microwave apparatus for testing breast integrity based on Huygens principle: Clinical validation on 16 subjects. *IET Conference Publications*, v. 2017, n. CP732, p. 1–5, 2017. Cited once at page 76.
- SANTORELLI, A. *A compact and low-cost microwave radar prototype for breast health monitoring*. Thesis (Doctoral) — McGill University, 2017. Cited once at page 70.

SASAKI, K. et al. Measurement and image-based estimation of dielectric properties of biological tissues —past, present, and future—. *Physics in Medicine & Biology*, IOP Publishing, v. 67, n. 14, p. 14TR01, 7 2022. ISSN 0031-9155. Available from Internet: <<https://iopscience.iop.org/article/10.1088/1361-6560/ac7b64>>. Cited once at page 31.

SBM. *Número de mamografias ainda é baixo no Brasil. Veja o porquê - SBM*. 2018. Available from Internet: <<https://www.sbmastologia.com.br/noticias/numero-de-mamografias-ainda-e-baixo-no-brasil-veja-o-porque/>>. Cited once at page 36.

SELVARAJ, V. et al. Breast Tissue Tumor Analysis Using Wideband Antenna and Microwave Scattering. *IETE Journal of Research*, Taylor & Francis, v. 67, n. 1, p. 49–59, 2021. ISSN 0974780X. Available from Internet: <<https://doi.org/10.1080/03772063.2018.1531067>>. Cited once at page 60.

Shah Karam, S. A.; O'LOUGHLIN, D.; ASL, B. M. A novel sophisticated form of dmas beamformer: Application to breast cancer detection. *Biomedical Signal Processing and Control*, v. 74, p. 103516, 2022. ISSN 1746-8094. Available from Internet: <<https://www.sciencedirect.com/science/article/pii/S1746809422000386>>. Cited once at page 47.

SHAO, W.; MCCOLLOUGH, T. Advances in Microwave Near-Field Imaging: Prototypes, Systems, and Applications. *IEEE Microwave Magazine*, IEEE, v. 21, n. 5, p. 94–119, 2020. ISSN 15579581. Cited once at page 82.

SHERE, M. et al. MARIA® M5: A multicentre clinical study to evaluate the ability of the Micrima radio-wave radar breast imaging system (MARIA®) to detect lesions in the symptomatic breast. *European Journal of Radiology*, Elsevier Ireland Ltd, v. 116, p. 61–67, 7 2019. ISSN 0720048X. Available from Internet: <<https://linkinghub.elsevier.com/retrieve/pii/S0720048X19301512>>. Cited 3 times at pages 32, 68, and 81.

SHUMAKOV, D. S.; NIKOLOVA, N. K. Fast quantitative microwave imaging with scattered-power maps. *IEEE Transactions on Microwave Theory and Techniques*, Institute of Electrical and Electronics Engineers Inc., v. 66, n. 1, p. 439–449, 1 2018. ISSN 00189480. Cited once at page 65.

SIEGEL, R. L. et al. Cancer statistics, 2023. *CA: A Cancer Journal for Clinicians*, v. 73, n. 1, p. 17–48, 1 2023. ISSN 0007-9235. Available from Internet: <<https://onlinelibrary.wiley.com/doi/10.3322/caac.21763>>. Cited once at page 28.

SIPOS, D.; GLEICH, D. Sfew radar with an integrated static target echo cancellation system. *Sensors*, v. 21, n. 17, 2021. ISSN 14248220. Cited once at page 52.

SONG, H. et al. Detectability of Breast Tumor by a Hand-held Impulse-Radar Detector: Performance Evaluation and Pilot Clinical Study. *Scientific Reports*, Nature Publishing Group, v. 7, n. 1, 12 2017. ISSN 20452322. Cited 3 times at pages 32, 76, and 77.

STANCOMBE, A. E.; BIALKOWSKI, K. S. Portable biomedical microwave imaging using software-defined radio. *Asia-Pacific Microwave Conference Proceedings, APMC, IEICE*, v. 2018-Novem, p. 572–574, 2019. Cited once at page 79.

SUGITANI, T. et al. A Compact 4 x 4 Planar UWB Antenna Array for 3-D Breast Cancer Detection. *IEEE Antennas and Wireless Propagation Letters*, v. 12, p. 733–736, 2013. ISSN 1536-1225. Available from Internet: <<http://ieeexplore.ieee.org/document/6545333/>>. Cited once at page 77.

TAJIK, D. *Quantitative Microwave Imaging for Breast Cancer Detection Advances in Real-Time Quantitative Near-Field*. 206 p. Thesis (Doctoral) — McMaster university, 2022. Cited once at page 65.

TAJIK, D.; TRAC, J.; NIKOLOVA, N. K. Quality Control of Microwave Equipment for Tissue Imaging. *IEEE Journal of Electromagnetics, RF and Microwaves in Medicine and Biology*, Institute of Electrical and Electronics Engineers Inc., v. 4, n. 1, p. 52–60, 3 2020. ISSN 24697249. Available from Internet: <<https://ieeexplore.ieee.org/document/8747500/>>. Cited once at page 65.

TAKAHASHI, K.; MIWA, T. Near-Range SFCW UWB Radar Based on Low-Cost Software Defined Radio. In: *2019 IEEE Radar Conference (RadarConf)*. IEEE, 2019. p. 1–6. ISBN 978-1-7281-1679-2. Available from Internet: <<https://ieeexplore.ieee.org/document/8835490/>>. Cited once at page 85.

TAKAHASHI, K.; MIWA, T. A Local Oscillator Phase Compensation Technique for Ultra-Wideband Stepped-Frequency Continuous Wave Radar Based on a Low-Cost Software-Defined Radio. *Sensors*, v. 21, n. 3, p. 780, 1 2021. ISSN 1424-8220. Available from Internet: <<https://www.mdpi.com/1424-8220/21/3/780>>. Cited once at page 52.

TAYLOR, J. D. *Advanced Ultrawideband Radar*. Boca Raton, FL : CRC Press, Taylor & Francis Group, 2016.: CRC Press, 2016. 1–475 p. ISBN 9781315374130. Available from Internet: <<https://www.taylorfrancis.com/books/9781315374130>>. Cited once at page 49.

TICE, J. A.; KERLIKOWSKE, K. Screening for Breast Cancer in Women With Dense Breasts. In: *Breast Cancer Screening*. Elsevier, 2016. p. 241–263. ISBN 9780128024942. Available from Internet: <<https://linkinghub.elsevier.com/retrieve/pii/B9780128022092000103>>. Cited once at page 40.

TING, J.-W.; OLOUMI, D.; RAMBABU, K. FMCW SAR System for Near-Distance Imaging Applications—Practical Considerations and Calibrations. *IEEE Transactions on Microwave Theory and Techniques*, Institute of Electrical and Electronics Engineers Inc., v. 66, n. 1, p. 450–461, 1 2018. ISSN 0018-9480. Available from Internet: <<http://ieeexplore.ieee.org/document/7945518/>>. Cited once at page 51.

TMDV. *Translational Medical Device Lab | NUI Galway*. 2021. Available from Internet: <<https://tmdlab.ie/>>. Cited once at page 73.

TOYA, A. et al. 125 mW 102.4 GS/s Ultra-High-Speed Sampling Circuit for Complementary Metal–Oxide–Semiconductor Breast Cancer Detection System. *Japanese Journal of Applied Physics*, IOP Publishing, v. 52, n. 4S, p. 04CE07, 4 2013. ISSN 0021-4922. Available from Internet: <<https://iopscience.iop.org/article/10.7567/JJAP.52.04CE07https://iopscience.iop.org/article/10.7567/JJAP.52.04CE07/meta>>. Cited once at page 77.

UBT. *UBT - Company*. 2021. Available from Internet: <<https://www.ubt-tech.com/en/microwave-imaging-technology/>>. Cited once at page 82.

- UTTERBACK, J. M. *Mastering the dynamics of innovation*. Elsevier, 1995. v. 12. ISSN 09234748. ISBN 9780875847405. Available from Internet: <<https://linkinghub.elsevier.com/retrieve/pii/0923474895900039>>. Cited once at page 84.
- VISPA, A. et al. UWB device for breast microwave imaging: phantom and clinical validations. *Measurement: Journal of the International Measurement Confederation*, Elsevier Ltd, v. 146, p. 582–589, 2019. ISSN 02632241. Available from Internet: <<https://doi.org/10.1016/j.measurement.2019.05.109>>. Cited once at page 76.
- VORST, A. V.; ROSEN, A.; KOTSUKA, Y. *RF/Microwave Interaction with Biological Tissues*. Hoboken, NJ, USA: John Wiley & Sons, Inc., 2005. ISBN 9780471752059. Available from Internet: <<http://doi.wiley.com/10.1002/0471752053>>. Cited once at page 31.
- WANG, L. Early Diagnosis of Breast Cancer. *Sensors*, v. 17, n. 7, p. 1572, 7 2017. ISSN 1424-8220. Available from Internet: <<http://www.mdpi.com/1424-8220/17/7/1572>>. Cited once at page 30.
- WANG, L. Microwave Sensors for Breast Cancer Detection. *Sensors*, v. 18, n. 2, p. 655, 2 2018. ISSN 1424-8220. Available from Internet: <<http://www.mdpi.com/1424-8220/18/2/655>>. Cited once at page 61.
- WEHNER, D. R. *High Resolution Radar*. [S.l.]: Artech House, 1995. ISBN 0890061947. Cited once at page 53.
- WHITE, M. C. et al. Age and cancer risk: A potentially modifiable relationship. *American Journal of Preventive Medicine*, Elsevier, v. 46, n. 3 SUPPL. 1, p. S7–S15, 3 2014. ISSN 07493797. Available from Internet: <<http://dx.doi.org/10.1016/j.amepre.2013.10.029>>. Cited once at page 27.
- WHO. *Breast fact sheet*. 2020. Available from Internet: <<https://gco.iarc.fr/today/data/factsheets/cancers/20-Breast-fact-sheet.pdf>>. Cited once at page 28.
- WHO. *Breast Cancer Inequities*. 2023. Available from Internet: <<https://www.who.int/initiatives/global-breast-cancer-initiative/breast-cancer-inequities>>. Cited once at page 28.
- WÖRTGE, D. et al. Comparison of X-ray-Mammography and Planar UWB Microwave Imaging of the Breast: First Results from a Patient Study. *Diagnostics*, v. 8, n. 3, p. 54, 8 2018. ISSN 2075-4418. Available from Internet: <<http://www.mdpi.com/2075-4418/8/3/54>>. Cited once at page 36.
- WORTGE, D. et al. Prototype system for microwave breast imaging: Experimental results from tissue phantoms. In: *2018 11th German Microwave Conference (GeMiC)*. IEEE, 2018. v. 2018-Janua, p. 399–402. ISBN 978-3-9812668-8-7. Available from Internet: <<https://ieeexplore.ieee.org/document/8335114/>>. Cited once at page 65.
- YANG, R. et al. *High-Resolution Microwave Imaging*. Singapore: Springer Singapore, 2018. 1–552 p. ISBN 978-981-10-7136-2. Available from Internet: <<http://link.springer.com/10.1007/978-981-10-7138-6>>. Cited 2 times at pages 48 and 53.

- YUKSEL, H. et al. A Wideband Fully Integrated Software-Defined Transceiver for FDD and TDD Operation. *IEEE Journal of Solid-State Circuits*, v. 52, n. 5, p. 1274–1285, 5 2017. ISSN 0018-9200. Available from Internet: <<https://ieeexplore.ieee.org/document/7835655/>>. Cited once at page 57.
- ZASTROW, E. et al. Development of Anatomically Realistic Numerical Breast Phantoms With Accurate Dielectric Properties for Modeling Microwave Interactions With the Human Breast. *IEEE Transactions on Biomedical Engineering*, v. 55, n. 12, p. 2792–2800, 12 2008. ISSN 0018-9294. Available from Internet: <<http://ieeexplore.ieee.org/document/4564184/>>. Cited once at page 43.
- ZENG, X. *Time Domain Systems for Microwave Imaging : Accuracy Evaluations and Prototype Design*. 1 - 54 p. Thesis (Doctoral) — Chalmers University of Technology, 2013. Cited once at page 75.
- ZENG, X. *Xuezhi Zeng / Chalmers*. 2021. Available from Internet: <<https://www.chalmers.se/en/staff/Pages/Xuezhi-Zeng.aspx>>. Cited once at page 74.
- ZENG, X.; OROZCO, L. G.; FHAGER, A. Phase calibration of a software defined radio system for medical applications. In: *Asia-Pacific Microwave Conference Proceedings, APMC*. [S.l.]: Institute of Electrical and Electronics Engineers Inc., 2019. v. 2019-Decem, p. 1414–1416. ISBN 9781728135175. Cited 2 times at pages 55 and 75.
- ZHURBENKO, V. Challenges in the design of microwave imaging systems for breast cancer detection. *Advances in Electrical and Computer Engineering*, v. 11, n. 1, p. 91 – 96, 2011. Cited once at page 97.

Appendix

APPENDIX A

Publications During Candidature

This Appendix listed all publications that underwent the Ph.D. candidate's contribution. It was divided into two groups, one related to this Thesis subject that contributes to this presented work; and another one not related to this Thesis subject but has contributed to the development of writing and researching skills.

A.1 Thesis Related

A.1.1 First Author

The listed publications, including one journal, one proceeding, and two conferences, originated from this Thesis research are described in the following:

- a) Journal: Dionísio Carvalho, Alexandre J.Aragão, Bruno Sanches, Hugo Daniel Hernandez, Wilhelmus Van Noije, " Experimental evaluation of a Software-Defined Radio through a Breast Phantom aiming at Microwave Medical Imaging",
In: **Microprocessors and Microsystems (Elsevier)**, 2021, pp - 104381,
DOI: <https://doi.org/10.1016/j.micpro.2021.104381>.
- b) Proceeding: D. de Carvalho, A. de Jesus Aragão; F. Brito Filho, H. Daniel Hernandez and W. A. Noije, "Analysis of Breast Cancer detection based on Software-Defined Radio Technology," In: **XXVII Brazilian Congress on Biomedical Engineering**, published in IFMBE Proceedings - Springer, 2020, pp. 439–444,
DOI: 10.1007/978-3-030-70601-2.
- c) Conference: D. Carvalho, A. J. Aragão, A. Ferrari, B. Sanches and W. Noije, "Software-Defined Radio Assessment for Microwave Imaging Breast Cancer Detection,"

In: **2020 IEEE Nordic Circuits and Systems Conference (NorCAS)**, Oslo, Norway, 2020, pp. 1-6,
DOI: 10.1109/NorCAS51424.2020.9265007.

- d) Conference: D. Carvalho, A. J. Aragão, and W. Noije, "Synthetic Pulse based on SFCW Modulation: a Proposition for Microwave Imaging" In: **2022 IEEE Sixth Ecuador Technical Chapters Meeting (ETCM)**, Quito, Ecuador, 2022
DOI: 10.1109/ETCM56276.2022.9935767.

A.1.2 Co-author

- a) A. de Jesus Aragão, D. de Carvalho, B. Sanches and W. A. M. Van Noije, "An improved confocal algorithm for breast cancer detection using UWB signals," In: **2020 IEEE 11th Latin American Symposium on Circuits and Systems (LASCAS)**, San Jose, Costa Rica, 2020, pp. 1-4,
DOI: 10.1109/LASCAS45839.2020.9069034.
- b) A. de Jesus Aragão, B. Sanches, D. de Carvalho and W. A. M. Van Noije, "Low-cost portable system prototype for breast cancer detection using UWB signals," In: **2020 IEEE 13th International Congress on Image and Signal Processing, BioMedical Engineering and Informatics (CISP-BMEI)**, Chengdu, China, 2020, pp. 715-720, DOI: 10.1109/CISP-BMEI51763.2020.9263688.
- c) A. de Jesus Aragão, D. Carvalho and W. A. M. Van Noije, "A firmware platform for breast cancer microwave imaging," In: **2021 IEEE Fifth Ecuador Technical Chapters Meeting (ETCM)**, Cuenca, Ecuador, 2021,
DOI: 10.1109/ETCM53643.2021.9590727.
- d) BRITO FILHO, F. A.; CARVALHO, D.; NOIJE, W. A. M. V. ., "Near Field Radar System Modeling for Microwave Imaging and Breast Cancer Detection Applications", In **XXVII Brazilian Congress on Biomedical Engineering**, published in IFMBE Proceedings - Springer, 2020, pp. 338 - 343, DOI: 10.1007/978-3-030-70601-2.

A.2 Not Thesis Related

- a) H. Hernandez, D. Carvalho, B. Sanches, L. C. Severo and W. Van Noije, "Current mode 1.2-Gbps SLVS transceiver for readout front-end ASIC," 2017 IEEE International Symposium on Circuits and Systems (ISCAS), 2017, pp. 1-4,
doi: 10.1109/ISCAS.2017.8050227.

-
- b) D. de Carvalho, B. Sanches, M. De Carvalho and W. Van Noije, "A flexible stand-alone FPGA-based ATE for ASIC manufacturing tests," 2018 IEEE 19th Latin-American Test Symposium (LATS), 2018, pp. 1-6, doi: 10.1109/LATW.2018.8347236.
 - c) N. R. de Menezes, H. D. Hernandez, D. Carvalho and W. Van Noije, "All-digital FPGA-based RF pulsed transmitter with hardware complexity reduction techniques," 2020 33rd Symposium on Integrated Circuits and Systems Design (SBCCI), 2020, pp. 1-5, doi: 10.1109/SBCCI50935.2020.9189929.
 - d) H. Hernández et al., "A Monolithic 32-Channel Front End and DSP ASIC for Gaseous Detectors," in IEEE Transactions on Instrumentation and Measurement, vol. 69, no. 6, pp. 2686-2697, June 2020, doi: 10.1109/TIM.2019.2931016.
 - e) J. Adolfsson et al., "The upgrade of the ALICE TPC with GEMs and continuous readout," in Journal of Instrumentation, vol. 16, no. 03, pp. P03022, March 2021, doi: 10.1088/1748-0221/16/03/p03022.
 - f) J. Adolfsson et al., "SAMPA Chip: the New 32 Channels ASIC for the ALICE TPC and MCH Upgrades," in Journal of Instrumentation, vol. 12, no. 04, pp. C04008, April 2017, doi: 10.1088/1748-0221/12/04/c04008.

APPENDIX B

BladeRF 2.0 - SFCW C code

This Appendix is related to the C code developed and compiled to performs the BladeRF 2.0 transceiver operation as a SFCW radar. It is based on the libraries from (Nuand, 2023).

```

1  /**
2   * \brief:          Command line interface
3   * \details:       Compatible Cross Compile
4   * \author:        Dionisio Carvalho
5   * \date:          sep/2021
6   * \revision       1.0
7   */
8
9  #include <stdio.h>
10 #include <stdlib.h>
11 #include <string.h>
12 #include <stdint.h>
13 #include <time.h>
14 #include <signal.h>
15 #include <unistd.h>    //for usleep
16 #include <stdbool.h>
17 #include <libbladeRF.h>
18
19 #include "color.h"
20 #include "sdr_breast_config.h"
21
22 #define  FREQ_INIT  1000 // MHz - Initial SFCW frequency
23 #define  FREQ_STOP  6000 // MHz - Final SFCW frequency
24 #define  FREQ_SIZE   50  // MHz increment in MHz of Steps

```

```
25 #define FREQ_STEP (FREQ_STOP - FREQ_INIT)/FREQ_SIZE
26
27 typedef struct sc16q11_t {
28     int16_t i;
29     int16_t q;
30 }SC16Q11_T;
31 struct sdr_resources {
32     uint64_t                id;
33     bool                    tx1_active;
34     bool                    tx2_active;
35     bool                    rx1_active;
36     bool                    rx2_active;
37     uint32_t                tx1_gain;
38     uint32_t                tx2_gain;
39     uint32_t                rx1_gain;
40     uint32_t                rx2_gain;
41     bladerf_frequency       frequency;
42     bladerf_bandwidth       bandwidth;
43     bladerf_sample_rate     samplerate;
44     char                    *fpga_binary;
45 };
46 static const struct sdr_resources sdr_resources[] =
47 { [SDR1_ID] = {
48     .id                = SDR1_ID,
49     .tx1_active        = ON,
50     .tx2_active        = ON,
51     .rx1_active        = OFF,
52     .rx2_active        = OFF,
53     .tx1_gain          = 66,
54     .tx2_gain          = 66,
55     .rx1_gain          = 0,
56     .rx2_gain          = 0,
57     .frequency         = SDR1_FREQUENCY,
58     .bandwidth         = SDR1_BANDWIDTH,
59     .samplerate        = SDR1_SAMPLERATE,
60     .fpga_binary       = SDR1_FPGA_BINARY
61     }
62 };
63 struct channel_config {
64     bladerf_channel       channel;
65     bladerf_frequency     frequency;
66     bladerf_bandwidth     bandwidth;
```



```

67     bladerf_sample_rate    samplerate;
68     bladerf_gain           gain;
69 };
70
71
72 typedef struct sdr_channel_t{
73     int32_t                 slot_ID;
74     bool                    sdr_is_open;
75     bool                    mcu_is_open;
76     uint64_t                status;
77     struct channel_config   config;
78     struct bladerf_devinfo  dev_info[SDR_DEVICES_MAX];
79     struct bladerf          *dev[SDR_DEVICES_MAX];
80     bladerf_fpga_size fpga_size[SDR_DEVICES_MAX];
81
82 }SDR_CHANNEL_T;
83
84 static SDR_CHANNEL_T sdr_channel;
85
86 //-----
87 FILE *p_data_rx;
88 FILE *p_data_tx;
89
90 //-----
91 static int init_sync(struct bladerf *dev)
92 {
93     int status;
94     /* These items configure the underlying asynch stream used by
95     * the sync interface. The "buffer" here refers to those used
96     * internally by worker threads, not the user's sample buffers.
97     */
98     const unsigned int num_buffers      = 16;
99     /* Must be a multiple of 1024 */
100    const unsigned int buffer_size      = 8192;
101    const unsigned int num_transfers    = 8;
102    const unsigned int timeout_ms       = 3500;
103    /* Configure both the device's x1 RX and TX channels for
104    * use with the synchronous interface.
105    * SC16 Q11 samples *without* metadata are used. */
106    status = bladerf_sync_config(dev,
107                                BLADERF_FORMAT_SC16_Q11,
108                                num_buffers,

```

```

109         buffer_size ,
110         num_transfers ,
111         timeout_ms);
112     if (status != 0) {
113         fprintf(stderr, "Failed to configure RX sync : %s\n",
114             bladerf_strerror(status));
115         return status;
116     }
117
118     status = bladerf_sync_config(dev,
119         BLADERF_TX_X1 ,
120         BLADERF_FORMAT_SC16_Q11 ,
121         num_buffers ,
122         buffer_size ,
123         num_transfers ,
124         timeout_ms);
125     if (status != 0) {
126         fprintf(stderr, "Failed to configure TX sync : %s\n",
127             bladerf_strerror(status));
128     }
129     return status;
130 }
131 //-----From lib-----
132 int process_tx_rx(...)
133 ...
134 //-----
135 //-----From lib-----
136 int sync_rx(struct bladerf *dev)
137 { ... }
138 //-----From lib -----
139 int configure_channel_frequency_rx(struct bladerf *dev,
140     struct channel_config *ch)
141 { ...}
142
143 //-----From lib-----
144 int configure_channel_frequency(struct bladerf *dev,
145     struct channel_config *ch)
146 {...}
147
148 }
149 //-----From lib-----
150 int configure_channel_sample_rate(struct bladerf *dev,

```

```

151         struct channel_config *ch)
152     {...}
153 }
154 //-----From lib-----
155 int configure_channel_bandwidth(struct bladerf *dev,
156                               struct channel_config *ch)
157 {...}
158
159 //-----From lib-----
160 int configure_channel_gain(struct bladerf *dev,
161                           struct channel_config *ch)
162 {...}
163 //-----From lib-----
164 int configure_channel(struct bladerf *dev,
165                      struct channel_config *ch)
166 {...}
167 //-----From lib-----
168 void print_dev_info(struct bladerf_devinfo* dev_info)
169 {...}
170
171 //-----
172 // Configure Channel, Frequency, Bandwidth, Sample-rate, Gain
173 //-----
174 int sdr_config(void)
175 {
176     int status;
177
178     if(sdr_channel.sdr_is_open)
179     {
180         // Configuring the FPGAs availables.
181         for(uint32_t i = 1 ;
182             i < sizeof(sdr_resources)/sizeof(struct sdr_resources);
183             i++)
184             {
185
186 sdr_channel.config.channel=      sdr_resources[i].tx1_active;
187 sdr_channel.config.frequency =  sdr_resources[i].frequency;
188 sdr_channel.config.bandwidth=   sdr_resources[i].bandwidth;
189 sdr_channel.config.samplerate=  sdr_resources[i].samplerate;
190 sdr_channel.config.gain =       sdr_resources[i].tx1_gain;
191
192 fprintf(stdout,"dev_info[" YELLOW_TEXT("%i") "]" instance %d: ",

```

```

193 i, sdr_channel.dev_info[i-1].instance);
194
195 if((int32_t)sdr_channel.dev_info[i-1].instance >= 0)
196     {
197 status = configure_channel(sdr_channel.dev[i-1],
198                             &sdr_channel.config);
199 if(status != 0)
200     {
201 fprintf(stderr, \
202 "Failed to configure SDR channel %lu. Exiting.\r\n", \
203         sdr_resources[i].id);
204         i--;
205         For( ; i >= 1 ; i--)
206     {
207 fprintf(stdout, "Closing SDR %u\r\n", i);
208 bladerf_close(sdr_channel.dev[i-1]);
209     }
210         return 1;
211     }
212     else
213     {
214 fprintf(stdout, \
215 "\r\t\t\t\t" YELLOW_TEXT("SDR %lu configured [") GREEN_TEXT("Y")
216 YELLOW_TEXT("]\r\n"), \
217 sdr_resources[i].id);
218 enable_sdr_outputs(sdr_channel.dev[i-1]);
219     }
220     }
221     else
222     {
223 fprintf(stdout, \
224         "\r\t\t\t\t" YELLOW_TEXT("SDR %lu configured [")
225 RED_TEXT("N") YELLOW_TEXT("]\r\n"),
226         \sdr_resources[i].id);
227     }
228     }
229 fprintf(stdout, "Devices configured successful!\r\n");
230     }
231 return 0;
232 }
233
234 //-----

```

```
235 // Closing devices previous opened
236 //-----
237 void sdr_close(void)
238 {
239     for(uint32_t i = 1 ;
240         i < sizeof(sdr_channel.dev_info)/sizeof(struct bladerf_devinfo);
241         i++)
242     {
243         if((int32_t)sdr_channel.dev_info[i-1].instance >= 0)
244             {
245                 fprintf(stdout,"Closing SDR %d\r\n",i);
246                 bladerf_close(sdr_channel.dev[i-1]);
247             }
248     }
249 }
250
251 //-----
252
253
254
255 //-----
256 #ifdef MAIN
257 int main(int argc, char **argv)
258 #else
259 int sdr_init(int argc, char **argv)
260 #endif
261 {
262     SC16Q11_T rx_data;
263     SC16Q11_T tx_data;
264     p_data_rx = fopen("saida.sc16q11","wb");
265     p_data_tx = fopen("entrada.sc16q11","rb");
266     int status;
267     //Open Devices without check if FPGA is programmed.
268     for(uint32_t i = 1 ;
269         i <= sizeof(sdr_channel.dev_info)/sizeof(struct bladerf_devinfo);
270         i++)
271     {
272         bladerf_init_devinfo(&sdr_channel.dev_info[i-1]);
273         fprintf(stderr,\
274             "Initializing SDR channel\r\t\t\t\t%d\n", i);
275         sdr_channel.status = bladerf_open_devinfo(&sdr_channel.dev[i-1],
276             &sdr_channel.dev_info[i-1]);
```

```

277         if(sdr_channel.status == 0)
278         {
279 sdr_channel.status = bladerf_get_devinfo(sdr_channel.dev[i-1],
280         &sdr_channel.dev_info[i-1]);
281         if(sdr_channel.status != 0)
282         {
283 fprintf(stderr, \
284 "Unable to open device:\r\t\t\t\t" YELLOW_TEXT("%s") "\r\n",
285 \sdr_channel.dev_info[i-1].serial);
286         }
287         else
288         {
289         // Serial, USB, Instance
290         print_dev_info(&sdr_channel.dev_info[i-1]);
291         //Configure FPGA FILE
292 sdr_channel.sdr_is_open = TRUE;
293 if(!bladerf_is_fpga_configured (sdr_channel.dev[i-1]))
294     {
295 sdr_channel.status = bladerf_get_fpga_size (sdr_channel.dev[i-1],
296 \&sdr_channel.fpga_size[i-1]);
297 fprintf(stdout, \
298 "FPGA Size is : %d\r\n", \
299 sdr_channel.fpga_size[i-1]);
300 switch(sdr_channel.fpga_size[i-1])
301 {
302 case 49:         bladerf_load_fpga (sdr_channel.dev[i-1],
303 SDR_FPGA_STD_49);         break;
304 case 301:        bladerf_load_fpga (sdr_channel.dev[i-1],
305 SDR_FPGA_STD_301);        break;
306 default:        fprintf(stdout, "Falha : %d\r\n",
307 sdr_channel.fpga_size[i-1]);        break;
308         }
309     fprintf(stdout, \
310         "FPGA is %s\r\n", \
311         bladerf_is_fpga_configured(sdr_channel.dev[i-1])?\
312         "configured" : "not configured");
313         } } } }
314
315         // check for FPGA is loaded.
316
317 //-----
318 //Calling task to configure the BladeRF 2.0

```

```

319 //-----
320 sdr_config();
321
322 //-----
323 //SFCW routine
324 //-----
325
326 for(uint32_t i = 1 ;
327 i <= sizeof(sdr_channel.dev_info)/sizeof(struct bladerf_devinfo);
328 i++)
329 {
330 for(uint64_t step_counter = 0 ;
331     step_counter <= FREQ_STEP ;
332     step_counter++ )
333 {
334 sdr_channel.config.frequency =
335 FREQ_INIT*1000000 + (step_counter*FREQ_SIZE*1000000);
336 //-----
337 //Transmitter routine - Task configure_channel_frequency_rx
338 //-
339 status = configure_channel_frequency(sdr_channel.dev[i-1],
340 &sdr_channel.config);
341 //-----
342 //Receiver routine - Task configure_channel_frequency_rx
343 //-----
344 status = configure_channel_frequency_rx(sdr_channel.dev[i-1],
345 &sdr_channel.config);
346 fprintf(stdout,"Set frequency of SDR step %3d to %lldMHz\r\n",
347 step_counter,
348 (uint64_t)sdr_channel.config.frequency/1000000);
349 {
350 fprintf(stderr, "[" YELLOW_TEXT("DUMMY") "]
351 Receiving samples of RX...\r\n");
352 status = sync_rx(sdr_channel.dev[i-1]);
353     }
354     usleep(10000); // T=1/PRF => T = 10e-3 segundos
355
356     }
357     fclose(p_data_rx);
358     fclose(p_data_tx);
359 }
360

```

```
361     while(1)
362     {
363         char c;
364         //sleep(20000);
365     fprintf(stdout, "Press \"Y\" to close this program\r\n");
366         c = getchar();
367         if(c == 'y' || c == 'Y')
368         {
369             sdr_close();
370             //closing_Serial();
371             exit(0);
372             //break;
373         }
374     }
375
376     #endif //MAIN
377
378     return status;
379
380 }
```